

4-1-2005

Blast Assessment of Load Bearing Reinforced Concrete Shear Walls

Katie Wheaton

Clay Naito

Follow this and additional works at: <http://preserve.lehigh.edu/engr-civil-environmental-atlss-reports>

Recommended Citation

Wheaton, Katie and Naito, Clay, "Blast Assessment of Load Bearing Reinforced Concrete Shear Walls" (2005). ATLSS Reports. ATLSS report number 05-08.: <http://preserve.lehigh.edu/engr-civil-environmental-atlss-reports/62>

This Technical Report is brought to you for free and open access by the Civil and Environmental Engineering at Lehigh Preserve. It has been accepted for inclusion in ATLSS Reports by an authorized administrator of Lehigh Preserve. For more information, please contact preserve@lehigh.edu.



LEHIGH
UNIVERSITY

**BLAST ASSESSMENT OF
LOAD BEARING REINFORCED CONCRETE
SHEAR WALLS**

By

**Katie Wheaton, Graduate Student Researcher
Clay Naito, Principal Investigator**

April 2005

ATLSS REPORT NO. 05-08

**ATLSS is a National Center for Engineering Research
on Advanced Technology for Large Structural Systems**

117 ATLSS Drive

Bethlehem, PA 18015-4729

Phone: (610)758-3525

Fax: (610)758-5902

www.atlss.lehigh.edu

Email: inatl@lehigh.edu

1. Table of Contents

1. Table of Contents.....	2
2. Table of Figures.....	4
3. Abstract.....	7
4. Introduction	8
5. Blast Demands and Structural Resistance.....	9
5.1. Blast Load Demand	9
5.2. Structural Resistance to Blast	12
6. Research Significance.....	14
7. Prototype Building.....	15
7.1. Progressive Collapse Analysis.....	18
8. Qualitative Push-Over Analysis	21
8.1. Pressure Distribution Demand.....	21
8.2. Finite Element Analysis.....	23
8.3. Pushover Failure Modes	27
9. “System” Dynamic Analysis	28
9.1. Structural Resistance	29
9.1.1. Stiffness Properties	29
9.1.2. Moment-Curvature	31
9.1.3. Critical Displacements.....	36
9.2. Nonlinear Dynamic Response	41
9.2.1. Equivalent SDOF Model	41
9.2.2. Static Resistance Curve	44
9.2.3. Wall Response	48
9.3. Damage Quantification	50
9.3.1. Dynamic and Impulsive Response of 1 st Floor Wall	52
9.3.2. Pressure-Impulse Curve.....	54
10. “Component” Dynamic Analysis.....	58

10.1. Static Resistance Curve	58
10.2. Equivalent SDOF Model	61
10.3. Pressure vs. Impulse Curve.....	63
10.4. Summary of Component Model Method	64
10.5. Component Analysis with Bi-linear Approximation	66
11. Conclusions and Recommendations	69
12. References	71
Appendix A: Mathcad Program to Solve System Model Equivalent SDOF Model.....	72
Appendix B: Mathcad Program to Solve Component Model Equivalent SDOF Model	77

2. Table of Figures

Figure 1: Blast Load Effects	10
Figure 2: Idealized Blast Load (Exponential vs. Triangular).....	12
Figure 3: Building Shell Layout	15
Figure 4: Plan View of Prototype Building	16
Figure 5: Floor Diaphragm Details at Prototype Shear Wall.....	16
Figure 6: Cross Section 1-A	17
Figure 7: Cross Section 1-B.....	17
Figure 8: Cross Section 1-C.....	17
Figure 9: Wall Reinforcement Details	18
Figure 10: Isometric View of Prototype Shear Wall.....	18
Figure 11: Potential Progressive Collapse Scenario	20
Figure 12: Elevation Section 1-D	20
Figure 13: Blast demand scenarios	21
Figure 14: Reflective pressure demand on wall.....	22
Figure 15: Normalized Blast Pressures Compared	22
Figure 16: FE Model Constraints	23
Figure 17: FE Model Concrete Mesh	24
Figure 18: FE Model Reinforcement	24
Figure 19: FE Model Applied Load Distribution	25
Figure 20: Strain Distribution in Longitudinal Reinforcement at Initiation of Yield	26
Figure 21: Principal Strain Distribution in Concrete at Crushing.....	26
Figure 22: Equivalent SDOF System.....	28
Figure 23: Wall System	30
Figure 24: Wall Cross-Sections (Transverse Reinforcement Not Illustrated)	31
Figure 25: Fiber Analysis Details	32
Figure 26: Concrete Constitutive Properties.....	33
Figure 27: Steel Constitutive Properties	33

Figure 28: Moment Curvature Response of Wall	34
Figure 29: Comparison of Moment-Curvature Graphs at Nominal Capacity	35
Figure 30: Formation of Plastic Hinges	37
Figure 31: Formation of Plastic Hinge	38
Figure 32: Curvature Along Wall at Ultimate Load Level for 2 nd Floor, Outer Wall.....	39
Figure 33: Curvature Along Wall in Plastic Hinge Region	40
Figure 34: Convergence of Plastic Hinge Rotation for Increasing Discretization	40
Figure 35: Plastic Hinge Reaches Ultimate Curvature	41
Figure 36: Assumed Shape Functions	43
Figure 37: Static Resistance of Equivalent SDOF Model.....	45
Figure 38: Example Dynamic Response History of Wall.....	49
Figure 39: Assumed rebound response	50
Figure 40: (a) Long Duration Loading (b) Short Duration Loading	50
Figure 41: Normalized Dynamic Response of Wall under Quasi-Static Load	51
Figure 42: Normalized Dynamic Response of Wall under Dynamic Load	51
Figure 43: Normalized Dynamic Response of Wall Under Impulse Load	52
Figure 44: Curvature along first floor outer wall at ultimate.....	53
Figure 45: Response Curve of First and Second Floor Wall	54
Figure 46: Pressure vs. Impulse Curve (System Model)	55
Figure 47: Three Regimes of Loading (System Model)	56
Figure 48: FEMA Performance Levels (System Model).....	57
Figure 49: System Model vs. Component Model	58
Figure 50: Static Resistance Curve (System vs. Component Model)	61
Figure 51: Pressure vs. Impulse Curve (Component & System Models)	63
Figure 52: Flow Chart of Dynamic Response Methodology (Component Model).....	64
Figure 53: Flow Chart of Pressure vs. Impulse Curve Methodology	65
Figure 54: Maximum Response of Elastic-Plastic SDOF System Due to Triangular Load (Biggs 1964).....	66
Figure 55: Effective Bi-linear Resistance Curve	67

Figure 56: Pressure vs. Impulse Curve (Bi-Linear & System Models)68

3. Abstract

Assessment of a structure's blast capacity has become an important focus in structural engineering. In response to heightened terror awareness numerous existing structures must be evaluated for conformance with security standards. Determining the blast resistance of a structure is a first step towards evaluating the potential need for retrofit construction. Numerous methods can be employed to determine the blast resistance of a structure, oftentimes over-simplified or too complex. A common lateral load resisting system that is particularly vulnerable to blast loads is a reinforced concrete shear wall. The purpose of this paper is to outline a methodology to calculate the blast resistance of an existing shear wall, which will optimize the scope of results while minimizing the calculation complexity required.

This analysis couples a static FE model with an equivalent SDOF dynamic analysis. A prototypical corner shear wall with window openings is chosen for study. A static pushover FE model is developed which pinpoints the location of failure to be the 2nd floor, outer wall, becoming the subject of the dynamic analysis study. The 2nd floor wall is modeled two ways: as a system, including the stiffness contributions of adjoining wall sections, and as a component with fixed ends. A moment-curvature analysis determines the formation of plastic hinges, and the stages of failure are represented by a multi-linear static resistance curve. An equivalent SDOF model yields the dynamic response history of the wall. Pressure vs. impulse curves are created to describe the blast resistance of the wall at each damage stage. Comparison of the system and component methods reveals that the component model couples fewer calculations with a good quality response estimate for highly stiff walls. The component model overestimates the blast resistance of the wall by 7%, when compared to the system model results for blasts in the impulse region. A simplification of the resistance curve from multi-linear to bi-linear is also presented. This method yields values within 15% of the system model results and is recommended as a way of quickly determining the blast resistance of a structure at first yield or failure.

4. Introduction

Blast loads have been a design concern for structural engineers for many years. Originally, research and development was conducted to protect structures against accidental explosions, such as those that may occur in a chemical manufacturing plant or military ammunition depot. Recent terror events world wide, however, have created a shift in design philosophy from dealing with an expected explosive event of given size to an event of unknown magnitude that could occur at any time in any location on a structural system. Without a proper design approach these intentional explosive events have the potential for significant loss of life and economic damage.

In response to this growing concern many building owners are prioritizing protection against blast. This may take various forms including non-structural safeguards, such as a defended standoff distance and bag screening, or it may include complex analysis and design to create a blast hardened structure. The United States government has taken the lead in creating blast guidelines for its buildings. Currently all new and existing Department of Defense (DoD) facilities must conform to the Unified Facilities Criteria (U.S. Army Corp of Engineers 2005). Also, the Interagency Security Committee (ISC) of the General Services Administration (GSA) recently outlined specific standards for all leased buildings, which will affect any existing building considered for lease by GSA. It is apparent that many existing buildings must now be assessed for their conformance to these blast design guidelines. When it is necessary to design a structure to resist blast there are numerous approaches which may be employed. Existing design methods often oversimplify the problem or are too complex for an average design engineer to apply. To effectively enhance the blast resistance of our existing infrastructure, and to integrate blast resistance into new design, simplified accurate methods to determine a structure's strength under blast must be developed.

Reinforced concrete shear walls are commonly designed in the United States as a lateral resisting system to withstand earthquake and wind loads. The design of the shear wall to resist in-plane loads leaves them vulnerable to blast forces which typically generate out-of-plane loads captured by the large surface area of the wall. Shear wall systems often assist in the load bearing action of the building, supporting larger floor spans. Loss of such a component may lead to a progressive collapse. It is therefore advantageous for designers to have the ability to predict the blast resistance of such a structure in order to design a shear wall to withstand blast loads. The purpose of this research is to examine the blast resistance of a load bearing shear wall system by outlining a methodology that can be recreated in a time effective manner by engineers in practice.

5. Blast Demands and Structural Resistance

The first step in protecting a structure from blast loads is prevention. Prevention often takes the form of indirect measures such as surveillance and counter-terrorism intelligence or through direct physical measures such as that provided by a defended standoff distance. This creates a range between unregulated spaces through the use of concrete or steel barriers which prevent explosive carrying vehicles from approaching the structural system (General Services Administration 2003). While prevention can decrease the likelihood of an event, it cannot guarantee protection. For example, many structures are built in densely populated areas where a defended standoff distance is almost nonexistent. Therefore the second step, and primary task of the engineer, is to prevent loss of life by ensuring structural integrity during an explosion. A structure designed with enough ductility will absorb the energy of the blast while still remaining load bearing.

There are two fundamental tasks that must be conducted to ensure structural integrity under explosive events, determination of the *blast load demand* and *blast load resistance*. Blast load demand relates to the amount of energy a blast imparts to a structure, while blast load resistance is the physical strength of a structure to withstand a blast load. Many tools exist which can predict an explosion's blast demand. These have been well developed through research and are presented briefly in Section 5.1. Methods for determining the blast resistance of a structure are covered in the remaining portion of the report.

5.1. Blast Load Demand

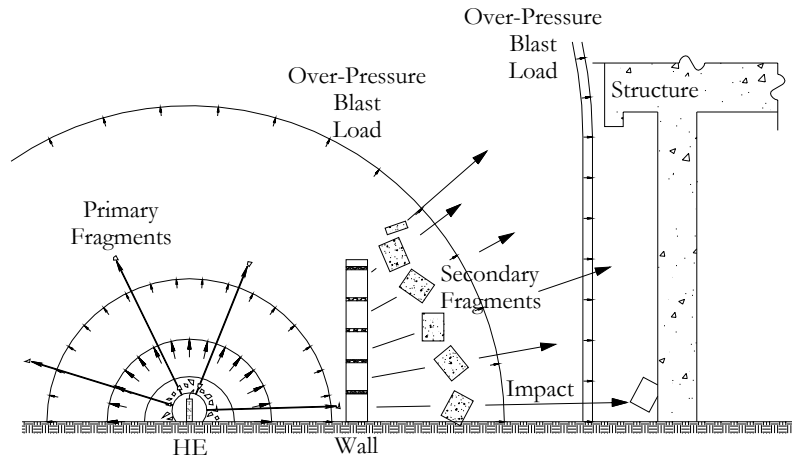
All structures are susceptible to damage from explosively generated blast loads. Given adequate time and explosive, any structure is vulnerable to collapse. A blast explosion is characterized by the rapid expansion of gas which generates a virtually instantaneous increase in local pressure (Mays and Smith 1995). As a result, a high-velocity, high-pressure wave propagates through the air, moving outward from its source and dissipating in energy as it travels. The characteristics of a blast load are dependent on many factors, most importantly, type and quantity of explosive and the location of the explosive relative to the structure.

The load demand caused by a detonation of a high explosive (HE) can be divided into four parts as shown in Figure 1 (a), impact of *primary fragments*, impact of *secondary fragments*, *over-pressure*, and *reflective pressure*. Primary fragments originate from the source of the explosion, often times placed within the bomb or casing. Secondary fragments consist of objects that are picked up and projected as the blast radiates. This can include equipment or other objects not securely attached to the ground, bricks from unreinforced walls, or portions of the structure itself. Primary and secondary fragments are both associated with significant casualties, but in most cases neither contributes to major structural damage.

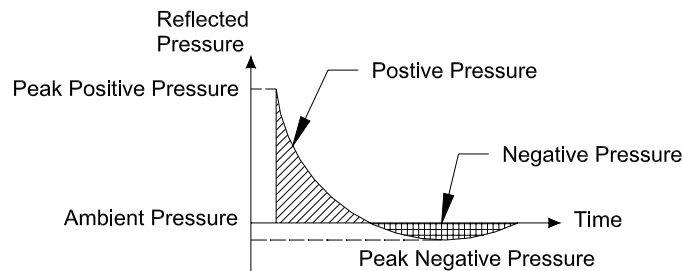
The initial increase in ambient pressure, which expands radially from the source of the explosion, is known as the over-pressure. The over-pressure is dependent on the size of the explosive and the distance from the explosion to the target. Thus a small size explosive at close range may generate the same demands as a large explosive in the distance. The *equivalent scaled distance*, Z , is used to compare the overpressures of explosions comprised of varying sizes and locations. The equivalent scaled distance is found from the equation, $Z = R/W^{1/3}$, where R [ft] is the distance from the explosion to the structure, and W [pounds of TNT] is the weight of the explosive (Conrath

1999). The blast effects of explosives other than TNT can be determined by multiplying W by an equivalency factor (DSWA 1998). For example the equivalency factor for Aluminum Nitrate and Fuel Oil (ANFO) would transform X pounds of ANFO into W pounds of TNT.

When the radiating over-pressure wave reaches an object perpendicular to its path the wave is reflected creating an elevated pressure demand. The magnitude of this reflected pressure is dependent on the shape of the object and the orientation of the object with respect to the blast wave. For a building element perpendicular to the radiating over-pressure wave a distributed reflected pressure is generated. This distributed pressure is assumed to have an instantaneous rise time to a peak positive pressure value which subsequently dissipates to atmospheric pressure over a few milliseconds. This is what is known as the reflected pressure, and it is the most destructive aspect of blast loading with respect to a structure. The positive pressure is followed by a negative pressure phase which is much lower in magnitude but longer in duration, usually over a range of 10-40 ms.



(a) Blast demands



(b) Pressure load profile

Figure 1: Blast Load Effects

An idealized pressure time response curve is presented in Figure 1 (b). The blast pressure is characterized by an instantaneous rise to peak positive pressure which occurs at time after the detonation. This peak pressure decreases exponentially to the negative phase. This pressure profile characterizes the *blast demand*. Three methods for determining the blast demand generated by conventional charge explosives have been developed by the military. These methods offer varied levels of complexity and detail. The least complex method utilizes charts such as those presented in Army Technical Manual TM5-1300 (U.S. Department of the Army 1990). These charts pertain to

accidental explosions and will yield a resulting pressure distribution for a given quantity of TNT, distance to the structure, and orientation of the structure to the blast. The second tool available from the Army Corps of Engineers is the computer program ConWep (Hyde 2003). ConWep generates the blast demands of conventional weapons as calculated from the equations and curves of Army Technical Manual TM 5-855-1 (U.S. Department of the Army 1998). The capabilities of ConWep include the calculation of an above ground air blast, ground shock, and the blast pressure on a concrete slab. The most complex of the currently available methods is the program BlastX (Britt et al. 2001). BlastX allows for the computation of pressure profiles on irregularly shaped structural geometries. BlastX has the capability to calculate the air blast generated by explosions inside or outside multiple room structures and will model the shock wave reflection off of walls, columns, and other structural elements.

The three methods described for assessing blast demand provide increasing levels of accuracy. For the majority of structural analysis, however the resulting pressure profiles may be simplified. The exponential pressure-time demand, Figure 1 (b), can be represented as a triangular distribution. For most cases, the negative pressure region has little effect on the behavior of the system and can be neglected. The area under the pressure – time profile is referred to as the *impulse*, $i = \int p(t)dt$. Equating the area under the exponential curve to the area under a triangular curve, as shown in Figure 2, the impulsive energy can be maintained, resulting in a reasonable approximation of the blast demand. The maximum positive pressure, p_o , remains the same for both curves. By equating the areas under both curves, the approximate curve will have a time duration of $t_{dl} = 2i / p_o$. Thus p_o and i will describes how much energy the blast is imparting to a structure, and therefore defines the blast demand on a structure. Often in blast assessment the responsibility of determining the specific threat level (i.e., weight of explosive and distance) is handled by an outside source. Thus, engineers in practice who are instructed to design a structure for a specific threat level will usually be given the blast demands in terms of pressure and impulse.

A typical blast demand on a structure has two features which are not commonly encountered by design engineers. This includes the large magnitude of the pressure demand and the dynamic aspect of the loading. These characteristics must be considered together. Applying the blast demand statically will in most cases significantly over estimate the demand. The impulsive nature of the pressure in combination with the mass and stiffness of the system allows the structure to resist dynamic loads in excess of its static load capacity (i.e. $t_d \ll T_n$). Methods for accounting for these effects are developed in detail in later sections.

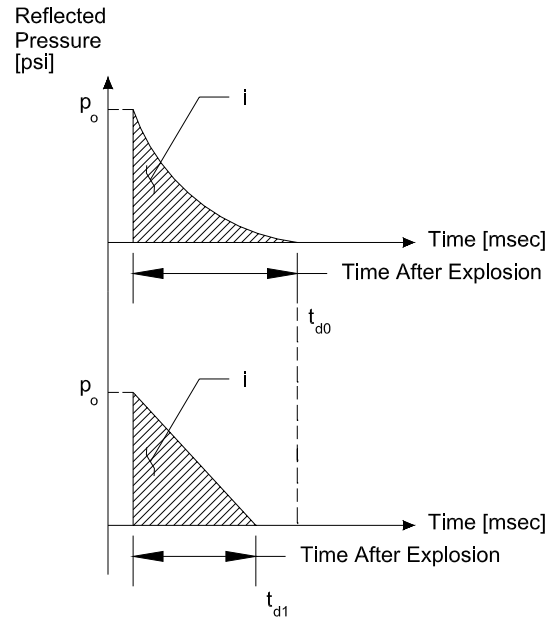


Figure 2: Idealized Blast Load (Exponential vs. Triangular)

When the combination of pressure level and impulse is extremely elevated, the structure has a tendency to become pulverized. This phenomenon is known as *brisance*. The risk of brisance is commonly associated with reinforced concrete structures. Brisance commonly occurs when the explosion occurs in close proximity to the structure. This distance has been estimated to occur at a scaled distance of $Z \leq 1.5 \text{ ft}/\text{lb}^{1/3}$ (McVay 1988). Thus for an explosion in close proximity to a structure, a portion of the system may be subject to demands in excess of the scaled distance limit. Elements within this range can be assumed to be instantaneously removed or to produce a static pull-down force on the remaining system. As an upper bound the pull down force can be assumed to be equal to twice the pre-existing gravity load.

5.2. Structural Resistance to Blast

The goal for a blast resistant design includes preventing local or progressive collapse of a component or structural system, minimizing global damage, or localizing damage to absorb the blast energy. Depending on the goal of the design, different analytical techniques can be utilized. Analytical techniques can be divided into three categories: coupled dynamic analysis, uncoupled dynamic analysis, and static analysis. Each analysis technique balances computational rigor with the amount of information attained. The specifics of the design goal will determine which level of analytical detail is required.

The most accurate analytical technique is a coupled blast analysis. In this technique the blast pressure demand changes as the structure deforms under the load application. These analyses are used for flexible structural systems of where isolated damage is expected. This technique is most commonly used for military applications such as blasts on ship hulls. This coupling between the load and the resistance requires advanced finite element techniques in which both the pressure wave and the nonlinear action of the structure is modeled. To accurately perform this analysis requires proper application of computational fluid dynamics and dynamic finite element (FE) analysis with

geometric and material nonlinearities. A few programs such as SHAMRC (Crepeau 2001) allow for coupled analysis, however, the computational effort and expertise required make these studies very uneconomical for bridge and building analysis. Fortunately, due to the stiffness and mass of typical building systems, the response of the structural elements can be assumed to be uncoupled from the blast load. In an uncoupled analysis the element is assumed to be rigid during the load application, thus the blast demand can be determined independently as discussed in the preceding section.

Uncoupled dynamic analysis includes finite element analysis and simplified techniques such as single degree of freedom (SDOF) analysis. Finite element methods can be conducted at varying levels of detail. Material and geometric nonlinearities, large deformations, and dynamic responses can all be accurately modeled. Such methods however require high level analytical tools (i.e. DYNA3D), costly computing time, and most importantly, advanced knowledge of nonlinear analysis. In the interest of time and money this technique is seldom used by designers.

As an alternative to complex dynamic analyses a less rigorous approach for design applications has been developed and implemented by the Government Security Agency (GSA). This static, linear analysis method is well documented by the GSA in the manual “*Progressive Collapse Analysis and Design Guidelines*” (General Services Administration 2003). The guide makes the assumption that a targeted structural element undergoes an instantaneous removal. The removal process is assumed to occur locally to the section of the building under evaluation. The remaining structure is then analyzed against a factored load of $2(DL+0.25*LL)$. If the remaining capacity is less than the demand the members must be strengthened. While this simplified calculation procedure provides a methodology for prevention of progressive collapse, it provides no information as to the actual response or damage states of a building under blast loads. It is a *threat independent* methodology, meaning that it cannot predict the blast resistance of a structure or the damage associated with an event of a given size.

To provide an effective and yet simple method for analysis of structures under blast loads a combined finite element and SDOF modeling method is developed. The method begins with a static elastic FE push-over analysis of the structural system. Using this tool the location of failure is qualitatively identified. The identified damage region is then examined using an equivalent SDOF system. The use of a SDOF model allows for material nonlinearities and dynamic action to be accounted for without significant computational time. The equivalent SDOF system captures the dynamic response history of the structure. Its elastic-plastic resistance behavior is considered, and the formations of plastic hinges determine critical displacement values that designate stages of failure. From this information, a pressure-impulse curve can be generated which quantifies the blast resistance of a structure. This analysis considers the case of a reinforced concrete wall, but it could be easily extended to other structural materials such as steel, precast concrete, or masonry.

This analysis technique can be conducted independently of the blast demand assessment. Therefore one individual can focus on calculating a structure’s resistance strength, while another can focus on calculating blast demands for different explosions. This method is time effective while still providing valuable dynamic response information to the designer. The method is presented in detail in the paper along with recommended model simplifications to reduce computation time and analytical rigor.

6. Research Significance

The purpose of this research is to examine the blast resistance of a load bearing shear wall system. While reinforced concrete shear wall systems have been used to successfully resist the effects of lateral demands generated from earthquakes and wind loads, the resistance to explosive loads has not been comprehensively examined. Shear walls are conventionally designed to resist lateral loads through in-plane action; however, blast forces typically generate out-of-plane loads. The large surface area of a wall provides an ideal area for capturing blast pressures, resulting in a complex, dynamic structural response. Exterior walls of the building are often a structure's first line of defense against an explosion, but rarely have cladding for protection. These systems often assist in the load bearing action of the building, supporting larger floor spans vulnerable to the risk of progressive collapse. It is therefore advantageous for designers to have the ability to predict the blast resistance of such a structure in order to design a shear wall to withstand blast loads.

This study presents the results of a simplified dynamic analysis method that can be utilized to determine the dynamic response of a structure and its stages of failure. The paper outlines a methodology that couples a static FE model with a SDOF dynamic analysis in order to reduce computation time while preserving the scope of results obtained. A prototypical building was chosen to represent commonly constructed office buildings in the United States. The building studied is a low rise structure, three stories high, with gravity bearing shear walls located at each corner. The system is designed for seismic demands and does not exhibit any special details for blast resistance. The paper provides a methodology for assessing the blast resistance of the prototype building and provides numerical examples. The strength of the wall is quantified through generation of pressure vs. impulse curves, delineating stages of failure by the FEMA performance level criteria. The wall is first examined as a complete system. Simplifying assumptions are then presented to reduce model complexity and calculation time. The analysis results for the two models are compared, with suggestions as to when it is appropriate to apply the simplified model.

7. Prototype Building

The prototypical building studied is a low-rise structure, three stories high with a rectangular footprint of approximately 140 ft by 60 ft. The lateral load resisting system is comprised of shear walls at all four corners of the building as shown in Figure 4 and Figure 3. The shear walls are designed for seismic zone 4. Perimeter columns are protected by cladding, and assumed to be far enough away from the center of the explosion so as not to be subject to structural damage. The system is designed using normal weight concrete with a 28 day compressive strength of 4 ksi. Live loads were taken to be 20 psf at the roof and 80 psf elsewhere. A superimposed dead load of 15 psf was assumed. Steel reinforcement is Grade 60, ASTM A706. Steel W-sections are ASTM A992 while steel channels are ASTM A36.

The north-east corner wall is chosen for the blast resistance assessment. It exhibits a regular geometry with architectural window openings integrated within the faces of the wall at each floor level. Coupling beams are located at the top and bottom of each opening. The perpendicular walls are cast monolithically. Reinforcement in each wall is symmetric and is detailed according to Figure 10. The size of longitudinal reinforcement decreases up the height of the wall. The corner shear wall being studied supports the gravity load of the floor diaphragm as shown in Figure 5. The floor is comprised of concrete over metal deck and is supported by steel channels attached to the shear wall with Nelson embed studs as shown in Figure 7. Additional wall and floor diaphragm details are shown in Figure 6 through Figure 9.

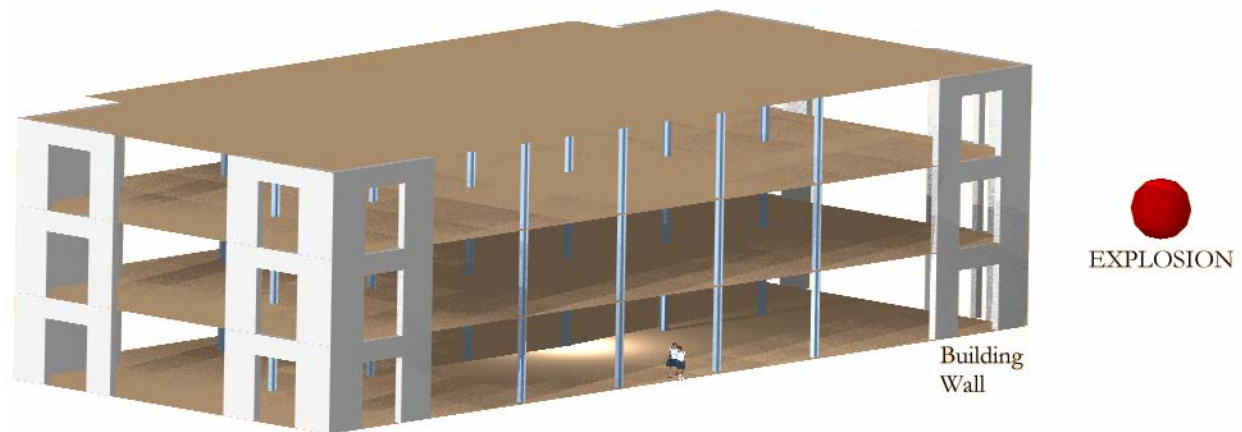


Figure 3: Building Shell Layout

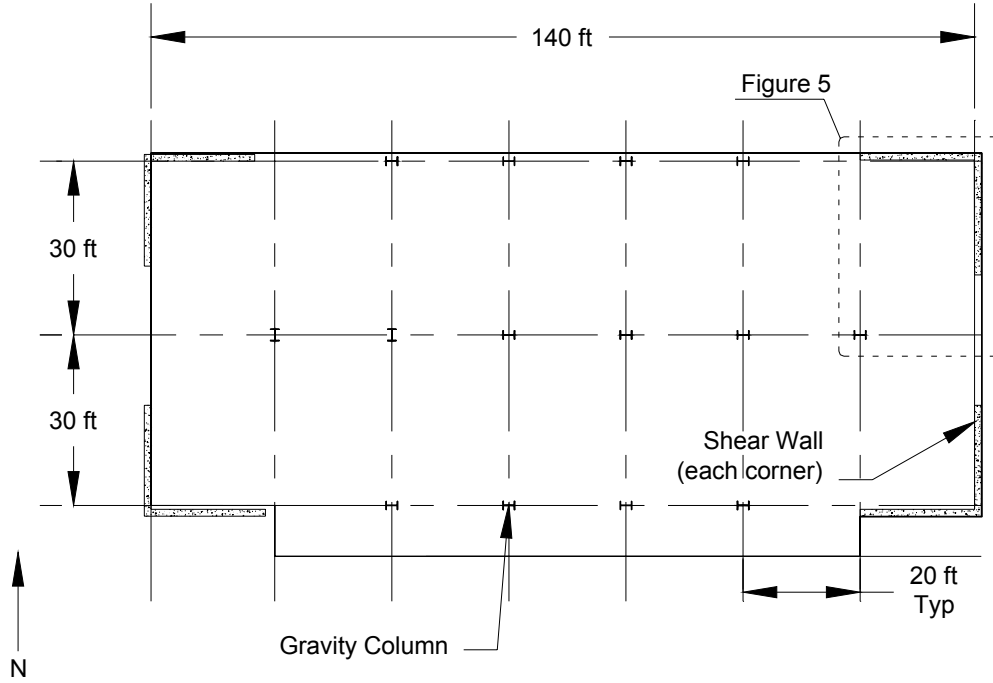


Figure 4: Plan View of Prototype Building

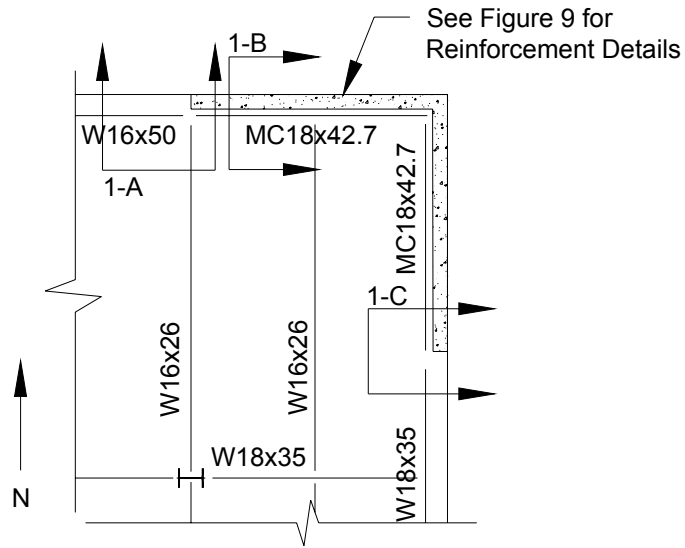


Figure 5: Floor Diaphragm Details at Prototype Shear Wall

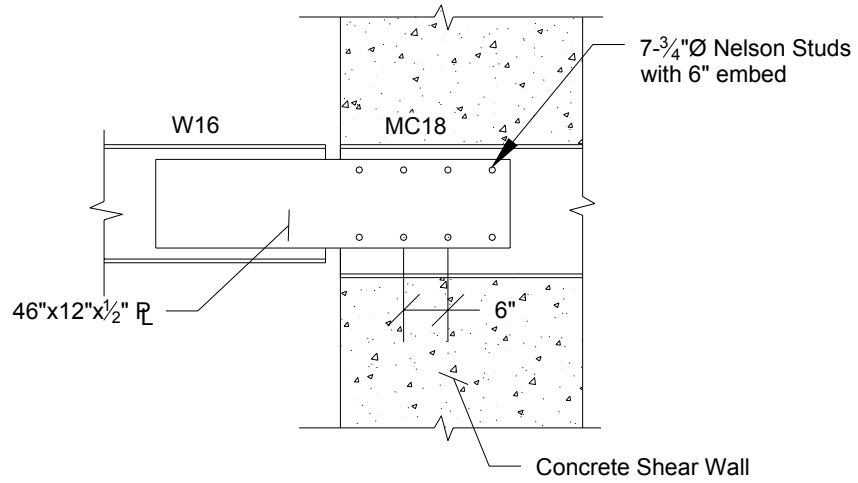


Figure 6: Cross Section 1-A

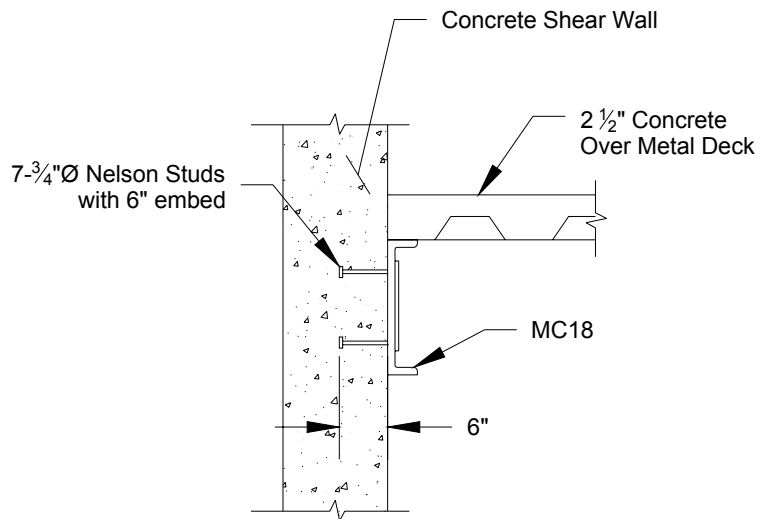


Figure 7: Cross Section 1-B

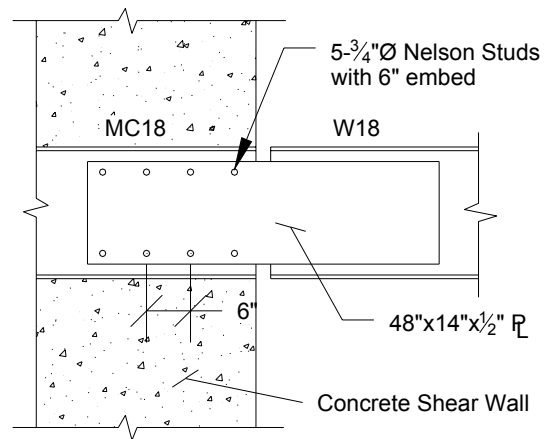


Figure 8: Cross Section 1-C

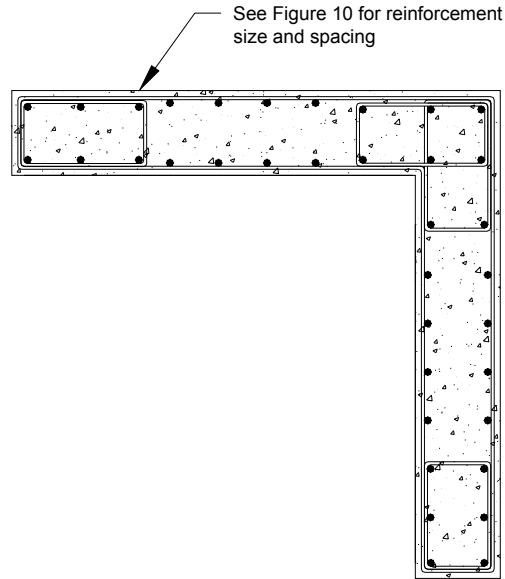


Figure 9: Wall Reinforcement Details

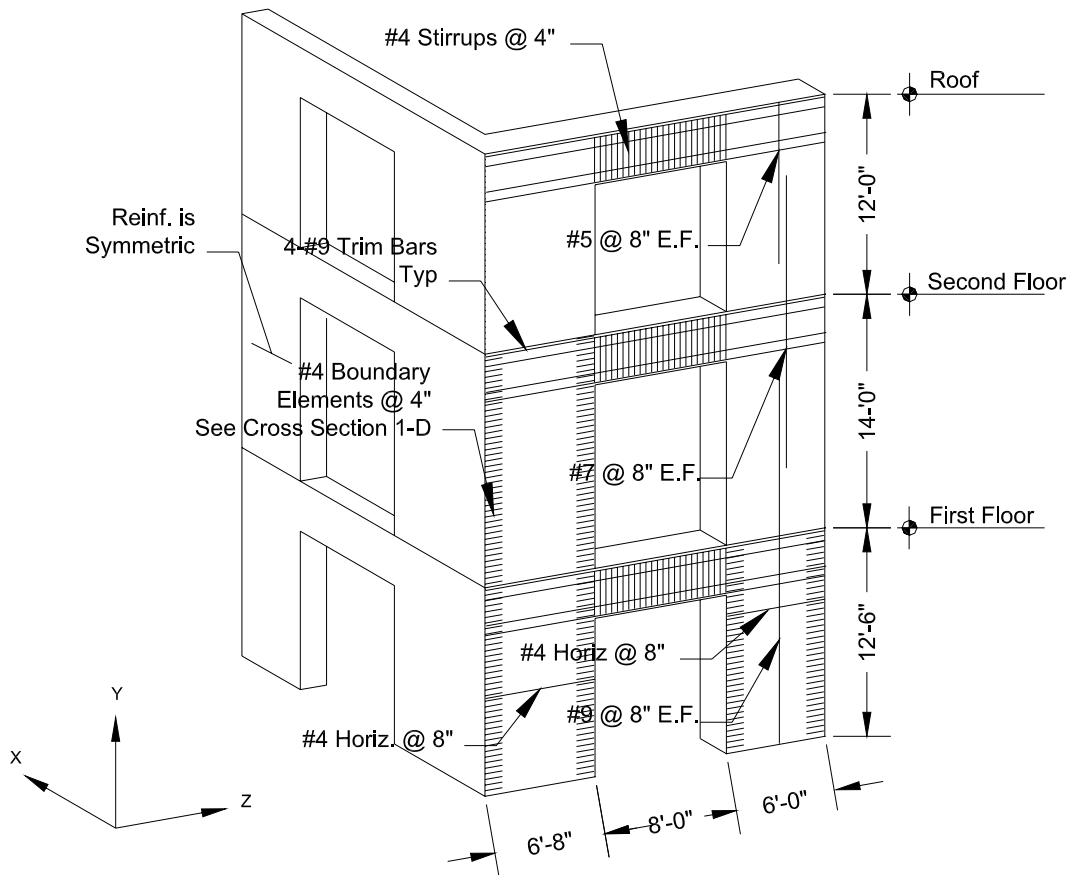


Figure 10: Isometric View of Prototype Shear Wall

7.1. Progressive Collapse Analysis

The locations of window openings in the prototype shear wall create 6 foot wide outer walls spanning from floor to

floor, which are particularly vulnerable to blast loads. Under a moderate blast load it is conceivable that both outer portions of the wall will be lost while the corner piece of the wall will remain intact. The integrity of the slab is examined for this condition. As shown in Figure 5 the W16 sections supporting the floor diaphragm frame into an MC18 section attached to the shear wall. The channel section is attached to the wall with 7-3/4" diameter Nelson studs, shown in Figure 7. In the event that the outer wall collapsed, the channel section would become a cantilever that is anchored by the remaining corner wall as shown in Figure 11. The cantilevered channel would be the only remaining section to carry the gravity load of the floor diaphragm. A shear capacity calculation of the remaining headed studs at the corner wall was performed in accordance with concrete design specifications (Precast/Prestressed Concrete Institute 1999). The capacity of one stud was found to be 18 kips. Assuming 6 studs remained attached to the corner wall, the total shear capacity is 108 kips. The shear as a result of gravity loads the headed studs to 80% of their capacity. Therefore the shear studs will not fail. But flexural calculations of the cantilevered channel give an allowable stress value of $F_b = 0.66 * F_y = 23.76$ ksi, while the maximum moment at the cantilevered end causes a tensile stress in the top flange of $f_b = 40$ ksi. Therefore the channel section will fail in flexure, precipitating a progressive collapse of the floor shown as illustrated in Figure 12.

It is apparent that the outer walls of the shear wall are an important structural element to maintain integrity of the floor diaphragm. Loss of the outer wall will lead to loss of a large portion of the floor. To enhance the integrity of this system a number of options could be pursued: the slab edge restraint to the corner wall could be strengthened, the slab could be designed as self supporting under a cantilever condition, or the shear wall could be strengthened. However, prior to conducting any of these rehabilitations it is important to quantify how the wall will be damaged and what level of damage is associated with a given blast. This study of the wall's inherent strength may preclude the need for any rehabilitation.

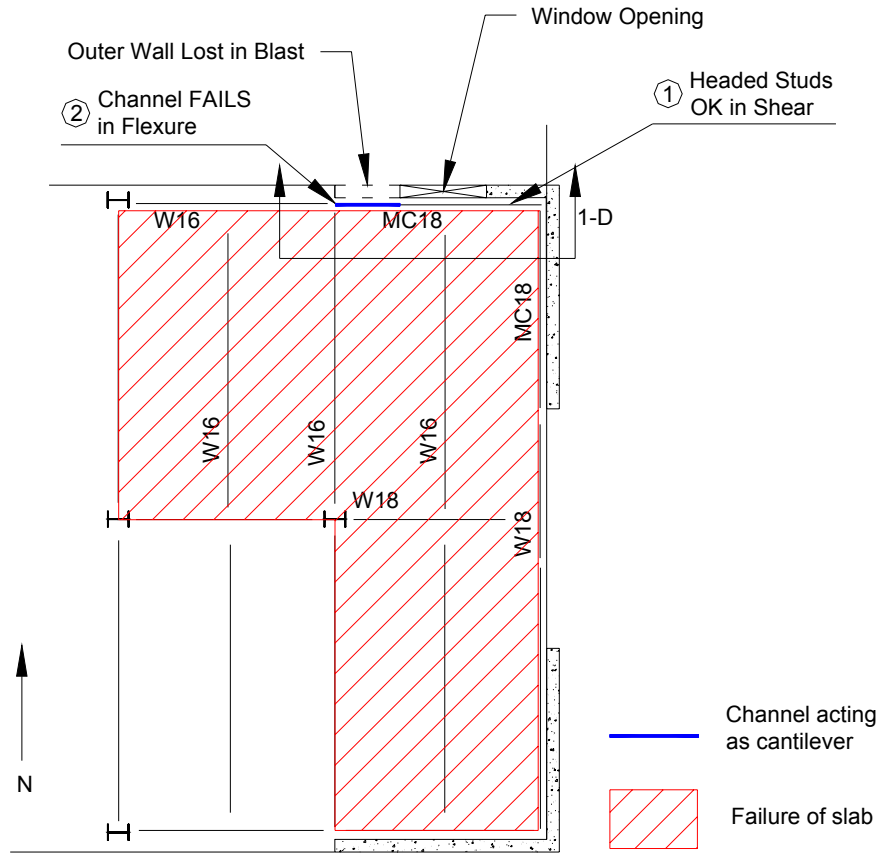


Figure 11: Potential Progressive Collapse Scenario

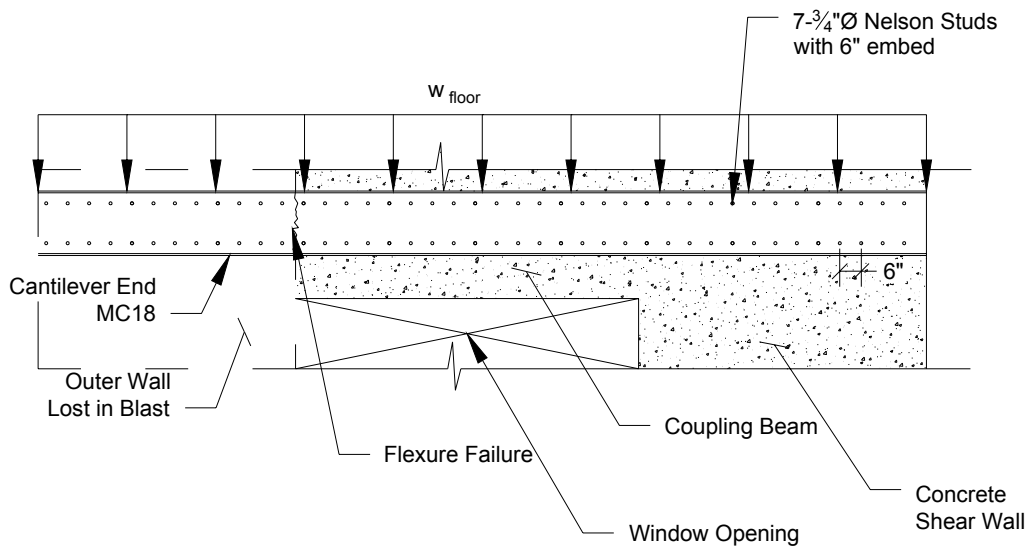


Figure 12: Elevation Section 1-D

8. Qualitative Push-Over Analysis

As a first step in analyzing the prototype shear wall under a blast load, a static push-over analysis is conducted on the wall system. This provides a qualitative estimate of the building response and determines the location where failure occurs in the wall. In order to perform the push-over analysis, the relative blast demand pressures along the height of the structure must be determined. For this study the software BlastX was used calculate the pressure distribution on the shear wall resulting from a blast (Britt et al. 2001). The use of this software is restricted and requests for the program may be directed to the US Army Engineer Research and Development Center.

8.1. Pressure Distribution Demand

A pushover analysis is conducted to determine the relative pressure distribution along the height of the structure. For a ground level explosion the pressure distribution changes from a high value at the bottom of the structure to a low value at the upper floors. This distribution can be determined using one of the many blast load tools available as discussed section 5. For this study Blast X is used. The program accounts for geometry and reflected surfaces when computing the pressure – time demands. An explosion would cause a continuous pressure distribution over the face of the structure. However, for simplicity the assumption is made that the pressure is uniform at each floor. Pressures are estimated using targets at the center of each wall component. The more target locations specified, the more detailed the pressure distribution will be. For this study the shear wall was divided into thirty regions with target locations placed in the center of each piece, as shown in Figure 13. The pressure levels and arrival times at each target vary according to its distance from the source of the explosion. The distance to the structural component increases with floor level, resulting in a decreased maximum pressure and increased arrival time. This is illustrated for one of the wall faces in Figure 14.

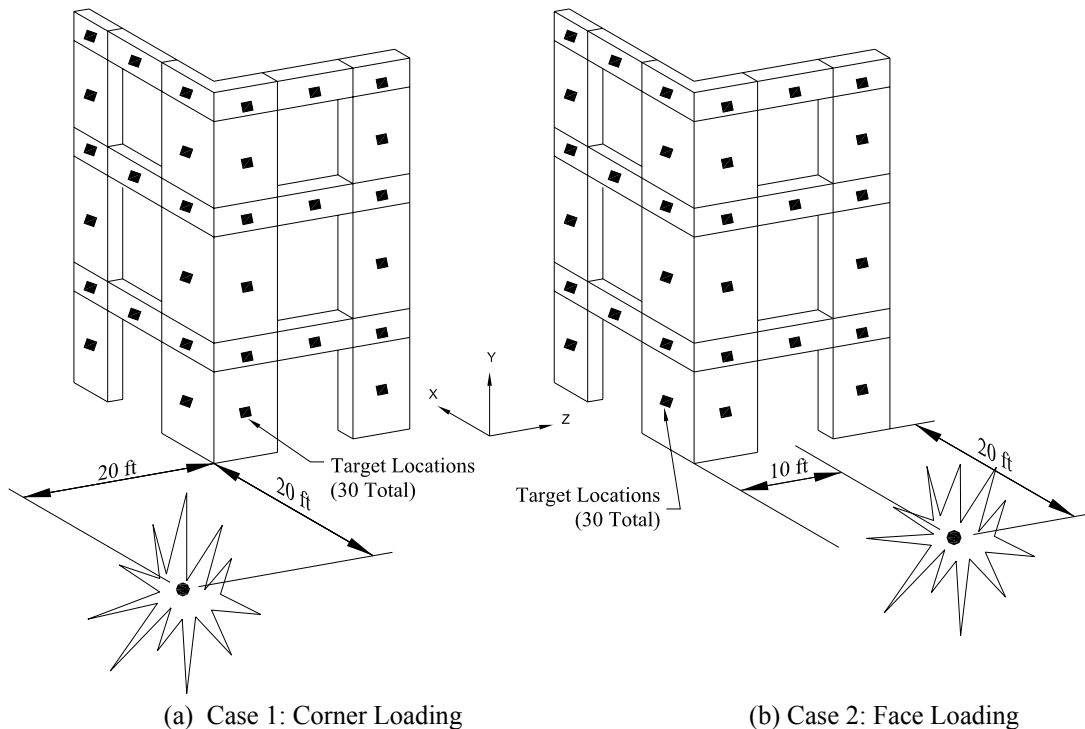


Figure 13: Blast demand scenarios

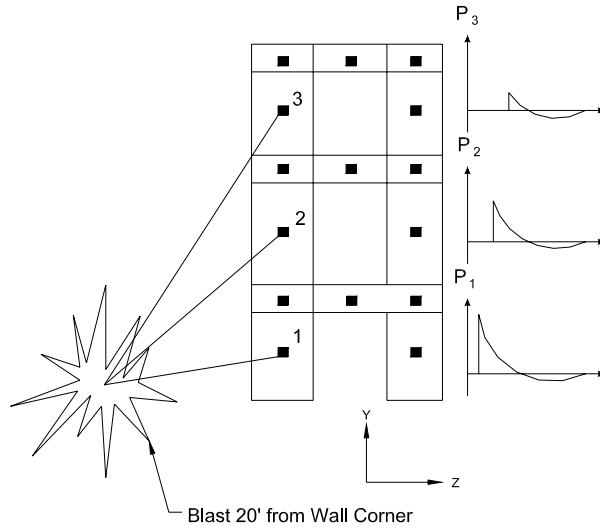
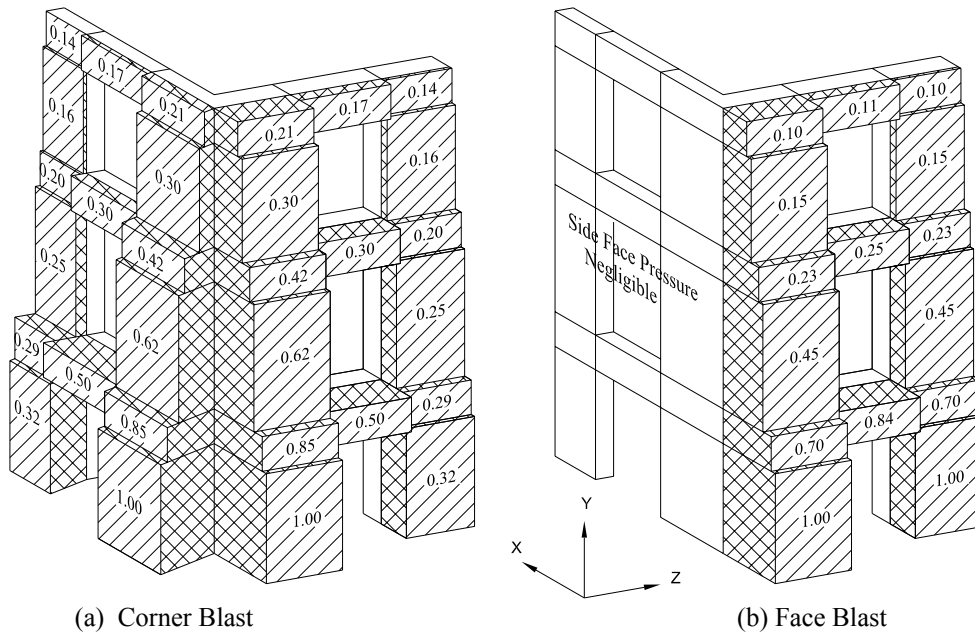


Figure 14: Reflective pressure demand on wall

When constructing a blast demand model the location of the explosion must be specified. Two scenarios were investigated, Case 1 located the bomb 20 ft from the corner of the shear wall and Case 2 located the bomb 20 ft directly in front of one wall, as show in Figure 13. The resulting pressure distributions are shown in Figure 15, with the pressure normalized to 1.0 for both cases. For the same explosive size it was determined that Case 2 had a maximum pressure magnitude that was 3 times larger than the maximum pressure of Case 1. This is because in Case 2, one wall takes the full brunt of the explosive load, while the side wall feels negligible pressure loads. Case 1 results in a symmetric loading case which would cause both walls to fail at the same time. This is a more catastrophic failure, therefore a corner blast load was chosen for the purposes of this study.



(a) Corner Blast

(b) Face Blast

Figure 15: Normalized Blast Pressures Compared

8.2. Finite Element Analysis

The blast pressure demand is used for a non-linear, static push-over analysis of the wall model. An actual blast load would act dynamically not statically on the wall, therefore results of the FE model are confirmed by dynamic response calculations later on. The finite element (FE) program Diana 8 (Witte 2002) was used to create the push-over model. When extracting the blast demand calculations from BlastX several simplifying assumptions were made. First the pressure is assumed to act uniformly over pieces of the wall as calculated in BlastX and act perpendicular to the wall's surface. Second, the delay in arrival time between the closest and furthest element is on the order of 4 ms, therefore the pressure loads are assumed to act simultaneously. Third, the structure is rigid with respect to the blast pressure; thus for simplicity the pressure does not change due to deformation of the structure. In addition the floor diaphragm is assumed to be rigid during a blast load; therefore the floor diaphragm will provide full bracing to the wall at each level. Lastly, the walls and coupling beams are taken to be axially rigid. The assumed constraints are shown as applied to the FE model in Figure 16.

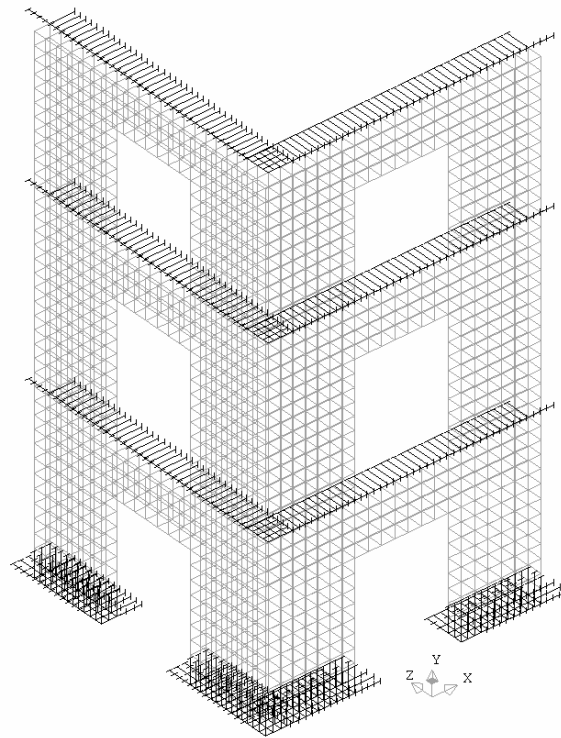


Figure 16: FE Model Constraints

The FE model was constructed using a 20 node isoparametric, solid brick element (CHX60), based on quadratic interpolation and Gauss integration. Approximately 12"x12"x12" (0.30x0.30x0.30 meters) elements were used to model the concrete illustrated in Figure 17. Diana allows for embedment of reinforcement elements into the concrete elements, creating a perfect bond with the concrete. All reinforcement was included in the model, as detailed as shown in Figure 18, including vertical, horizontal, and boundary reinforcement located in the walls and coupling beams. Plastic behavior of the concrete elements was modeled using Von Mises yielding at a stress of 3.4 ksi and work hardening was considered. Concrete cracking was governed by a tensile stress of 0.47 ksi and

compression stress of 4.0 ksi. Tension softening was brittle and constant shear retention was used. Reinforcement elements were also modeled with Von Mises yielding and work hardening, with a yield stress of 60 ksi.

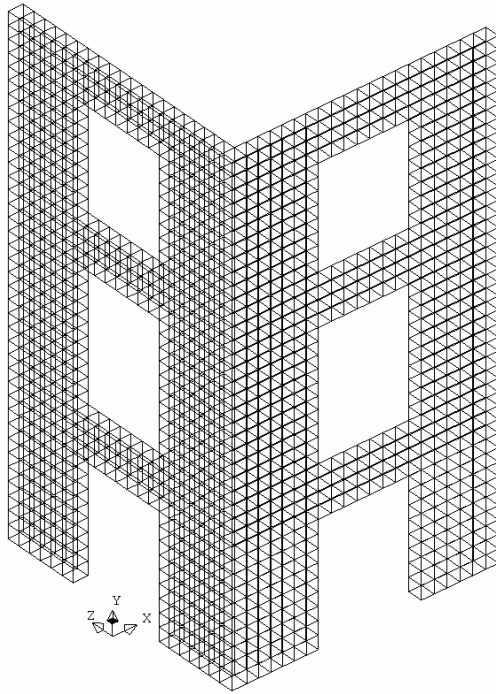
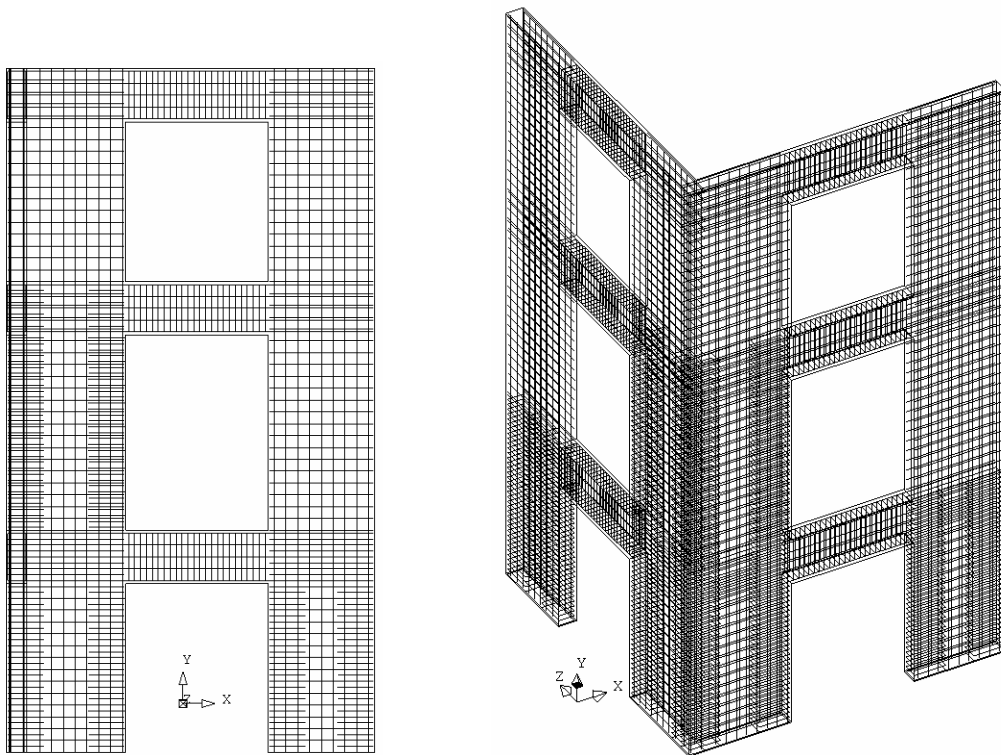


Figure 17: FE Model Concrete Mesh



Side Elevation View

Isometric View

Figure 18: FE Model Reinforcement

In the Diana FE model the wall was loaded statically under the blast demand distribution determined previously until a cross-section of the wall had formed a plastic hinge, as shown in Figure 19. Formation of a plastic hinge was assumed to initiate at the nominal flexural capacity. This was taken to be the point when the longitudinal reinforcement had reached a tensile strain of $\varepsilon_y = 0.002$, and the concrete had crushed in compression at a strain of $\varepsilon_c = -0.003$. Figure 20 shows the strain values of the outer longitudinal reinforcement, and Figure 21 shows the strain values of the concrete on the inside face of the wall.

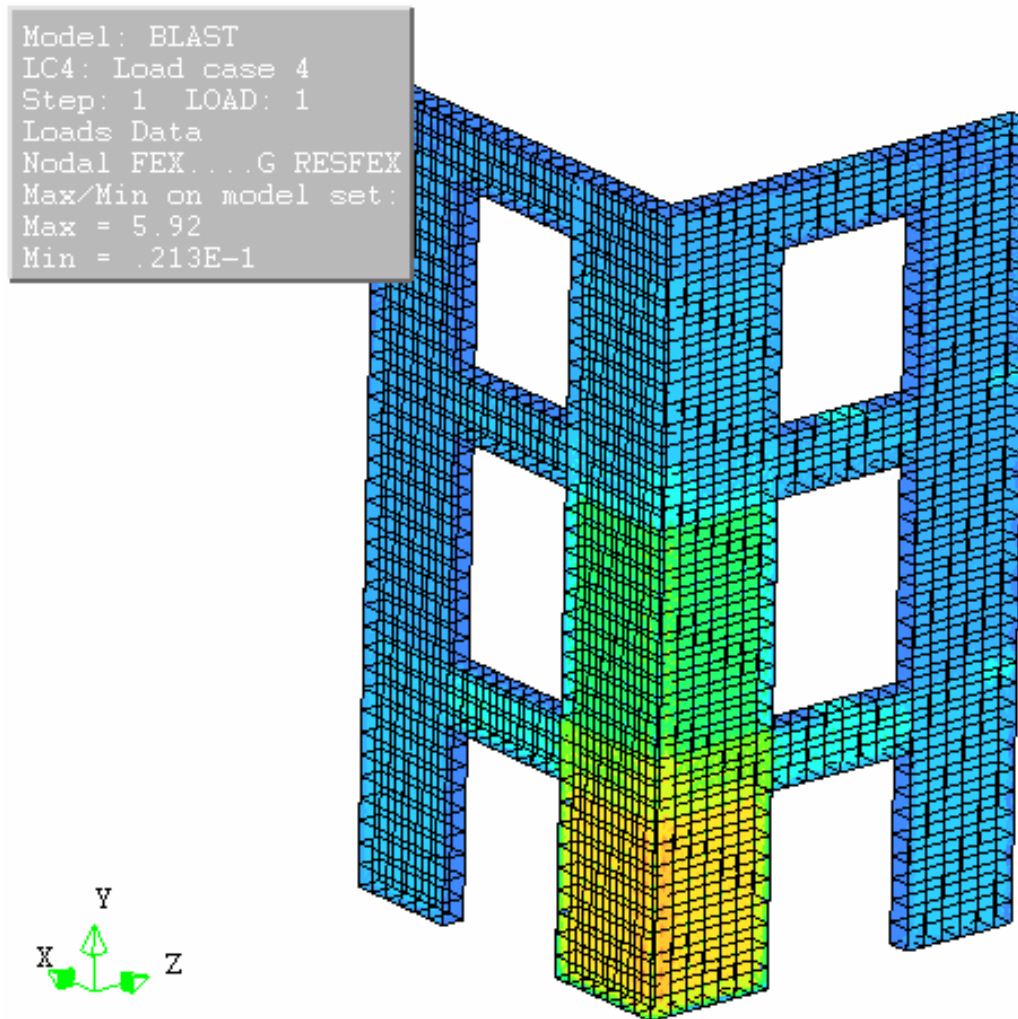


Figure 19: FE Model Applied Load Distribution

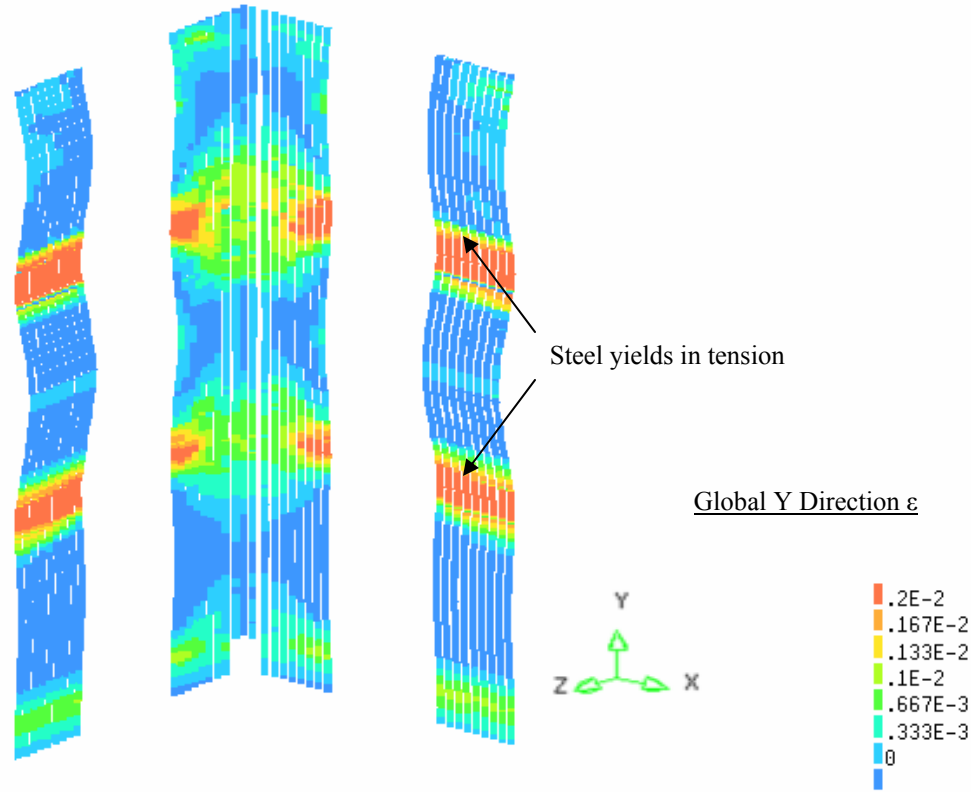


Figure 20: Strain Distribution in Longitudinal Reinforcement at Initiation of Yield

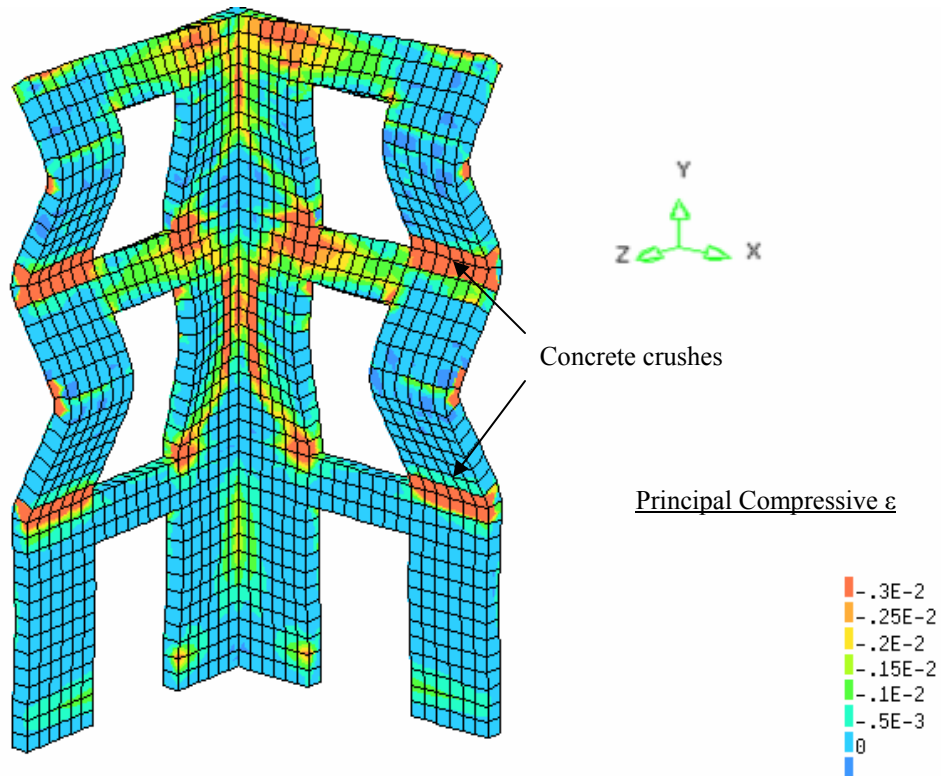


Figure 21: Principal Strain Distribution in Concrete at Crushing

8.3. Pushover Failure Modes

The window openings in the shear wall leave the outer wall sections more vulnerable to blast loads. As illustrated in the deformed shape of Figure 21 the corner portion of the shear wall is resistance to blast pressures. Under uniform loading the corner of the wall is stiffened by the two sections framing into it. While two-way action on the corner wall will lead to damage along the free edge of the wall, the remaining corner column will likely stay intact. Complete failure of this segment of the wall is unlikely under a conventional blast demand. Taking this into consideration, it was expected that failure would occur in the first floor, outer wall, where the blast pressure was highest. Figure 20 and Figure 21 however, show that the failure occurs in the 2nd floor, outer wall due to formation of hinges at the 2nd and 3rd floor levels. It can be seen that the 2nd floor, outer wall has the highest midspan displacement, as a result of its increased span and the reduction in longitudinal reinforcement up the height of the wall. Therefore the 2nd floor, outer wall will undergo the greatest curvature at each of its ends and form plastic hinges first. This portion of the wall becomes the “weak link” of the structure.

As the failure scenario illustrated in Figure 11 demonstrated, the loss of any of the outer walls will precipitate a catastrophic failure of the floor diaphragm framing into the shear wall. Therefore, when the 2nd floor outer wall fails the 3rd floor diaphragm framing into the shear wall will collapse, potentially producing a progressive collapse of the 2nd floor. It is apparent that when the 2nd floor, outer wall fails the integrity of the entire wall has been compromised. The subsequent dynamic analyses will focus on this outer portion of the wall to determine its resistance to blast loading.

9. “System” Dynamic Analysis

The FE model analyzed in Section 8.2 yielded a qualitative representation of the failure zone of the prototypical shear wall under a static load. The next analysis step is to determine the dynamic failure response of the wall. The dynamic response can be examined at different levels of complexity ranging from 3D nonlinear finite element, to multi-degree of freedom models (MDOF), to simplified single degree of freedom models (SDOF). Nonlinear dynamic FE studies are well within the capabilities of US engineering practice. Unfortunately the time and associated costs required to conduct these studies make them very impractical. As an alternative to an FE model, a less complex MDOF dynamic model can be analyzed. But this still requires time consuming numerical analysis. An analysis technique that has been used in the past by the Army Corps of Engineers and various blast analysts is the *equivalent SDOF method*. This method converts a MDOF system to a simple spring-mass SDOF system. Performing an equivalent SDOF analysis is time effective while still yielding the desired dynamic response history.

The equivalent SDOF model method equates the energies of the real and equivalent systems. In this procedure, the actual force, mass, and stiffness of the wall (F , M , and k) are transformed into an *equivalent* force, mass, and stiffness (F_e , M_e , and k_e) as shown in Figure 22. The equivalent system is chosen so that the deflection of the concentrated mass is the same as that of the midspan of the actual wall (Biggs 1964). The values of the equivalent parameters, as derived by dynamic theory, are shown in Eqns. 1-3 (Chopra 1995). The definition of the assumed shape function, $\phi(x)$, will be described in Section 9.2.

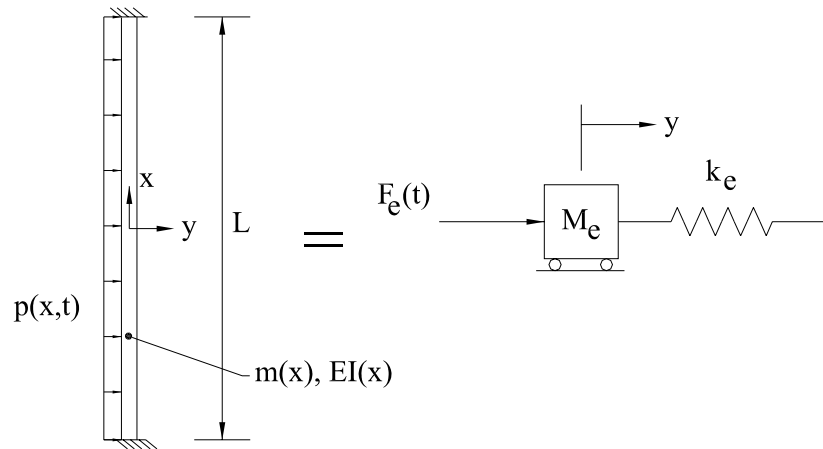


Figure 22: Equivalent SDOF System

$$M_e = \int_0^L m(x) [\phi(x)]^2 dx \quad \text{Eqn. 1}$$

$$k_e = \int_0^L EI(x) [\phi''(x)]^2 dx \quad \text{Eqn. 2}$$

$$F_e(t) = \int_0^L p(x,t) \phi(x) dx \quad \text{Eqn. 3}$$

$$M_e y'' + k_e y = F_e(t) \quad \text{Eqn. 4}$$

The equation of motion (EQM) that describes the behavior of the equivalent SDOF system is written in Eqn. 4. According to Eqn. 4 the EQM of the equivalent SDOF model can be solved only when the stiffness of the structure has been calculated. The full dynamic response of the wall will be governed by stages of inelastic behavior during which the stiffness of the wall will change. Therefore before the solution of the dynamic problem can be discussed it is necessary to quantify the inelastic behavior of the wall. This requires calculation of the flexural and polar moments of inertia. The moment-curvature behavior of the wall sections are then derived to determine when plastic hinges form along the wall. The stages of inelastic behavior are then delineated by calculating critical displacements, i.e. the midspan displacement of the wall when each hinge develops. This information will then be used to construct a static resistance curve which will describe the inelastic behavior of the wall for solution of the dynamic EQM. The steps of the analysis methodology are presented in detail in this section.

9.1. Structural Resistance

It was determined from the static push-over analysis that the wall fails first at the 2nd floor, outer wall. As described earlier, assumptions were made about the rigidity of the structure, namely, the floor diaphragm is assumed to prevent in-plane translation of the wall, and the walls and coupling beams are taken to be axially rigid. These assumptions are used to represent the symmetric wall system as shown in Figure 23. The degrees of freedom (DOF) reduce to three rotations at each joint. These rotations are symbolized as θ_{xn} , θ_{yn} , θ_{zn} , where n represents the joint number.

Applying the equivalent SDOF analysis technique to the prototypical shear wall requires critical thinking to determine what assumptions can be made and how the model should be constructed. As determined previously the failure occurs in the 2nd floor, outer wall, therefore the dynamic analysis will focus at this location. Two scenarios will be considered. The first regards the wall as a *system*, as shown in Figure 23, taking into account the flexural resistance of the adjoining walls. The second scenario considers the wall acting as a *component*, i.e. the end conditions of the wall are assumed to be fixed-fixed therefore the wall acts alone. The dynamic response of the wall acting as a system will be considered in this chapter. Chapter 10 will consider the wall acting as a component.

9.1.1. Stiffness Properties

In order to construct an equivalent SDOF model for the wall system the stiffness of the wall must be determined. This is done by first calculating the moment of inertia of each section of the idealized wall shown in Figure 23 and detailed in Figure 24. Transverse reinforcement provides minimal confinement for out-of-plane flexure therefore its contribution was neglected. According to the theory of concrete cracking, the actual moment of inertia will vary along the span of the wall depending on its deflection value. For blast design use of fully cracked, transformed sections provides a conservative estimate of the moment of inertia (Biggs 1964; Smith and Hetherington 1994). This assumption will be verified in the following sections. When computing the modular ratio E_s was taken to be 29,000 ksi and E_c was taken as 3605 ksi. In order to account for torsional stiffness of the framing coupling beams,

the polar moment of inertia was calculated for each section using the equation $J = \frac{bh(h^2 + b^2)}{12}$, where b = the width of the section and h = the height of the section (Gere and Timoshenko 1997). The fully cracked transformed and polar moment of inertias for each wall cross section are presented in Table 1.

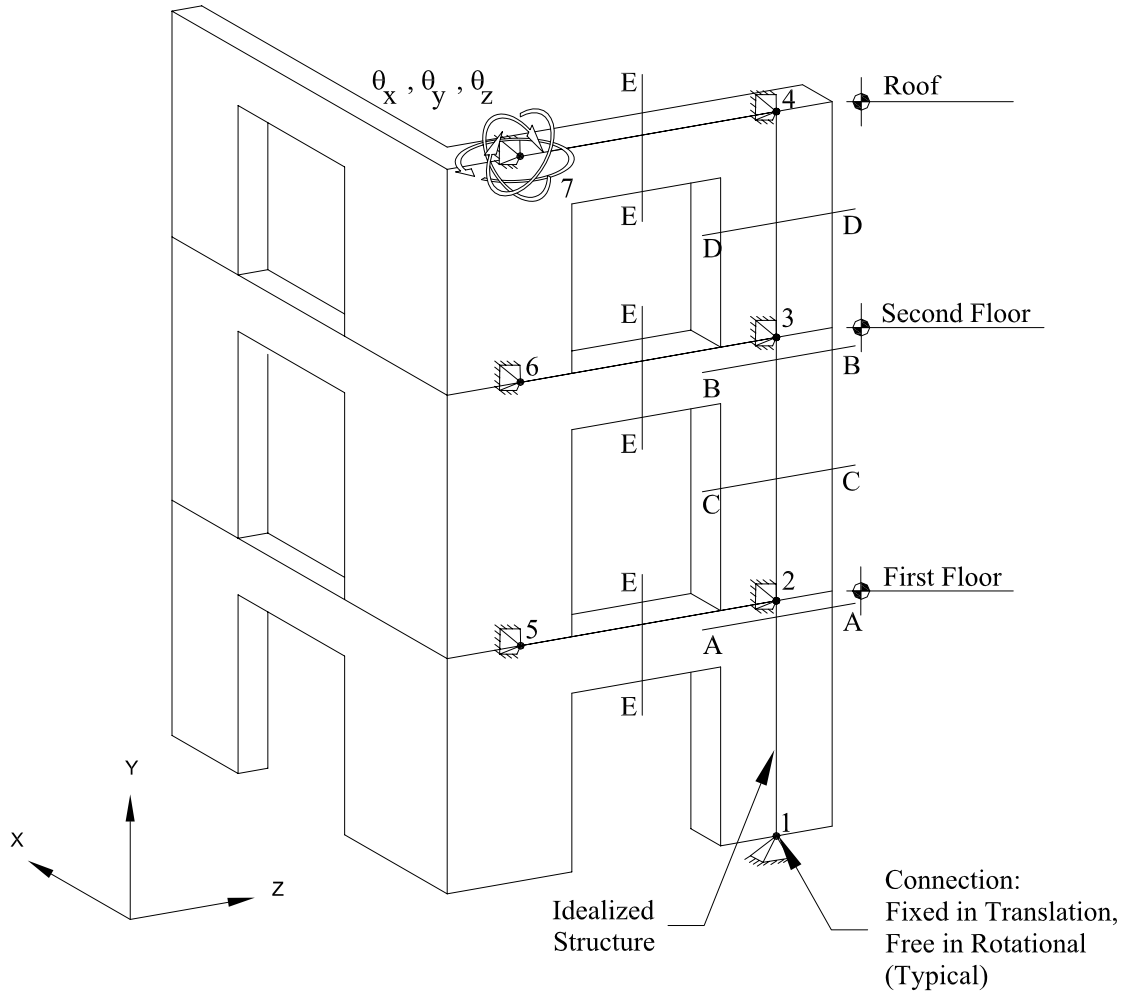


Figure 23: Wall System

Table 1: Moment of inertias of wall sections			
	$I_{z'z'} \text{ (in}^4\text{)}$	$I_{y'y'} \text{ (in}^4\text{)}$	$J \text{ (in}^4\text{)}$
Section A-A	5752	109082	4.5192×10^5
Section B-B	3766	91197	4.5192×10^5
Section C-C	4786	101088	4.5192×10^5
Section D-D	2981	82208	4.5192×10^5
Section E-E	18992	1982	6.2664×10^4

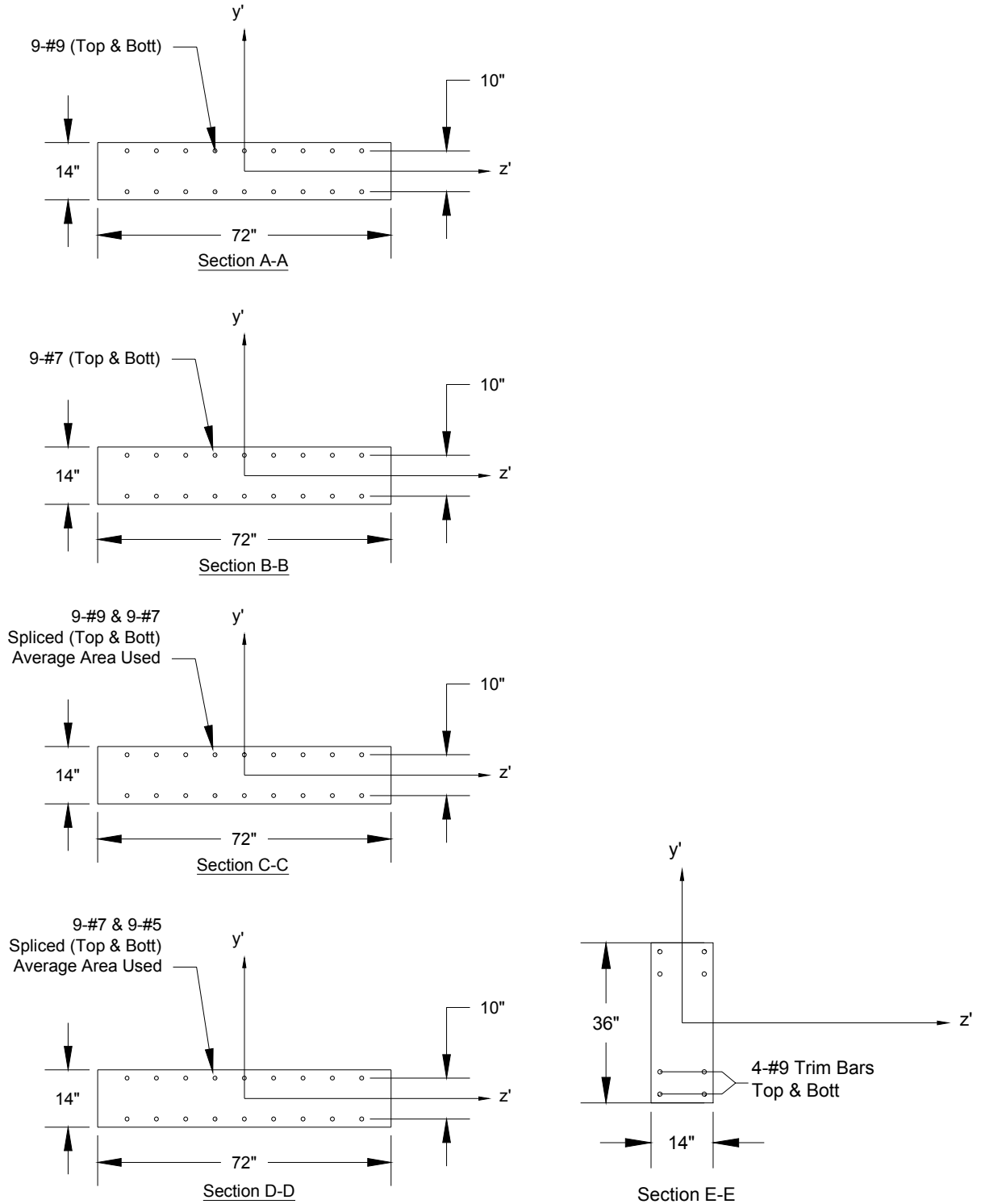


Figure 24: Wall Cross-Sections (Transverse Reinforcement Not Illustrated)

9.1.2. Moment-Curvature

To determine the ability of a structure to withstand a blast, the inelastic capacity of each element must be assessed. The level of inelastic capacity is computed in terms of ductility defined as the ratio of the ultimate deformation to

the deformation at first yield. The ductility of ordinary reinforced concrete walls subject to lateral loads are typically on the order of 4.5 (International Code Council 2003). However, since blast loading occurs out-of-plane of the wall the actual level of inelastic resistance must be computed for the system and conditions in question. This is conventionally determined according to the moment-curvature response of the section. The points of concrete cracking, steel yield, concrete crushing, and ultimate capacity can be correlated to points on a moment-curvature graph.

9.1.2.1. Fiber Element Analysis

Developing a fiber-element model is an accurate method for finding the moment-curvature graph of a cross-section. In a fiber-element model a structure is represented by numerous cross-sectional slices along its length and each cross-section is subdivided into horizontal fibers, as shown in Figure 25. Each fiber is governed by a nonlinear, longitudinal stress-strain relationship dependent on the material type it represents (i.e. steel or concrete). The model is loaded by stepping the strain in each fiber increases according to a linear strain profile, as shown in Figure 25. The axial forces are equated to the axial force present in the cross-section and the resulting moment is computed. The corresponding curvature is the gradient of the strain profile.

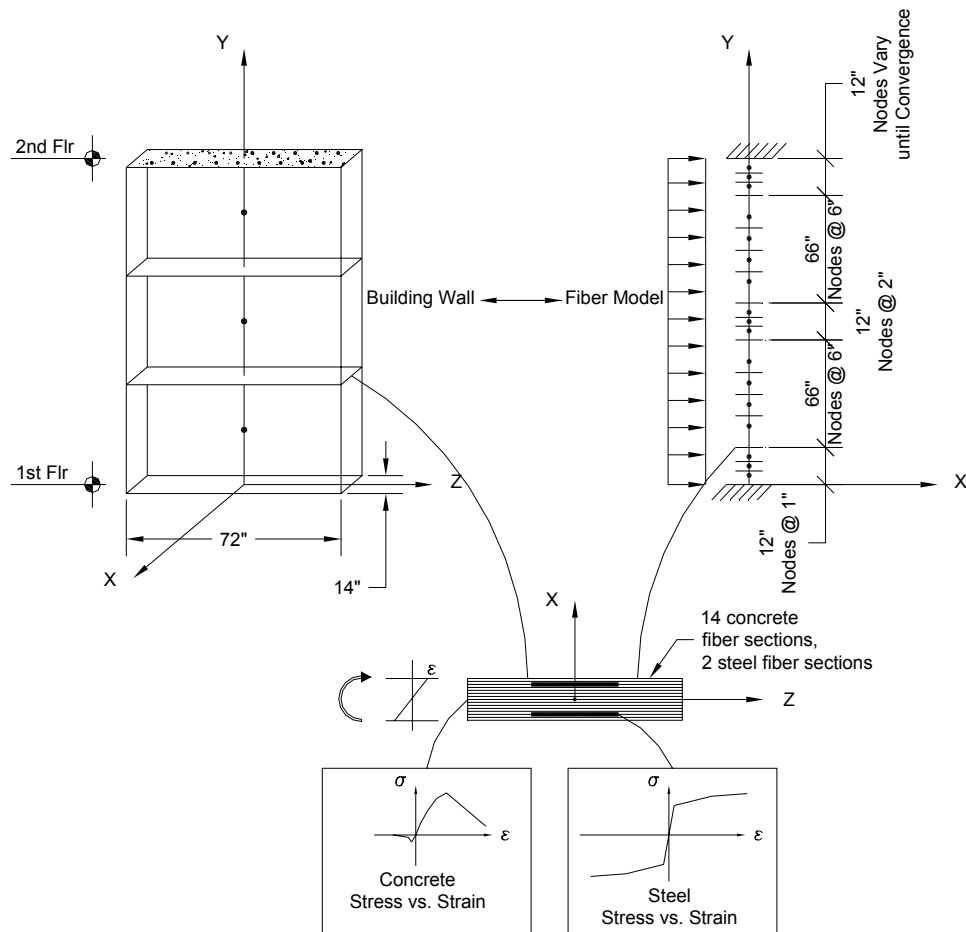


Figure 25: Fiber Analysis Details

For this analysis the program DRAIN-2DX (Prakash et al. 1993) was used to construct a fiber-element model. An inelastic fiber element was used (element 15) accounting for strain hardening, yield of steel, and cracking and crushing of concrete. The element model is of “distributed plasticity” type, which accounts for the spread of inelastic behavior along the member length. This is opposed to a “lumped plasticity” model which uses the concept of zero-length “plastic hinges”. Shear behavior is assumed to be elastic. Uniform loading is represented as point loads placed at nodes along the length of the member. The ends of the wall were taken to be completely fixed. The material properties as specified for steel or concrete fibers are shown in Figure 26 & Figure 27.

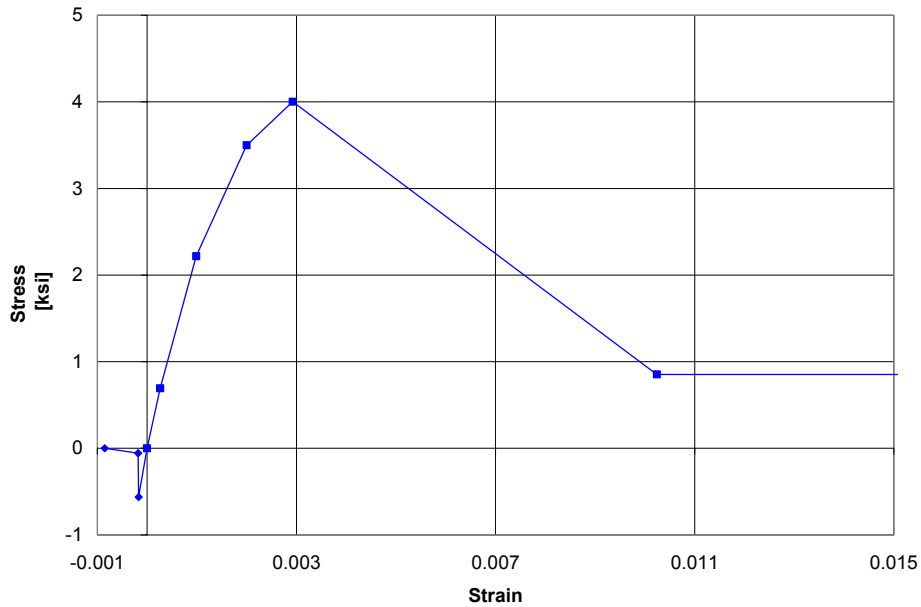


Figure 26: Concrete Constitutive Properties

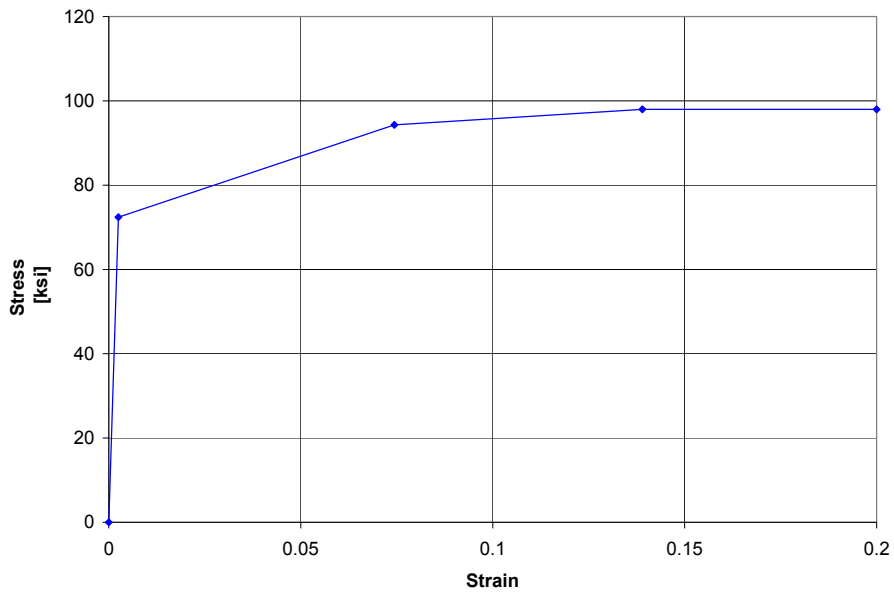


Figure 27: Steel Constitutive Properties

The fiber model for the wall is based on the as-built reinforcement details. The concrete was assumed to be unconfined, as the boundary elements of the wall were not designed to provide confinement. The wall reinforcement is reduced along the height of the structure as the shear demand decreases. The longitudinal reinforcement in the second floor wall decreases from #9 to #7 bars as shown in Figure 10. It was assumed that the #9 bars are fully developed and extend 2/3 up the height of the second floor wall. The resulting moment-curvature graphs for Sections A-A and B-B are shown in Figure 28. Section C-C was assumed to behave as Section A-A with #9 reinforcement instead of #9 and #7 spliced. Section D-D was not analyzed because it was determined that failure will be localized at the top and bottom of the 2nd floor wall, therefore the 3rd floor cross-section will not affect subsequent analysis of the progression of failure.

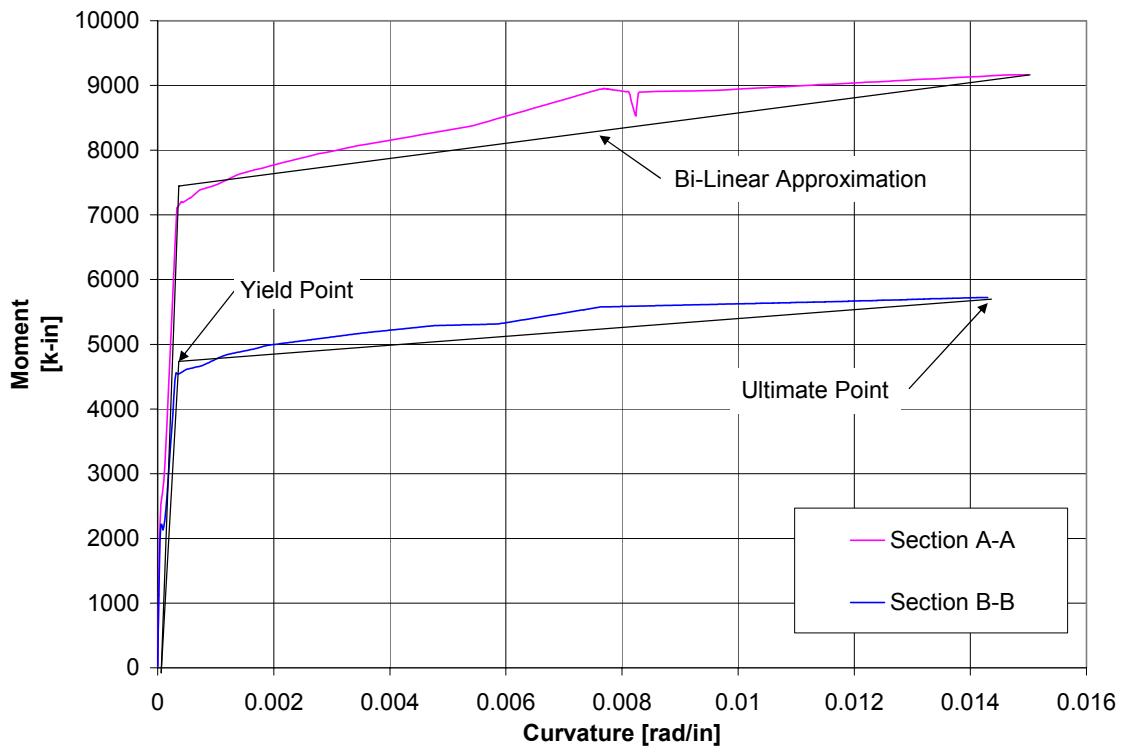


Figure 28: Moment Curvature Response of Wall

The stages of inelastic behavior are apparent by the shape of the moment-curvature graphs. Once cracking has occurred the moment-curvature relationship softens slightly and remains linear until the onset of yield. The major change in slope on the graph occurs when the *yield* point of tensile steel is reached, at a strain of 0.002, and the curvature greatly increases while the moment stays almost constant. After yield the internal lever arm of the section will increase, causes the moment to slowly rise until the wall reaches its ultimate strength. The *ultimate* capacity is assumed to be controlled by reinforcement fracture. Based on ASTM A706 mill certification reports, an ultimate strain of 0.140 is used.

The moment-curvature response is simplified to a bi-linear model for all subsequent analyses. These approximated values are tabulated in Table 2 and plotted in Figure 28. The yield and ultimate points determined in the DRAIN

analysis will determine when plastic hinges form and fail, as described subsequently.

	Section A-A		Section B-B	
	Curvature (rad/in)	Moment (k-in)	Curvature (rad/in)	Moment (k-in)
Yield Point	0.000367	7340	0.000271	5410
Failure Point	0.0149	9167	0.0143	5720

Table 2: Moment-Curvature Response

9.1.2.2. Section Analysis

In the practice of engineering it may not be practical to develop a fiber element model to determine a moment-curvature graph. In such cases a simplified calculation may be appropriate to estimate the moment-curvature behavior of a section (Park and Paulay 1975). Points on the graph can be calculated by a section analysis of the strain profile at various stages of inelastic behavior. The points are then connected linearly producing a simplified moment-curvature graph. Figure 29 shows the results of a section analysis for cross-sections A-A and B-B up to the nominal moment capacity of the sections. Three points are calculated, those of concrete cracking ($\epsilon_c = 0.0001$), yielding of the steel ($\epsilon_s = 0.002$), and crushing of the concrete ($\epsilon_c = -0.003$). In comparison, the moment-curvature graphs calculated by DRAIN are also shown on the graph. It can be seen that the hand calculation is a very close approximation to the DRAIN results. To determine the ultimate moment and curvature point, as was done in the DRAIN calculation, a section analysis could be performed based upon the ultimate steel strength at the point of steel fracture.

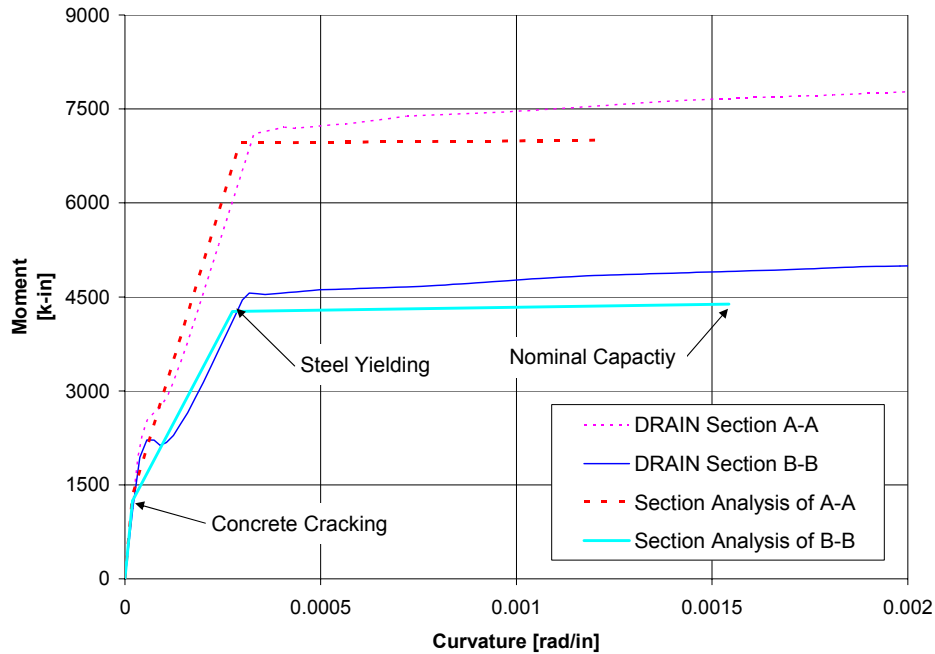


Figure 29: Comparison of Moment-Curvature Graphs at Nominal Capacity

9.1.3. Critical Displacements

With the inelastic behavior of the wall sections known the progression of damage in the wall can be determined. This is assessed by determining when and where plastic hinges form in the wall system. A *plastic hinge* will form when a section reaches its yield moment. Plastic theory predicts that under a large enough load, three hinges will form in succession in the 2nd floor wall before failure; a hinge at both ends and one in the middle. The magnitude of midspan deflections at the time each hinge forms are known as the *critical displacements*. These displacements are the benchmark to describe the transition of the wall through various stages of inelastic behavior.

When a plastic hinge forms, the rules of elementary beam theory describing deflection no longer apply. Therefore several assumptions will be made to simplify the deflection calculations during plastic behavior. The first assumption is that when a plastic hinge forms it will hold a constant moment, but as the load is increased it will hold no additional moment, essentially acting as a pin during the next stage of loading. Also, the formation of a hinge causes a local spike in curvature which results in additional plastic hinge rotation. This additional rotation is accounted for in the final stage of deflection when it has the largest effect.

To calculate the critical displacements the following procedure is used. First, the wall system is loaded statically according to the blast pressure distribution in Figure 15 (a). As shown in Figure 30, the load is incremented until a cross-section along the height of the wall reaches its yield moment, M_y , forming a plastic hinge. The first hinge forms at the top of the 2nd floor wall (Section B-B) when $M_B = M_{yB}$. The blast pressure is incremented again until the 1st floor cross-section (Section A-A) forms a plastic hinge at $M_A = M_{yA}$. The pressure then increases a third time until the last hinge formed in the middle of the 2nd floor wall (Section C-C) at $M_C = M_{yC}$. Note that the three stages of loading do not act independent of one another but rather they are additive.

The critical displacements, y_{el} , are calculated as the midspan deflection of the 2nd floor wall when each hinge forms. These deflections can be calculated by modeling the wall as a series of structural subassemblies as illustrated in Figure 30. This analysis can be conducted in any standard structural analysis program. For this analysis the program MASTAN (Ziemian and McGuire 2000) was used. The moments of inertia tabulated in Table 1 are used to define the stiffness of the members in the model. The pressure load varies up the height of the wall as determined by BlastX. P-delta effects are not included because the gravity floor loads acting axially on the wall are small enough in magnitude that the second-order moment at the maximum wall displacement is less than 5% of the yield moment. The displacement values calculated in when the three hinges form are found to be 0.341 in, 0.426 in, and 0.994 in, respectively. The critical displacements are tabulated in Table 3.

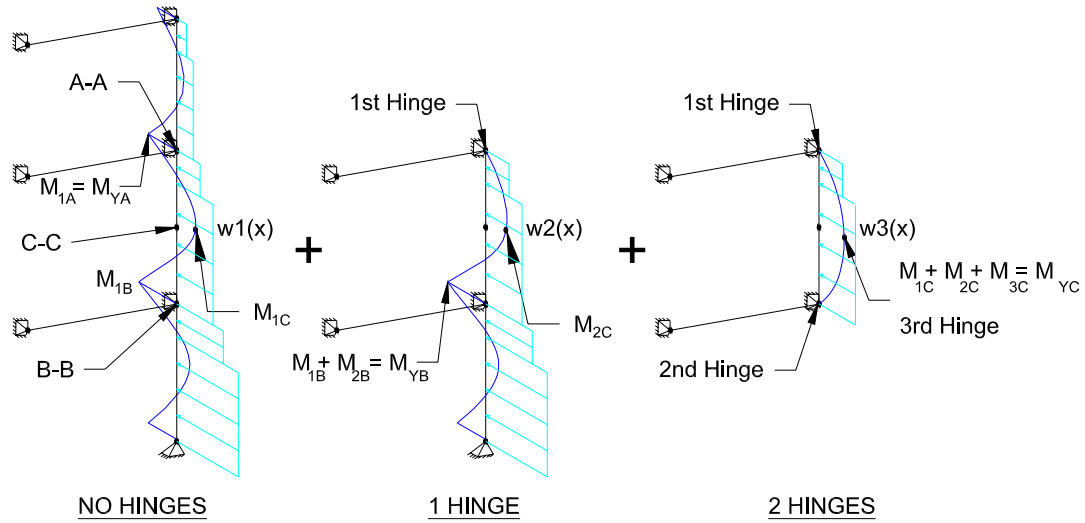


Figure 30: Formation of Plastic Hinges

	Displacement at midspan of wall (in)
y_{el1}	0.341
y_{el2}	0.426
y_{el3}	0.994
$y_{el,ultimate}$	1.340

Table 3: Critical Displacements

9.1.3.1. Ultimate Rotation Capacity

Having determined the critical displacements for the first three stages of inelastic behavior, one last critical displacement remains to be calculated. That is the displacement at failure. The wall will fail when one of the plastic hinges reaches its *ultimate rotation*, θ_u .

Figure 31 shows a portion of a concrete structure loaded uniformly to the point of yield and ultimate moments. The corresponding curvature for the two cases is shown for comparison. When M_y is reached at a cross-section a plastic deformation initiates, i.e., a plastic hinge forms, and the localized curvature increases as the plastic hinge rotates. As M_y increases to M_u , the inelastic curvature spreads over a length of the member, creating a *plastic hinge length*, l_p . The area under the curvature diagram is equal to the rotation at that section. Therefore the spike in curvature creates a localized increase in rotation at the plastic hinge, causing the maximum deflection in the member to increase also.

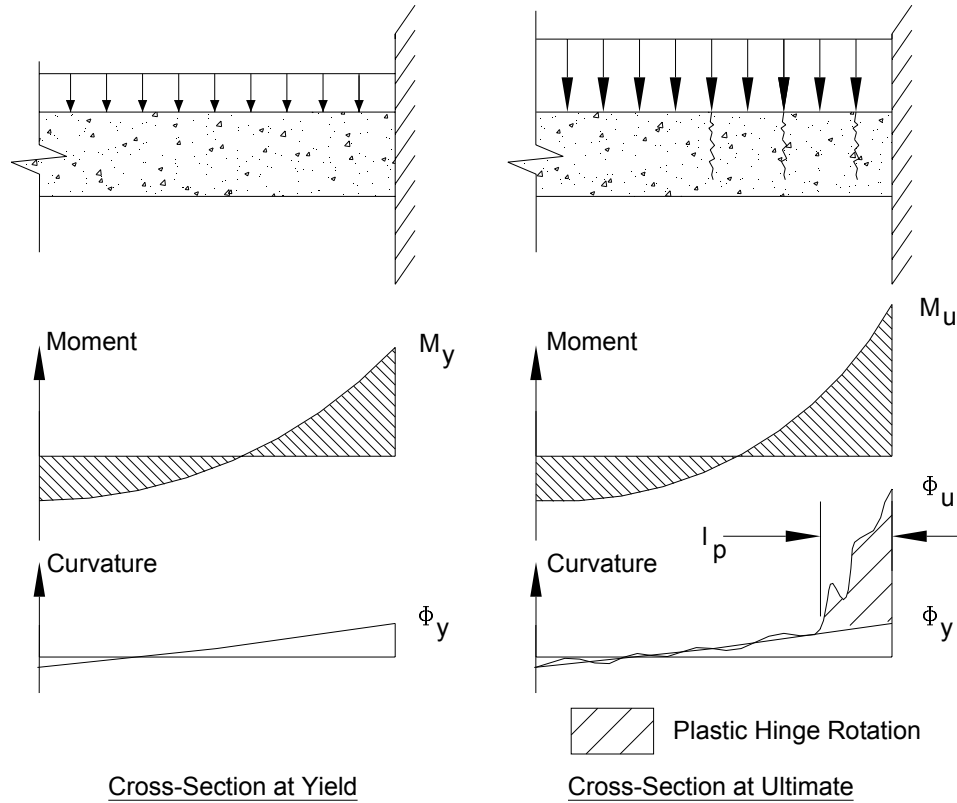


Figure 31: Formation of Plastic Hinge

The ultimate rotation value, θ_u , is calculated as the area under the curvature diagram when the curvature has reached ultimate, ϕ_u . As shown in Figure 31, the shape of the curvature distribution at ultimate capacity is irregularly shaped. The nature of crack propagation makes it hard to predict the value of the plastic hinge length, l_p . Some empirical formulas exist which try to predict l_p , but most pertain to highly confined concrete in seismic zones (Priestly et al. 1996). Baker's Equation (Institution of Civil Engineers 1964) has been widely used to find l_p for unconfined beam sections, but the equation was derived empirically from tests that did not include wall sections. For this analysis, it was determined that Baker's Equation overestimated the ductility of the wall and was therefore not used. Some researchers specify a rotation value to designate the point of hinge failure. For example, the US Army Corp of Engineers assumes that a rotation of two degrees or more will cause the compression face of a concrete beam to crush (U.S. Army Corp of Engineers 1998). But once again, this is usually applied for sections with high confinement and high ductility. These methods are summarized in Table 4.

<p>Columns in Seismic Zones (Priestly et al. 1996)</p>	$l_p = 0.08L + 0.15f_{ye}d_{bl} \geq 0.3f_{ye}d_{bl}$ <p>where, L = distance from the critical section to the point of contraflexure d_{bl} = diameter of longitudinal reinforcement</p>
---	--

	f_{ye} = characteristic yield strength
Unconfined Beams (Baker (Institution of Civil Engineers 1964))	$l_p = k_1 k_2 k_3 \left(\frac{z}{d}\right)^{1/4} d$
	<p>where,</p> <p>$k_1 = 0.7$ for mild steel</p> <p>$k_2 = (1+0.5*P/P_u)$</p> <p>$k_3 = 0.6$ when $f'_c = 5100$ psi or 0.9 when $f'_c = 1700$ psi</p> <p>P_u = ultimate capacity of member for axial load</p> <p>P = ultimate axial load for member</p> <p>d = effective depth of member</p>
U.S. Army Corps of Engineers	$\theta_u = 2^\circ$

Table 4: Plastic Hinge Length Estimates

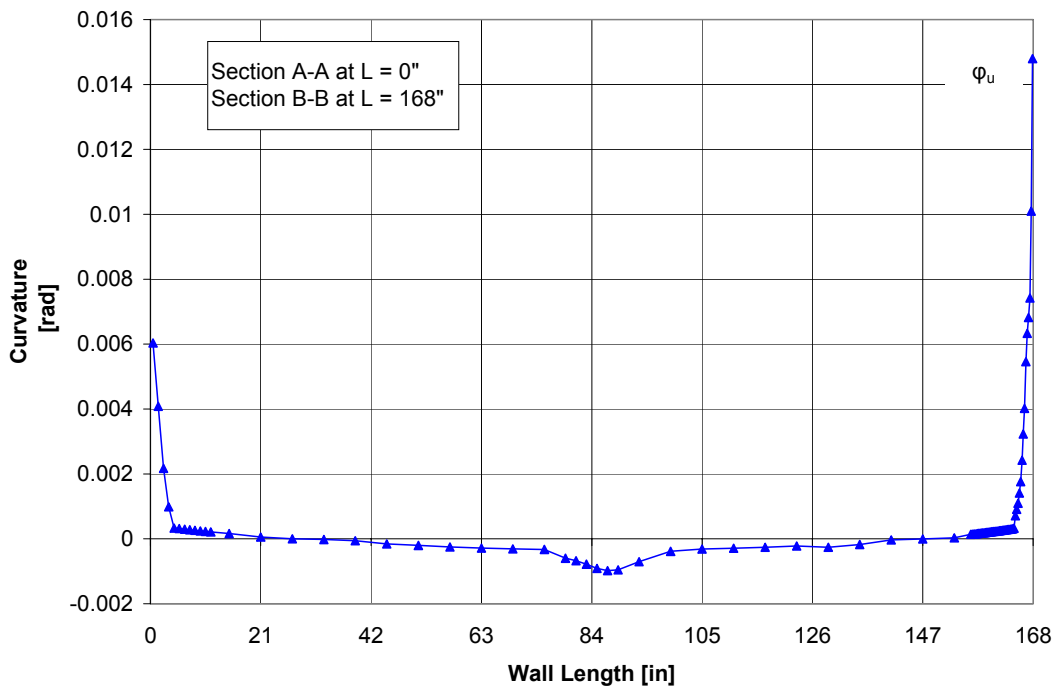


Figure 32: Curvature Along Wall at Ultimate Load Level for 2nd Floor, Outer Wall

In order to calculate the ultimate rotation value we refer back to the fiber element model developed in Section 9.1.2.1. The fiber-element model yields the curvature along the length of the wall for a given uniform load. The curvature profile at ultimate is graphed in Figure 32. It can be seen that the curvature increases to $\phi_u = 0.0148 \text{ rad/in}$ at $L = 168''$, therefore the plastic hinge at Section B-B will be the location of failure. Figure 33 shows a close-up view of the ultimate curvature at Section B-B. In order to give an accurate representation of the ultimate curvature profile, the nodes from $L = 156''$ to $L = 168''$ were discretized at various densities until the ultimate rotation value converged. Figure 34 shows the ultimate rotation plotted vs. the number of elements/inch. The model converges at a discretization of $1/4''$ or 4 elements / inch. The curvature profile

approximates the plastic hinge length to be 4". Summing the area under the curvature diagram, the ultimate rotation at Section B-B was calculated to be $\theta_u = 0.90$ degrees or 0.016 radians.

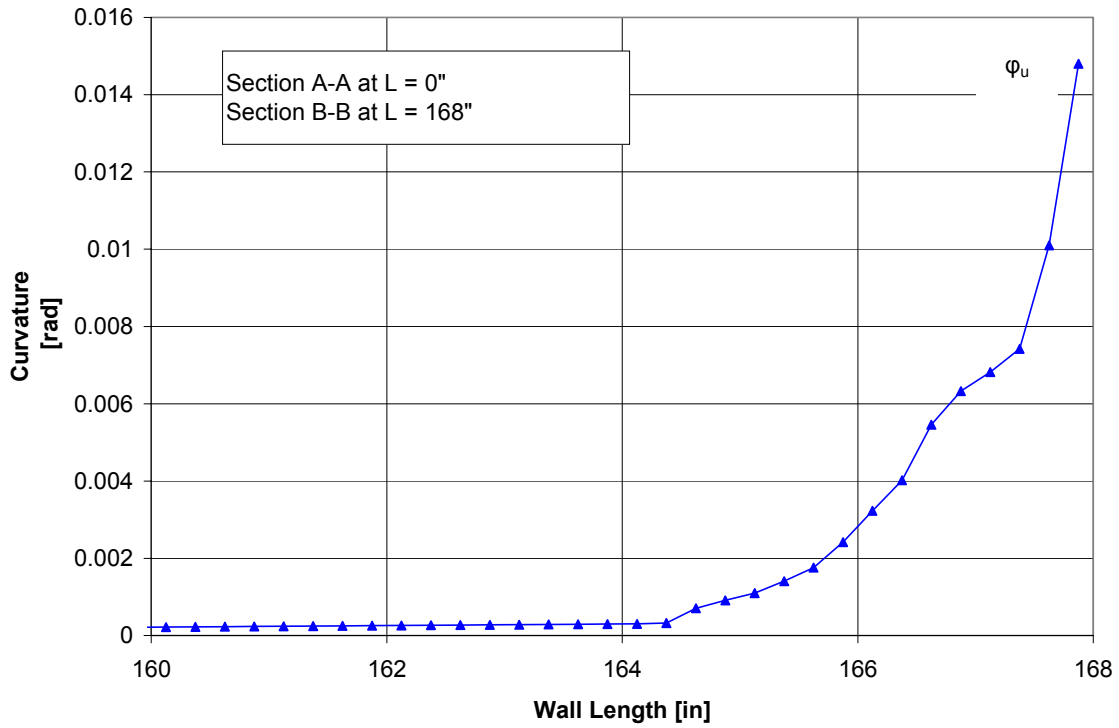


Figure 33: Curvature Along Wall in Plastic Hinge Region

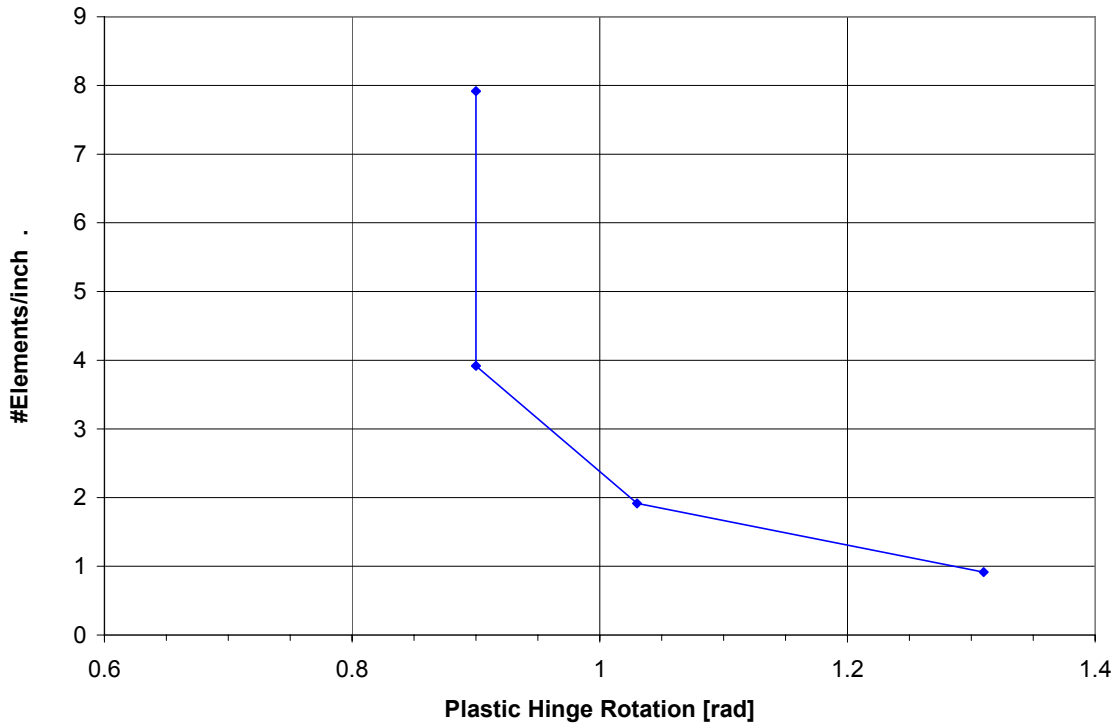


Figure 34: Convergence of Plastic Hinge Rotation for Increasing Discretization

9.1.3.2. Displacement at Failure

Assuming that the elastic deformation of the wall is small compared to the plastic, the critical displacement value at failure can now be determined. The displaced shape after three hinges have formed is assumed to be that shown in Figure 35. As derived from the DRAIN model, the wall will fail when Section B-B reaches a rotation of $\theta_u = 0.016 \text{ rad/in}$. According to similar triangles and assuming that $\tan(\theta) \approx \theta$, the critical displacement at failure is defined as $y_{el,u} = \theta_u * \frac{L}{2}$. Therefore $y_{el,u} = 1.340''$. The ductility of the wall is equal to

$\mu = \frac{\Delta_u}{\Delta_y} = \frac{1.340}{0.341} = 3.93$. The critical displacement values at each inelastic stage are summarized in Table 3.

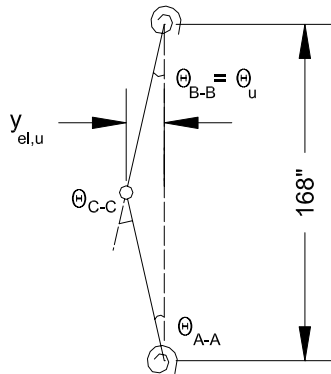


Figure 35: Plastic Hinge Reaches Ultimate Curvature

9.2. Nonlinear Dynamic Response

Section 9.1 outlined a procedure to determine the inelastic behavior of the wall under a static pushover. A moment-curvature analysis of the wall system sections revealed when plastic hinges formed and failed. The locations of plastic hinges were also determined in a structural analysis model of the wall system and the critical displacements corresponding to hinge formation were calculated. With this information the equivalent SDOF model can now be analyzed under a dynamic blast load.

9.2.1. Equivalent SDOF Model

As shown in Figure 22 an equivalent SDOF model equates the actual force, mass, and stiffness of the wall (F , M , and k) to an *equivalent* force, mass, and stiffness (F_e , M_e , and k_e). The SDOF system is developed to have the same deflection as the midspan of the actual system. The equivalent parameters are defined in Eqns. 1-3. The equivalent system is equated to the real system using *shape functions*, $\varphi(x)$, derived directly from the displaced shape of the real wall, $v(x)$. The assumed shape function must satisfy two criteria. First, the shape must be the same as that resulting from the static deflection under application of the dynamic load. The second criterion is that the magnitude of the displaced shape shall be normalized to unity at the midpoint (Biggs 1964). For a given failure stage the shape

function is calculated by the equation $\varphi(x) = \frac{v(x)}{v_{mid}}$, where v_{mid} is equal to the displacement at midspan.

As shown in Figure 36 the 2nd floor wall will go through four stages of inelastic behavior before failure, therefore four shape functions are required to capture the behavior. The equation for the displaced shape of the real wall can be directly computed using theoretical principals of structural analysis. While this method is very accurate the time required is prohibitive for this purpose. As an alternative the shape function can be approximated by creating a computer model of the wall in a standard structural analysis program. The MASTAN model developed in Section 9.1 can be used to calculate the displacement equations, $v(x)$, of the 2nd floor wall during the first three stages of inelastic behavior. As shown in Figure 30, the moment values at the ends and middle of the 2nd floor wall are computed by the analysis program. Since the loading is a uniform load the equation of moment as a function of the wall length, $M(x)$, can be calculated by fitting a parabolic curve to these three points. Applying the elementary beam theory the equation for displacement, $v(x)$, can be derived using Eqn. 5 (Ugural and Fenster 1995).

$$EIv(x) = \int_0^x dx \int_0^x M(x) dx + c_1x + c_2 \quad \text{Eqn. 5}$$

The constants c_1 and c_2 correspond to the homogeneous solution of the differential equations and are evaluated from the boundary conditions. The constant $\frac{c_1}{EI}$ is equal to the value of rotation, θ , at Section A-A (the wall base of the

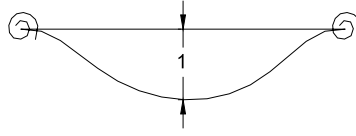
2nd floor, outer wall). The constant $\frac{c_2}{EI}$ is equal to the value of the displacement, v , at Section A-A, which will always be assumed to equal zero. The moment and displacement equations derived from the MASTAN model are shown in Table 5. The equation for the displaced shape of Stage 4 can be calculated directly because the shape is assumed to be bi-linear with maximum displacement at the center as shown in Figure 35. The assumed shape

functions for Stages 1-4 are normalized using the equation $\varphi(x) = \frac{v(x)}{v_{mid}}$, and the results are shown in Figure 36.

	M(x)	v(x)
Stage 1	$1.27x^2 - 217x + 6152$	$6.12 * 10^{-9} x^4 - 2.10 * 10^{-6} x^3 + 1.78 * 10^{-4} x^2 + 3.48 * 10^{-4} x$
Stage 2	$0.18x^2 - 37.9x + 1189$	$8.86 * 10^{-10} x^4 - 3.66 * 10^{-7} x^3 + 3.44 * 10^{-5} x^2 + 3.48 * 10^{-4} x$
Stage 3	$0.49x^2 - 82.3x$	$2.28 * 10^{-9} x^4 - 7.67 * 10^{-7} x^3 + 1.08 * 10^{-2} x$
Stage 4		$0.016x \quad \text{for } x < \frac{L}{2}$ $-0.016x + 2.68 \quad \text{for } x > \frac{L}{2}$

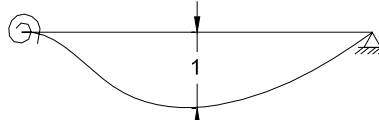
Table 5: Moment and Computed Deflection Equations

Stage 1



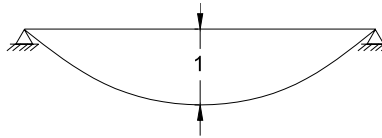
$$\varphi1(x) = 1.77 * 10^{-8} x^4 - 6.07 * 10^{-6} x^3 + 5.15 * 10^{-4} x^2 + 1.03 * 10^{-3} x$$

Stage 2



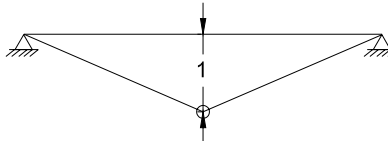
$$\varphi2(x) = 8.92 * 10^{-9} x^4 - 3.69 * 10^{-6} x^3 + 3.46 * 10^{-4} x^2 + 3.53 * 10^{-3} x$$

Stage 3



$$\varphi3(x) = 4.01 * 10^{-9} x^4 - 1.35 * 10^{-6} x^3 + 1.90 * 10^{-2} x$$

Stage 4



$$\varphi4(x) = \frac{2x}{L} \quad \text{for } x < \frac{L}{2}$$

$$\varphi4(x) = \frac{-2x}{L} + 2 \quad \text{for } x > \frac{L}{2}$$

Figure 36: Assumed Shape Functions

As illustrated by Figure 36 there are four shape functions describing the behavior of the wall as it goes through the elastic, elastic-plastic, and plastic stages. Therefore Eqns. 1 – 3 must be solved four times using each of the shape functions, an example of which is shown in Eqn. 6. F_e is a function of $p(x)$ and therefore will vary according to the magnitude of the blast load. The values of M_e and k_e are tabulated in Table 6.

$$\begin{aligned}
 M_e &= \int m(x) * \phi^2(x) dx \\
 &= \int_0^{168} 0.227 * (1.77 * 10^{-8} x^4 - 6.07 * 10^{-6} x^3 + 5.15 * 10^{-4} x^2 + 1.03 * 10^{-3} x)^2 dx \quad \text{Eqn. 6} \\
 &= 15.97
 \end{aligned}$$

	M_e (lb-sec²/in)	k_e (lb/in)
Stage 1	15.97	589,264
Stage 2	18.40	336,113
Stage 3	19.19	185,204
Stage 4	12.69	0

Table 6: Equivalent Mass and Stiffness

9.2.2. Static Resistance Curve

In order to calculate the dynamic response of the wall a *static resistance curve* must be derived. The resistance of an element is the internal force which restores the element to its unloaded static position (Biggs 1964). Thus the maximum resistance is the total load that the wall can support statically. The slope of the resistance curve is the stiffness value for a given stage of inelastic behavior, and the area under the resistance curve represents the potential energy, PE , that the wall can resist. The values for y_{el} in Table 3 and the equivalent stiffness values, k_e , in Table 6 allow calculation of the resistance values, R_e , using the equation $R_e = k_e * y_{el}$. The results are graphed in Figure 37. It can be seen that the wall exhibits an elastic-plastic resistance curve with slope equal to the spring constants k_{1e} , k_{2e} , and k_{3e} corresponding to the formation of the three plastic hinges. After the third hinge forms, the wall is in the purely plastic phase and the stiffness drops to zero.

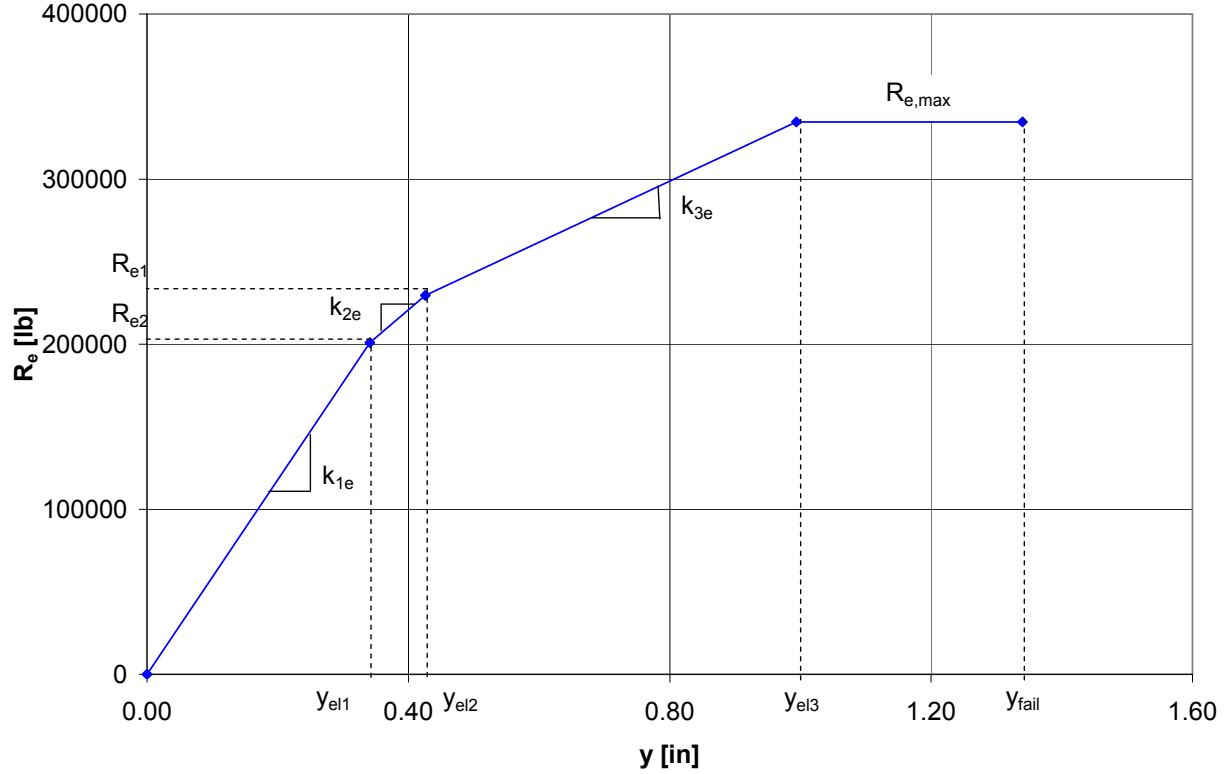


Figure 37: Static Resistance of Equivalent SDOF Model

As the wall goes from the elastic to the inelastic stages the EQM governing its behavior changes according to the resistance function in Figure 37. Because the parameters of the equivalent system change as the element progresses through the different stress ranges (see Table 6) a complete solution requires that each range be treated separately (Biggs 1964). The EQM for each stage are shown below in Eqns. 7-10. It is seen that damping has been neglected. This is because we are interested in the maximum displacement response of the wall. This occurs during the first cycle of oscillation when damping is relatively unimportant. Also, the energy dissipation in the wall will occur mainly through plastic deformation. Omitting damping leads to a slightly more conservative design overall (Smith and Hetherington 1994).

$$\text{Stage 1: } M_{1e}y'' + k_{1e}y = F_{1e}(t) \quad 0 < y < y_{1el} \quad \text{Eqn. 7}$$

$$\text{Stage 2: } M_{2e}y'' + [k_{2e}(y - y_{el1}) + R_{1e}] = F_{2e}(t) \quad y_{1el} < y < y_{2el} \quad \text{Eqn. 8}$$

$$\text{Stage 3: } M_{3e}y'' + [k_{3e}(y - y_{el2}) + R_{2e}]y = F_{3e}(t) \quad y_{2el} < y < y_{3el} \quad \text{Eqn. 9}$$

$$\text{Stage 4: } M_{4e}y'' + R_{e,max} = F_{4e}(t) \quad y_{3el} < y < y_m \quad \text{Eqn. 10}$$

The EQM is solved for each stage using an explicit numerical analysis method. A number of methods can be utilized for this analysis including the Central Difference Method and Newmark's Method. The procedure shown here is a constant velocity method (Biggs 1964). The procedure is described in Table 6 and is included in Appendix A as it was programmed.

<p>Initial variables defined outside loop:</p>	<p>t_d = duration of load (sec) t_{end} = end of numerical analysis (sec) Δt = time step of numerical analysis choose $\Delta t \leq 0.1 * T_n$</p>
<p>Initial calculations for t = 0:</p>	<p>$F1_{oe} = p_o * F1'_e$ (F_{oe} = max blast load) $F2_{oe} = p_o * F2'_e$ $F3_{oe} = p_o * F3'_e$ $F4_{oe} = p_o * F4'_e$ $y^{(0)} = 0$ (y = displacement) $f^{(0)} = \frac{F1_{oe}(t=0)}{M1_e}$ (f = blast force) $r^{(0)} = 0$ (r = resistance) $y''^{(0)} = f^{(0)} - r^{(0)}$ (y'' = acceleration) $y^{(1)} = \frac{1}{2} y''^{(0)} (\Delta t)^2$</p>
<p>Elastic Stage until $y = y_{el1}$:</p>	<p>$f^{(s)} = \frac{-F1_{oe}(\Delta t * s)}{t_d} + F1_{oe}$ $r^{(s)} = \frac{y^{(s)} * k1_e}{M1_e}$ $y''^{(s)} = (f^{(s)} - r^{(s)}) * \Delta t^2$ $y^{(s+1)} = 2y^{(s)} - y^{(s-1)} + y''^{(s)} (\Delta t)^2$</p>
<p>Stage 2 until $y = y_{el2}$ or rebound begins ($y = y_{max}$):</p>	<p>$f^{(s)} = \frac{-F2_{oe}(\Delta t * s)}{t_d} + F2_{oe}$ $r^{(s)} = \frac{k2_e(y^{(s)} - y_{el1}) + R1_e}{M2_e}$ $y''^{(s)} = (f^{(s)} - r^{(s)}) * \Delta t^2$ $y^{(s+1)} = 2y^{(s)} - y^{(s-1)} + y''^{(s)} (\Delta t)^2$</p>
<p>Stage 2 Rebound until $y = y_{el2}$</p>	<p>$f^{(s)} = \frac{-F1_{oe}(\Delta t * s)}{t_d} + F1_{oe}$</p>

	$r^{(s)} = \frac{r_{\max}^{Stage2} - k_{1e} (y_{\max}^{Stage2} - y^{(s)})}{M_{1e}}$ $y''^{(s)} = (f^{(s)} - r^{(s)}) * \Delta t^2$ $y^{(s+1)} = 2y^{(s)} - y^{(s-1)} + y''^{(s)} (\Delta t)^2$
<p>Stage 3 until $y = y_{el3}$ or rebound begins ($y = y_{\max}$):</p>	$f^{(s)} = \frac{-F_{3oe} (\Delta t * s) + F3_{oe}}{t_d M_{3e}}$ $r^{(s)} = \frac{k_{3e} (y^{(s)} - y_{el2}) + R_{2e}}{M_{3e}}$ $y''^{(s)} = (f^{(s)} - r^{(s)}) * \Delta t^2$ $y^{(s+1)} = 2y^{(s)} - y^{(s-1)} + y''^{(s)} (\Delta t)^2$
<p>Stage 3 Rebound until $y = y_{el3}$:</p>	$f^{(s)} = \frac{-F_{1oe} (\Delta t * s) + F1_{oe}}{t_d M_{1e}}$ $r^{(s)} = \frac{r_{\max}^{Stage3} - k_{1e} (y_{\max}^{Stage3} - y^{(s)})}{M_{1e}}$ $y''^{(s)} = (f^{(s)} - r^{(s)}) * \Delta t^2$ $y^{(s+1)} = 2y^{(s)} - y^{(s-1)} + y''^{(s)} (\Delta t)^2$
<p>Stage 4 until $y = y_{fail}$ or rebound begins ($y = y_{\max}$):</p>	$f^{(s)} = \frac{-F_{4oe} (\Delta t * s) + F4_{oe}}{t_d M_{4e}}$ $r^{(s)} = \frac{R_{e,\max}}{M_{4e}}$ $y''^{(s)} = \frac{F_{4oe} (t = s)}{M_{4e}} - \frac{k_{4e} y}{M_{4e}}$ $y^{(s+1)} = 2y^{(s)} - y^{(s-1)} + y''^{(s)} (\Delta t)^2$
<p>Stage 3 Rebound until $y = y_{fail}$:</p>	$f^{(s)} = \frac{-F_{1oe} (\Delta t * s) + F1_{oe}}{t_d M_{1e}}$ $r^{(s)} = \frac{r_{\max}^{Stage4} - k_{1e} (y_{\max}^{Stage4} - y^{(s)})}{M_{1e}}$

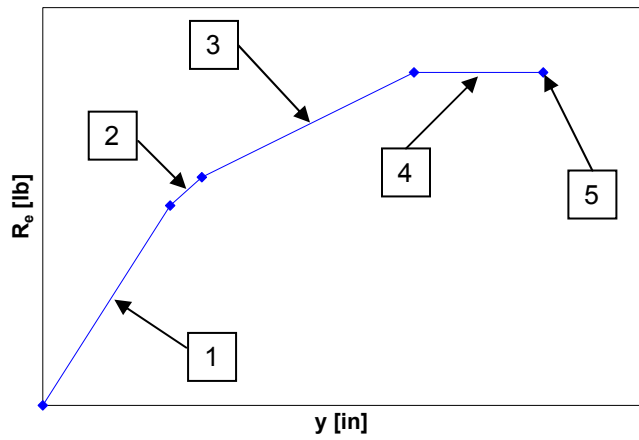
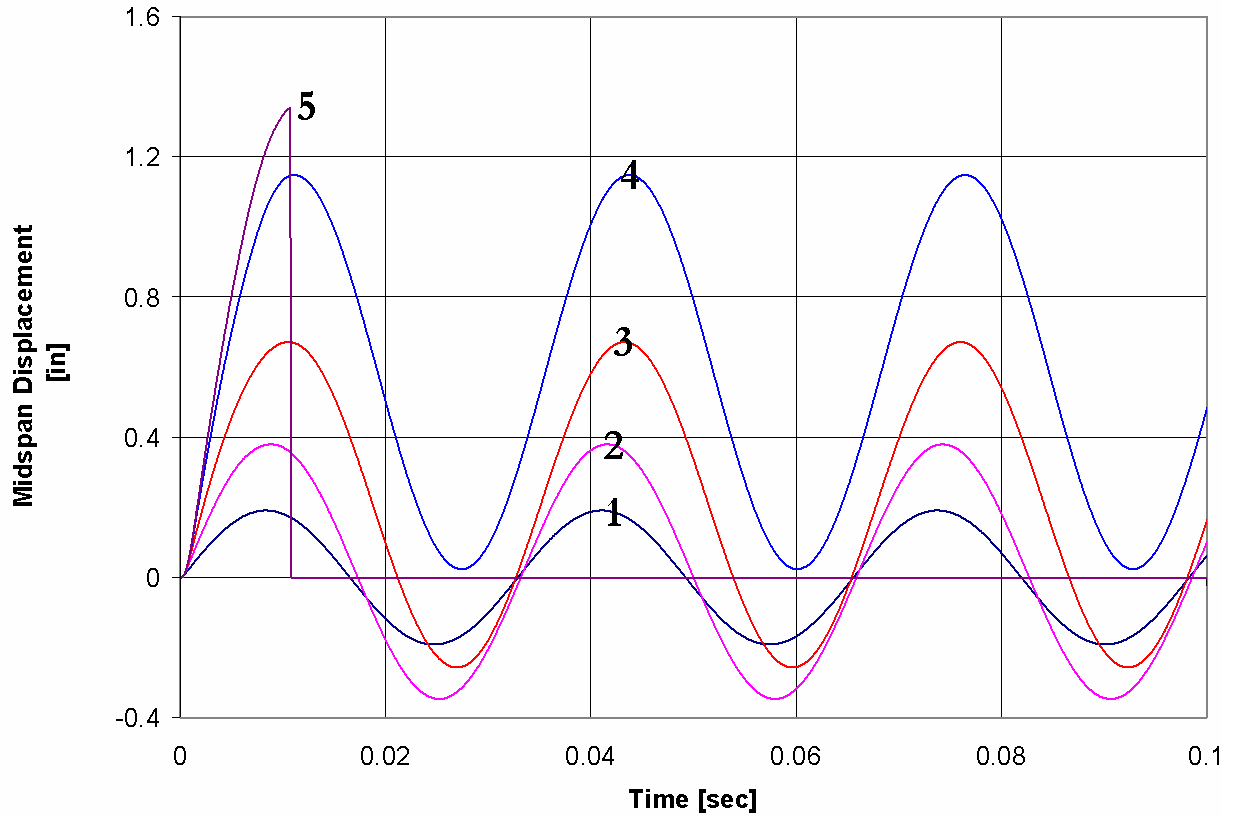
	$y''^{(s)} = (f^{(s)} - r^{(s)}) * \Delta t^2$ $y^{(s+1)} = 2y^{(s)} - y^{(s-1)} + y''^{(s)} (\Delta t)^2$
--	--

Table 7: Constant Velocity Numerical Analysis Procedure to Solve EQM

9.2.3. Wall Response

Solution of the EQM according to the numerical analysis procedure of Table 7 will yield the dynamic time history response of the wall for a specific blast demand. The procedure requires two input variables relating to the blast demand, the maximum pressure, p_o , and the impulse, i . The program then outputs the midspan displacement of the structure as a function of time. Figure 38 gives example time history responses at various stages. An illustration of the resistance curve shows the corresponding stage of inelastic behavior for each response. The values of p_o and i causing the response are also tabulated. It can be seen that because no damping is included in the EQM, the response of curves 1-4 will oscillate without decay. Curve 5 represents failure; therefore the response stops at the critical displacement value of 1.340", as derived in Section 9.1.3.2. This failure response is one of numerous combinations of p_o and i that will cause the wall to fail. It is useful to develop an "envelope" of blast demands which will define a failure zone as a function of p_o and i . A method of doing so is discussed in Section 9.3.2.

It should be noted in the numerical analysis procedure of Table 7 that specific calculation loops are required to describe the *rebound* response of the wall. This is in order to capture the correct resistance behavior of the wall as it oscillates dynamically. As the displacement of the wall increases, the resistance of the wall increases according to the slope of the static resistance curve, i.e. k_{1e} , k_{2e} , k_{3e} . When the wall reaches a peak oscillation it will then unload according to the initial elastic stiffness, k_{1e} . When the oscillation reaches a low point, the resistance once again increases along the slope of k_{1e} until the wall reaches a large enough displacement that the elastic-plastic stiffness once again applies. This behavior of moving up and down the static resistance curve is illustrated in Figure 39. The analysis procedure described in Table 7 and presented in Appendix A will calculate the complete response for blast loads in the dynamic and impulse ranges. For quasi-static loads the program should be used to calculate the maximum dynamic response only. If the dynamic response is required beyond the first oscillation peak, the program should be revised to capture a more advanced hysteretic behavior of the multi-linear resistance curve. Newmark's method with application of the Newton-Raphson iteration can be used. This advanced method of analysis was not employed for the purposes of this analysis, because the majority of blast loads will occur in the dynamic and impulsive regions only. See Section 9.3 for an explanation of the delineation of the quasi-static, dynamic, and impulse regions.



Stage	p_o (lb/in)	i (psi*s)
1	600	0.100
2	600	0.174
3	600	0.275
4	600	0.425
5	600	0.490

Figure 38: Example Dynamic Response History of Wall

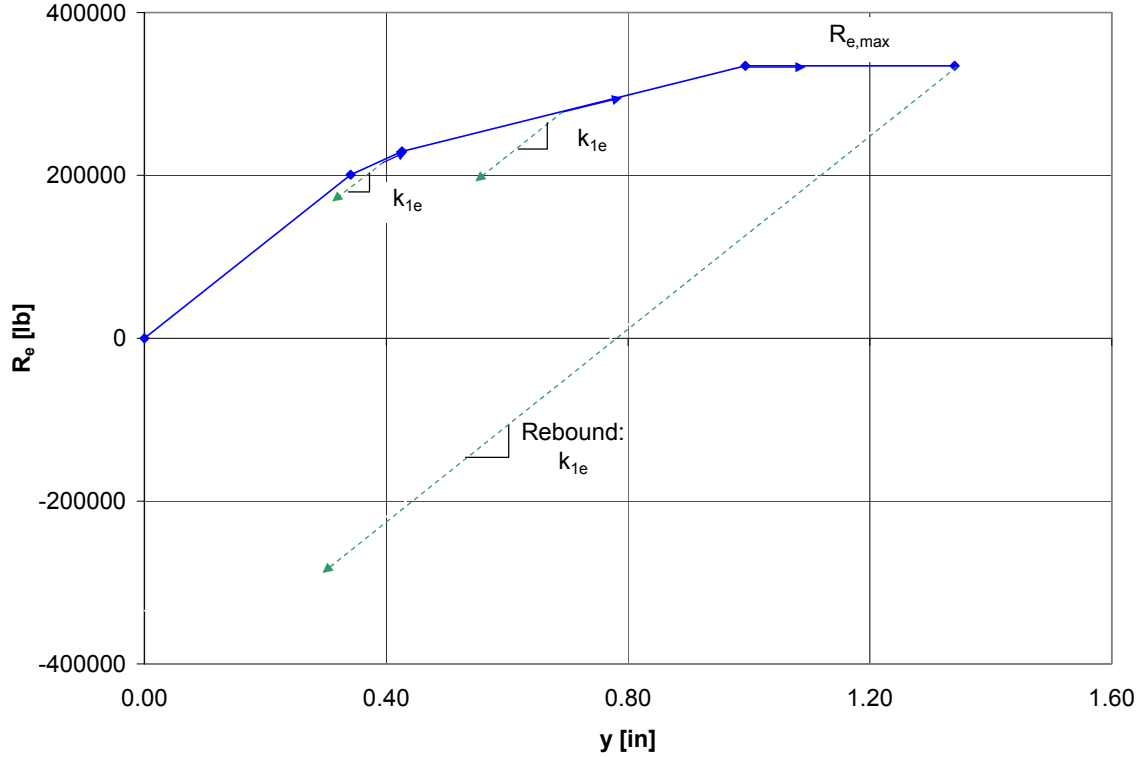


Figure 39: Assumed rebound response

9.3. Damage Quantification

Recall in Figure 2 the shape of the idealized blast curve. The blast curve is described by its maximum pressure value, p_o , and its time duration, t_d . Depending on the length of t_d compared to the natural period of the structure, T_n , the behavior of the structure will fall into one of three categories, quasi-static, dynamic, or impulsive. First consider the case when t_d is much longer than T_n . The pressure, p_o , changes so slowly that the force is considered constant up to the maximum displacement, as shown in Figure 40 (a). This loading regime is known as quasi-static. A quasi-static blast load would occur from an explosion that releases a virtually constant pressure for a relatively long time duration (~1-10 sec). This type of explosive loading is very rarely encountered with respect to intentional blast loading. The response history of the wall loaded by a quasi-static load is illustrated in Figure 41. The response is shown normalized with respect to the maximum static displacement, $(y_{sd})_o$, and is compared to the normalized blast demand. As characterized by a quasi-static load it can be seen that the wall undergoes many oscillations before the loading completes.

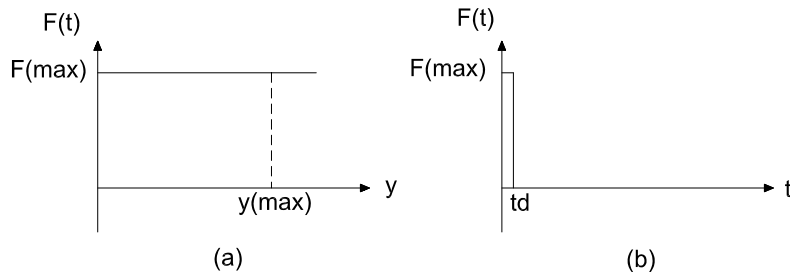


Figure 40: (a) Long Duration Loading (b) Short Duration Loading

The next case, shown in Figure 40 (b), is when t_d is much shorter than T_n . As shown in the response history graph of Figure 42 the loading is applied so quickly relative to the wall response that the wall reaches its maximum displacement after the blast load application has been completed. This is described as the impulsive region and represents most blast loading combinations. In between the two extreme cases lays the dynamic region, illustrated in Figure 43.

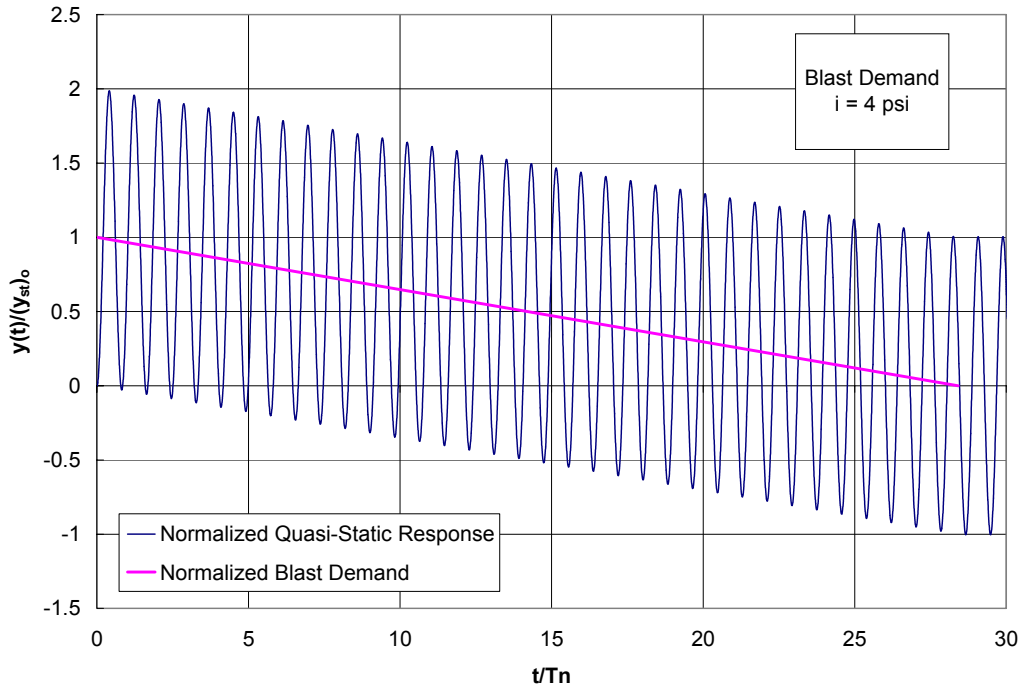


Figure 41: Normalized Dynamic Response of Wall under Quasi-Static Load

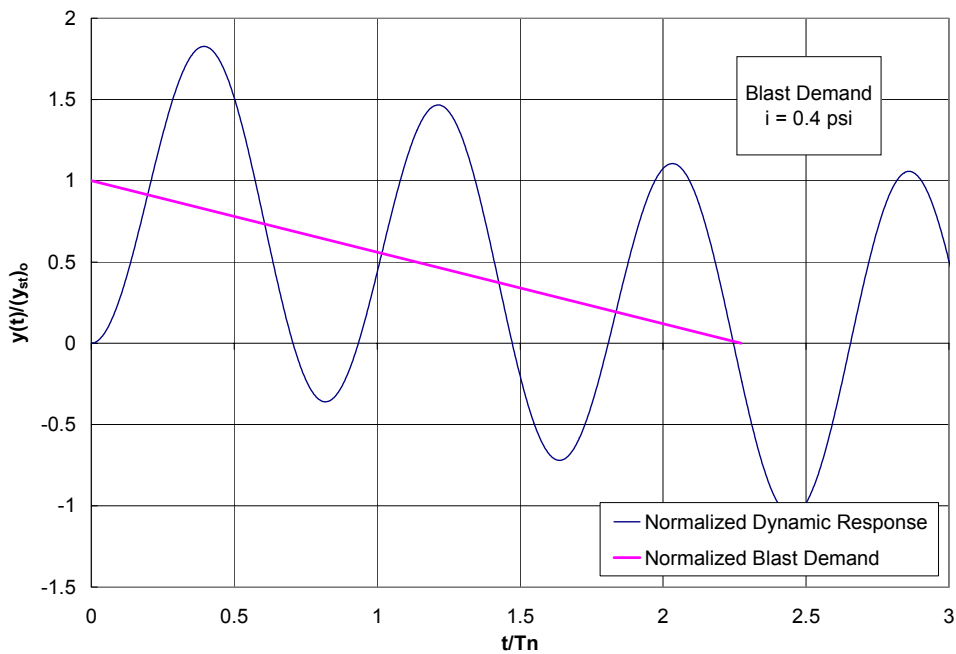


Figure 42: Normalized Dynamic Response of Wall under Dynamic Load

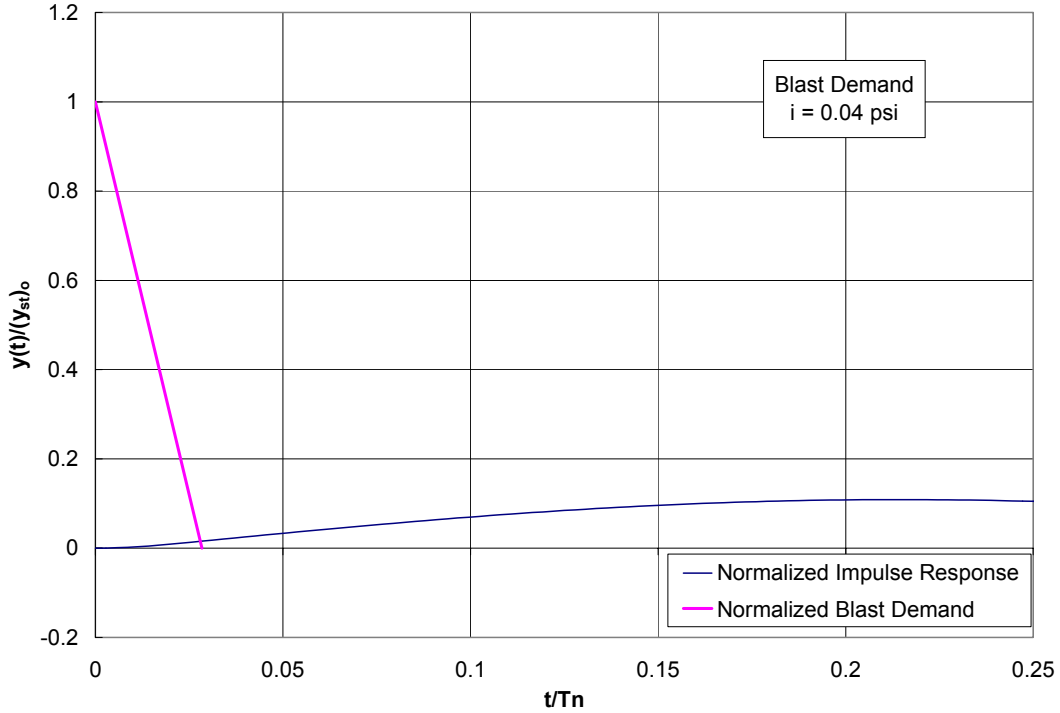


Figure 43: Normalized Dynamic Response of Wall Under Impulse Load

The three regimes can be delineated with respect to the relative duration of the blast load, t_d , and the period of the system, T_n . These regimes can be approximated as shown in Table 8 (Mays and Smith 1995).

$0.4 > t_d/T_n$	Impulsive
$0.4 < t_d/T_n < 40$	Dynamic
$40 < t_d/T_n$	Quasi-Static

Table 8: Regimes of Loading

9.3.1. Dynamic and Impulsive Response of 1st Floor Wall

As described previously, the FEM analysis in Diana indicated that failure would occur in the 2nd floor wall under a quasi-static load. Depending on the type of explosive a blast load may act in the quasi-static, impulsive, or dynamic range. Therefore it is prudent to check that our assumption holds true in the impulsive and dynamic zones as well. The dynamic response of the 1st floor wall can be determined through the procedure outlined in Chapter 9 and 10. Figure 44 shows the curvature diagram calculated in DRAIN-2DX for the 1st floor, outer wall. Note that the 1st floor wall has #9 longitudinal reinforcement along its entire length; therefore plastic hinges will form simultaneously at both ends of the wall where the moment peaks. Summing the area under the curvature diagram, the ultimate rotation value, θ_u , is calculated to be 0.022 rad or 1.25 degrees. According to the assumed failure geometry (see Figure 35) when the plastic hinge reaches θ_u the critical displacement value at failure will equal 1.650”.

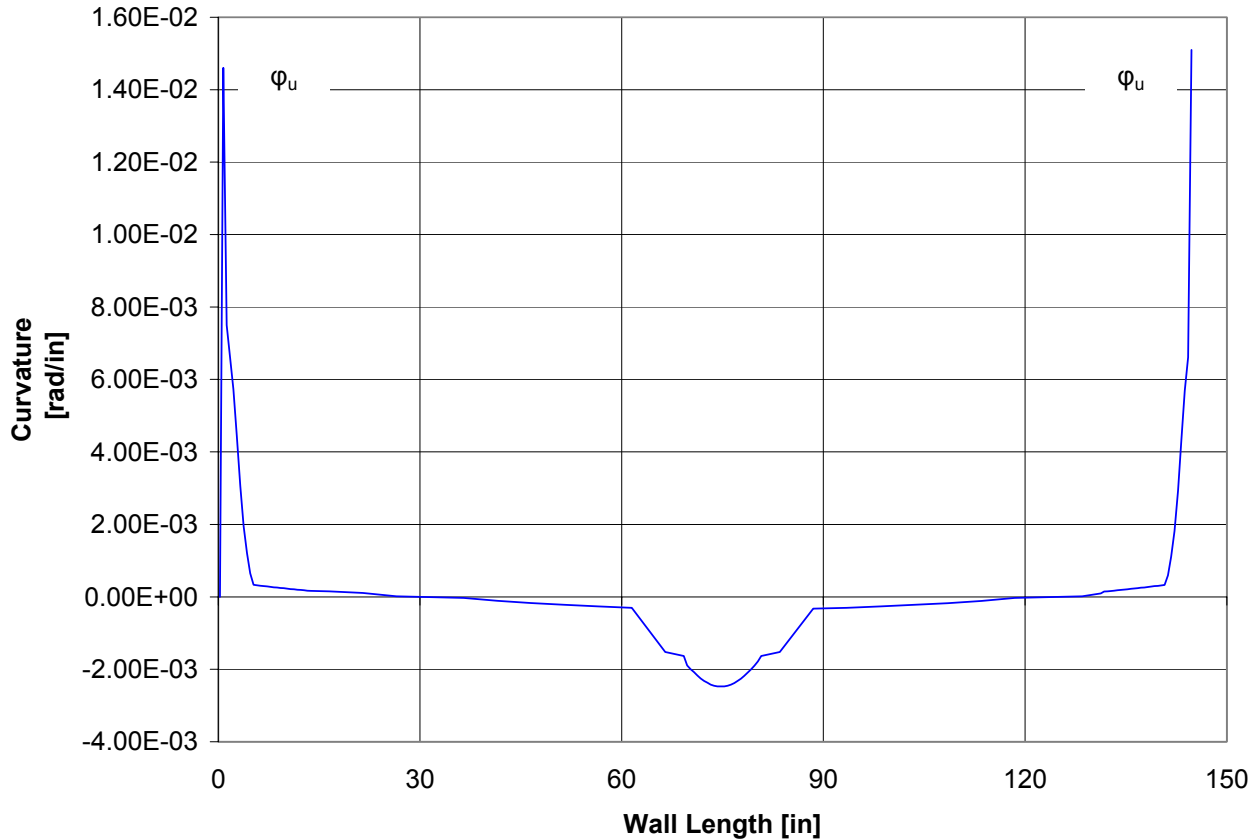


Figure 44: Curvature along first floor outer wall at ultimate

For simplicity the 1st and 2nd floor walls are modeled as components with fixed-fixed ends. This assumption will be validated as a legitimate simplification in the next chapter. Using the numerical analysis procedure outlined in Table 7 the EQM for the each wall is solved to determine the history response under a dynamic or impulsive load. A dynamic blast demand causing the 2nd floor, outer wall to fail is equal to ($p_o = 3460$ lb/in, $i = 0.96$ psi*sec). The corresponding pressure on the 1st floor, outer wall is equal to (4083 lb/in, 1.13 psi*sec), according to the normalized blast pressure distribution developed in Figure 15. The resulting response of both walls in Figure 45 shows that when the 2nd floor wall has reached failure, the 1st floor has achieved inelastic deformation but has not yet failed. In the impulse region the 2nd floor wall will fail with a blast demand of ($p_o = 70,000$ lb/in, $i = 0.49$ psi*sec). This corresponds to a demand of (82,600 lb/in, 0.57 psi*sec) on the 1st floor wall. Once again the 2nd floor, outer wall fails with only minimal damage to the first. The previous assumption made from the static pushover analysis that the 2nd floor wall fails first holds true under dynamic evaluation. For the quasi-static, impulse, and dynamic regions of loading the second floor wall will be lost before the first.

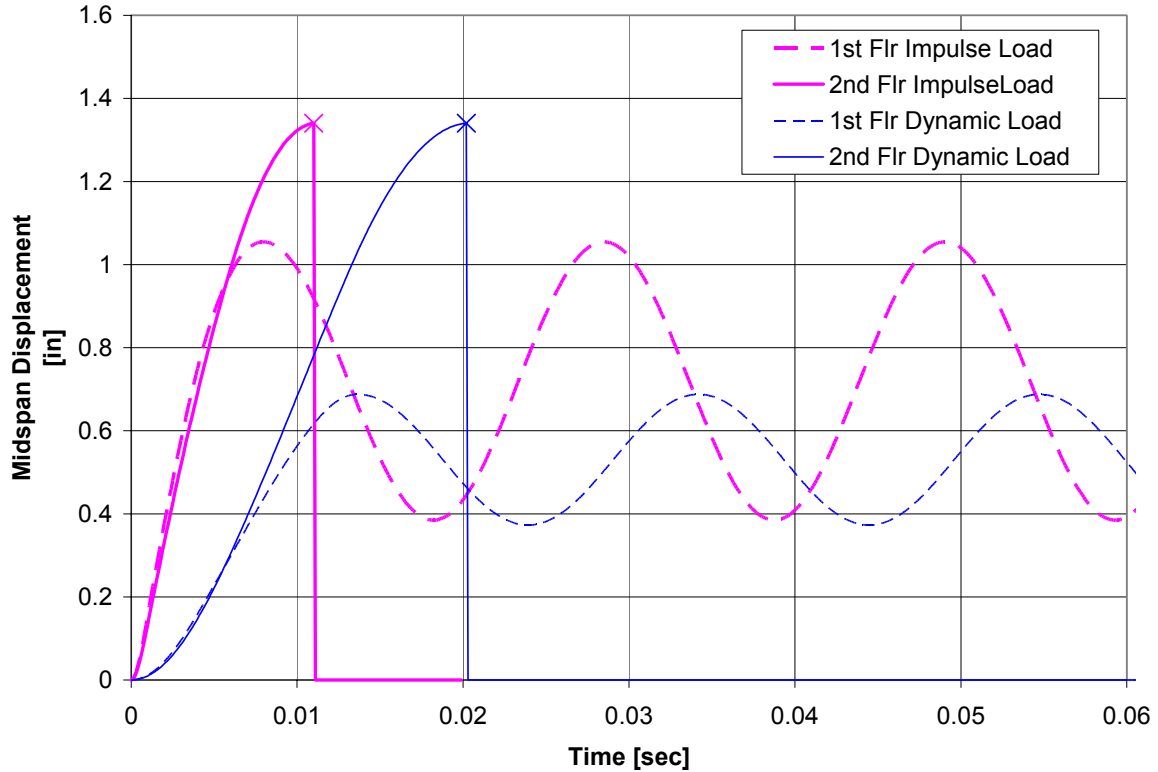


Figure 45: Response Curve of First and Second Floor Wall

9.3.2. Pressure-Impulse Curve

As shown in Figure 2 the blast demand is described by two criteria, maximum pressure and time duration, p_o and t_d respectively. The area under the blast curve is the impulse, i , imparted to the structure (i.e. $i = \frac{1}{2} * p_o * t_d$). As illustrated in Figure 38 the dynamic time history response of the system model has been calculated for a specific blast demand. It is informative to develop an “envelope” of blast demands, as a function of p_o and t_d , which will define the four failure stages in the wall. This can be done by graphing a *pressure vs. impulse curve*. A pressure vs. impulse curve is a very informative means to describe how much damage a structure will sustain under a variety of blast load magnitudes.

The pressure vs. impulse curve generated for the system model is illustrated in Figure 46. These curves were created by solving the EQM’s in Eqns 7-10. The numerical analysis technique outlined in Table 7 was modified slightly for the purposes of this analysis; see Appendix B for the revised MathCad program. The program was rewritten to input t_d and a critical displacement value, y_{el} (corresponding to one of the four failure stages). The program outputs the resulting pressure, p_o , which causes the structure to reach the specified failure level. The impulse corresponding to the failure level can then be calculated from the equation $i = \frac{1}{2} * p_o * t_d$. The program was run for 15 values of t_d ranging from 0.0005 sec to 5 sec. The program was also run for each critical displacement, y_{el1} , y_{el2} , y_{el3} , and $y_{el,u}$ (Stages 1-4).

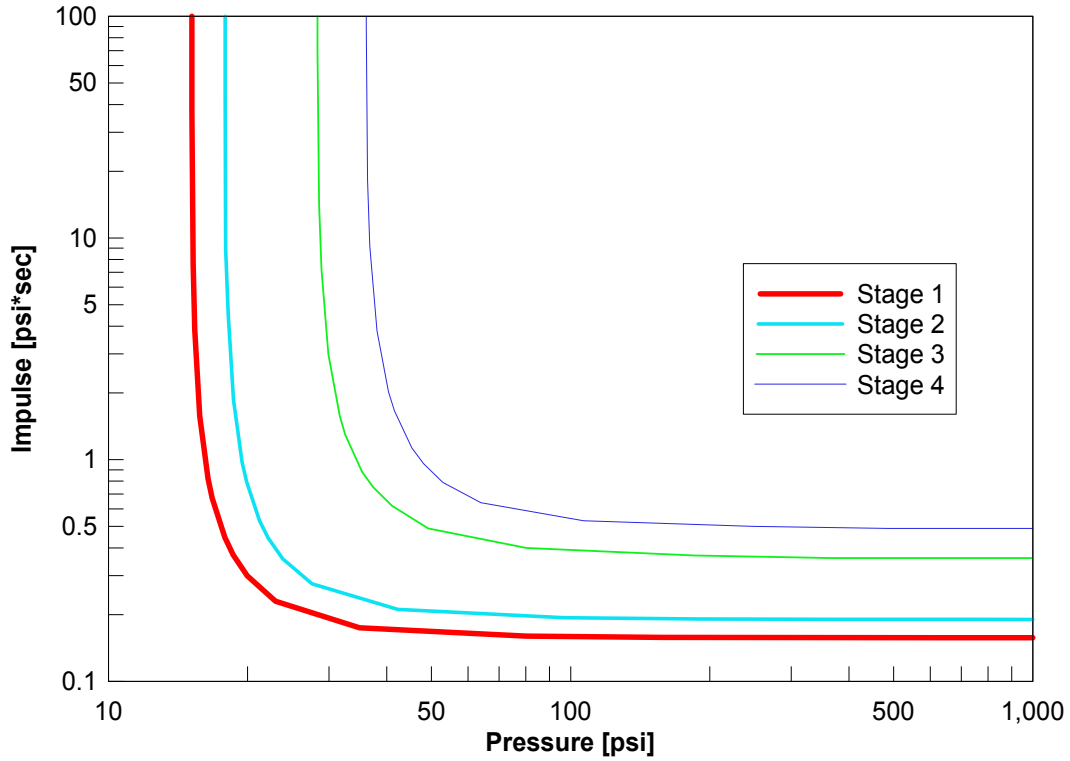


Figure 46: Pressure vs. Impulse Curve (System Model)

As discussed in Section 9.3 a blast demand will load a structure in one of three regions, quasi-static, dynamic, or impulsive. Using the criteria as tabulated in Table 8, lines delineating the three zones can be graphed on the pressure vs. impulse curve. It can be seen that for low pressures the wall is loaded in the quasi-static zone, high pressures correspond to the impulse zone, and in the middle is the dynamic zone.

For design purposes, it is convenient to name the four stages of failure according to the performance levels defined by FEMA (Applied Technology Council and Building Seismic Safety Council 1997). When one hinge has formed the structure is at the *Immediate Occupancy* (IO) level. When two hinges have formed it is the *Life Safety* (LS) level, three hinges is called the *Collapse Prevention* (CP) level, and when a hinge fails the structure is at *Collapse*. These performance levels define failure regions as illustrated on the pressure vs. impulse curve of Figure 48.

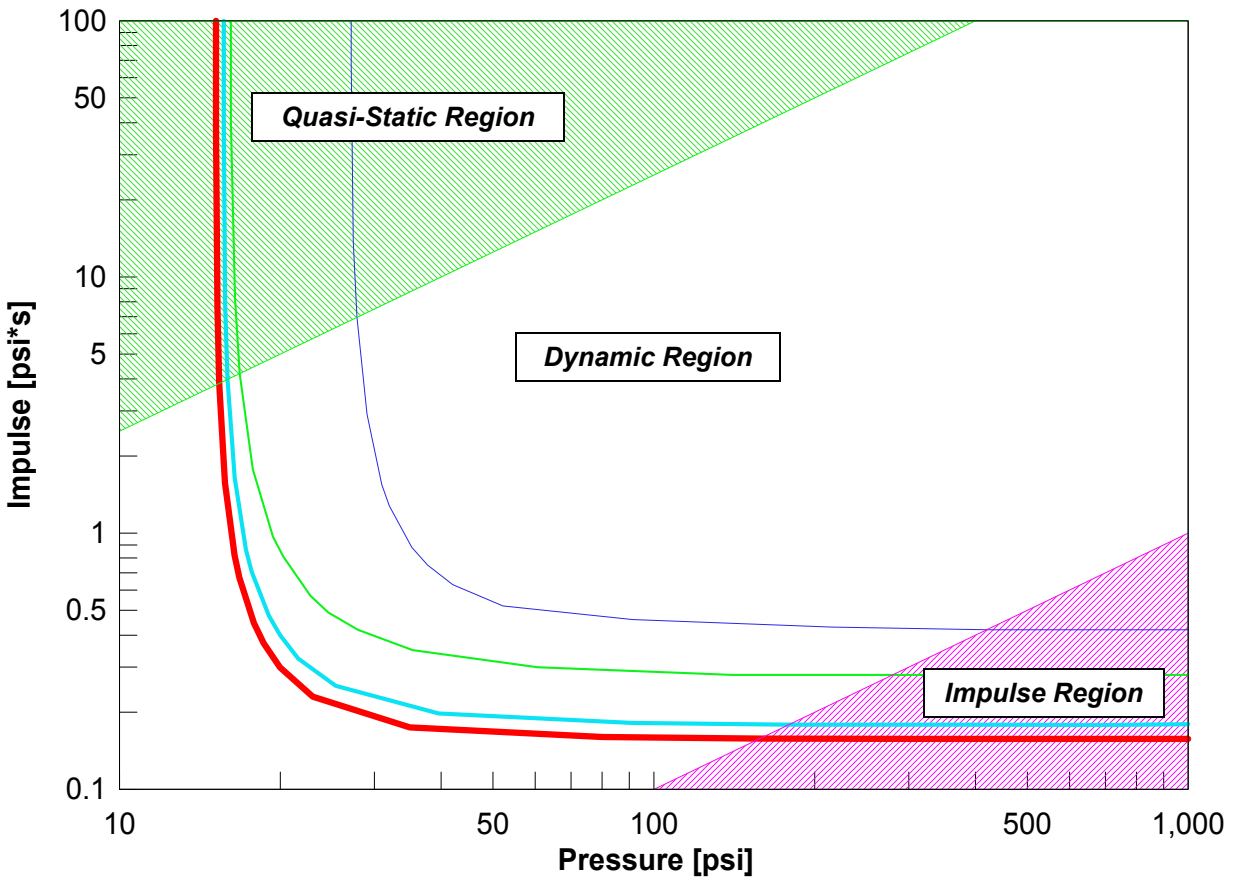


Figure 47: Three Regimes of Loading (System Model)

Development of the pressure vs. impulse curve for a specific structure is an advantageous tool for a designer. With the knowledge yielded by the graph, it is possible to determine for a given blast demand which performance level a structure will maintain. Instead of designing for the criteria of “fail” or “not fail”, the pressure vs. impulse graph allows a designer to determine what damage level a structure will incur. For example, say a wall system exists which is considered at risk for terrorist attacks. It is desired that the wall can resist an impulsive blast demand, i , of magnitude 0.3 psi*sec with a peak pressure, p_o , equal to 600 psi. The wall is part of a building which requires a Life Safety Level to be maintained under these demands. In order to determine if the wall is adequately designed for such blast criteria, the pressure vs. impulse curve is developed. From this chart the p_o vs. i can be mapped to determine the expected performance of the system. For example the coordinate $(p_o, i) = (600, 0.3)$ is plotted on the graph of Figure 48. The intercept lies in the LS range. Therefore the current blast resist capabilities of the wall would meet the design criteria. If the response had exceeded the Life Safety Level, retrofit options may be considered to increase the strength of the wall. A new pressure vs. impulse curve would have to be derived corresponding to the redesigned wall. Design time is always an important consideration in practice, and oftentimes simplifications are sought which will increase efficiency without loss of sufficient accuracy. As a means of simplifying the analysis method presented in Chapter 9, a component study of the wall is examined in the next chapter.

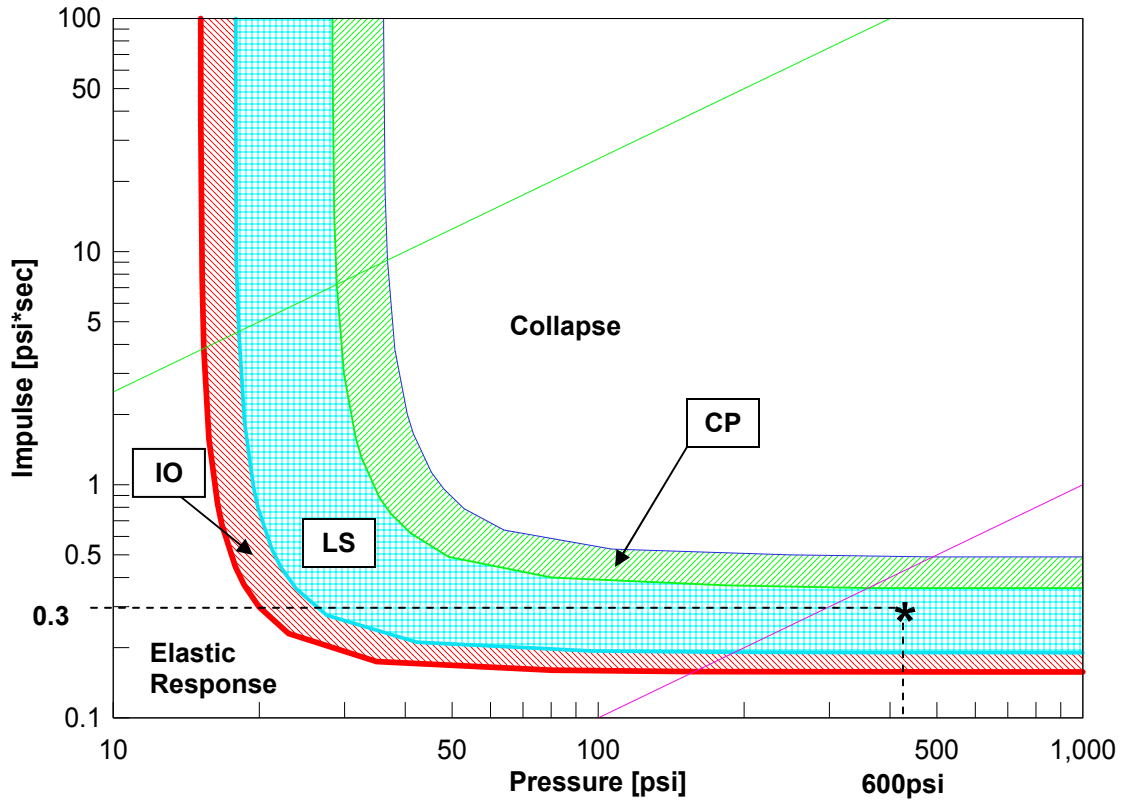


Figure 48: FEMA Performance Levels (System Model)

10. “Component” Dynamic Analysis

In the course of design it is advantageous to ascertain when simplifying assumptions can be made which do not deteriorate the required accuracy of the solution. The preceding chapter outlines a detailed methodology of finding the dynamic response of the 2nd floor, outer wall when acting as a *system* with the adjacent walls and coupling beams. Performing calculations to this level of detail may not always be desirable or necessary. A simplified model is developed which considers the 2nd floor, outer wall as a *component*. The component model assumes that the stiffness at the top and bottom of the wall is large enough so as to be considered fixed ends. In addition the blast load profile is assumed to act uniformly along the height of the wall component. Revising the system model using these simplifications yields the component model shown in Figure 49. The dynamic analysis outlined in Chapter 9 will now be replicated for the component wall. It will be shown that the component model can be analyzed with a substantial decrease in computational effort while still maintaining a comparable estimate of response.

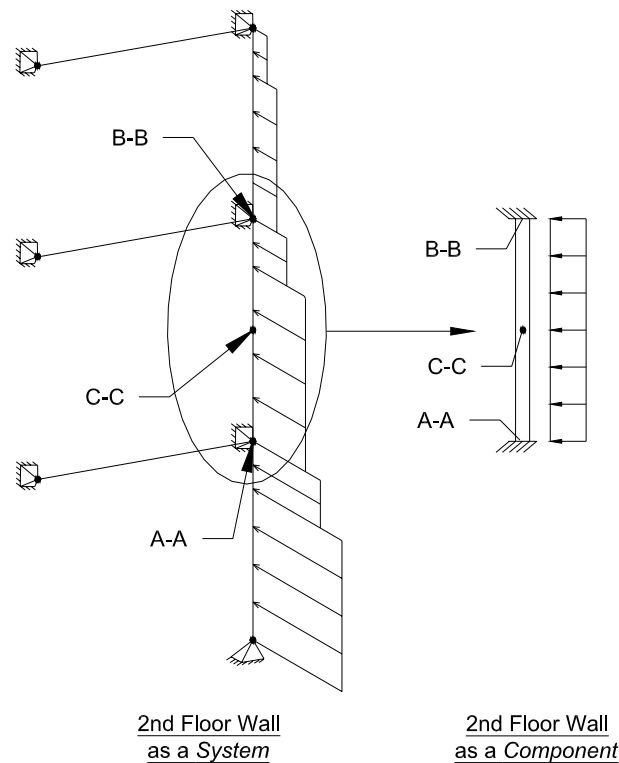


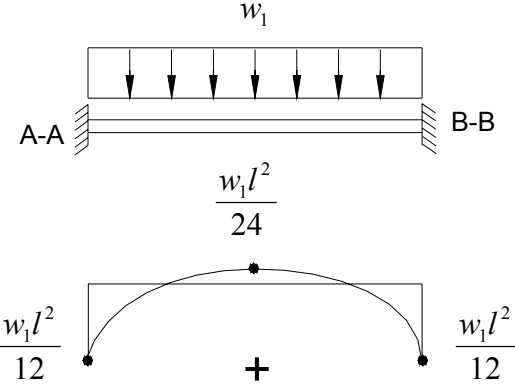
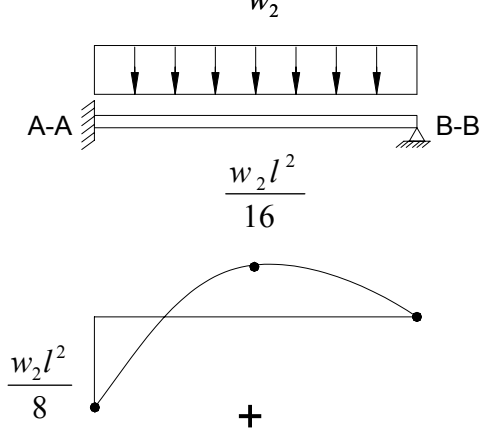
Figure 49: System Model vs. Component Model

10.1. Static Resistance Curve

As defined in Section 9.2.2 the static resistance of a structure can be represented in terms of wall resistance vs. midspan displacement (i.e. R vs. y_{el}). The slope of the graph is equal to the wall stiffness, k . The simplifications of the component model allow for its static resistance curve to be calculated with a few simple equations. The values of k and R for the component wall are derived according to the procedure in Table 9. The critical displacement values are then calculated using the equation $y_{el} = R/k$.

Recall that the yield moments for Sections A-A & B-B were derived in Chapter 10 as tabulated in Table 2, and the

yield moment for Section C-C was assumed to be that of Section A-A. The procedure to derive R and k for the component wall is as follows. First, a uniform distributed load, w_1 , is placed on the wall causing the moment at Section B-B to reach yield, M_{yB} , and form a plastic hinge. The total load acting on the wall is R_1 . At Stage 2 Section B-B now acts as a pin. A distributed load, w_2 , is added onto the wall so that the total moment of Stage 1 and 2 is equal to yield at Section A-A, M_{yA} . Therefore Section A-A forms a hinge and the total load acting on the wall is R_2 . In Stage 3 a distributed load, w_3 , is added to the wall so that the total moment of all three stages at Section C-C is yield, M_{yC} . For this analysis $M_{yC} = M_{yA}$, per the geometry of longitudinal reinforcement as discussed in Section 9.1.2. The stiffness at each stage is calculated from the deflected shape of the wall under a unit uniform load.

	<p><i>Stage 1 (Elastic) :</i></p> <ul style="list-style-type: none"> • $M_{yB} = \frac{w_1 l^2}{12}$ • $w_1 = \frac{12 M_{yB}}{l^2}$ • $R_1 = w_1 * l = \frac{12 M_{yB}}{l}$ • $k_1 = \frac{384 * EI}{L^3}$
	<p><i>Stage 2 (Elastic - Plastic) :</i></p> <ul style="list-style-type: none"> • $M_{yA} = \frac{w_1 l^2}{12} + \frac{w_2 l^2}{8}$ $= M_{yB} + \frac{w_2 l^2}{8}$ • $w_2 = \frac{8(M_{yA} - M_{yB})}{l^2}$ • $w_1 + w_2 = \frac{8 * M_{yA} + 4 * M_{yB}}{l^2}$ • $R_2 = (w_1 + w_2) * l$ $= \frac{8 * M_{yA} + 4 * M_{yB}}{l}$ • $k_2 = \frac{185 * EI}{L^3}$

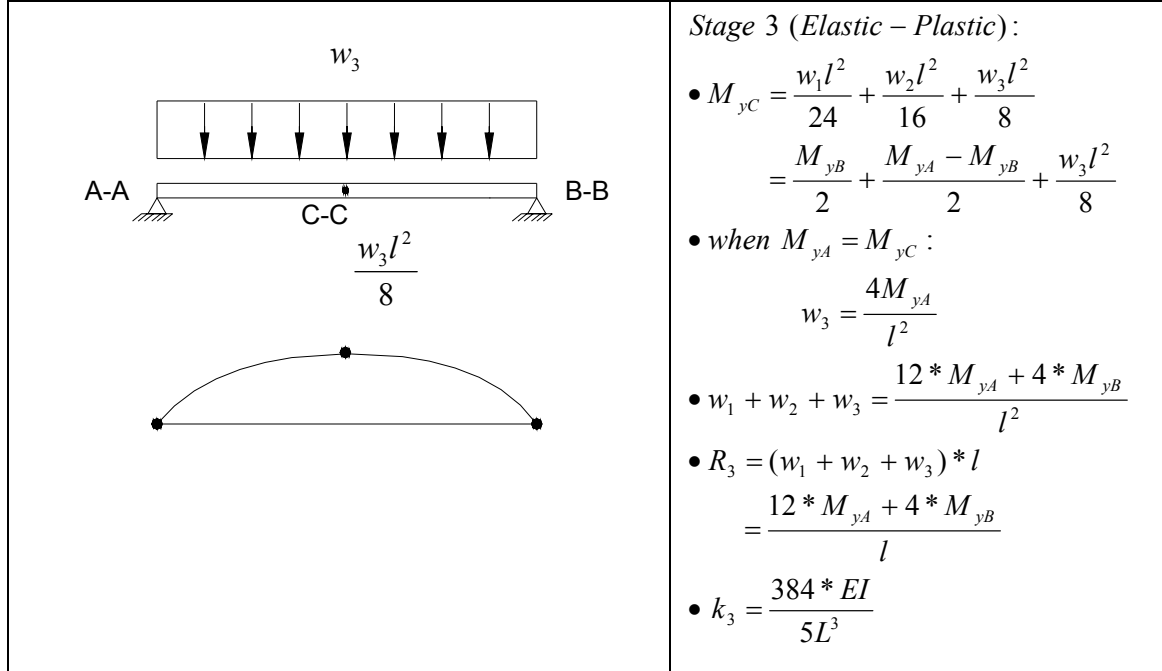


Table 9: Derivation of R and k for Component Model

The values of R , k , and y_{el} for the component model are tabulated in Table 10. Note that the resistance curve is in terms of the *actual* resistance parameters (R and k) as opposed to the *equivalent* resistance parameters (R_e and k_e). Transformation to the equivalent parameters for solution of the equivalent SDOF model will be described in the next section. These values are used to graph a static resistance curve, as shown in Figure 50. The graph is compared to the resistance curve calculated for the system model. The area under the resistance curve represents the potential energy, PE , which the wall can resist. The areas under both curves are compared in Table 10. As expected the component wall will absorb more energy than the system model because it is artificially stiffer due to the fixed-fixed assumptions used. Therefore dynamic analysis of the component wall should result in an over-approximation of the strength of the wall. This is true for all stages except for the first, which actually absorbs less energy than the system model. Subsequent analysis will show that this difference in energy absorption affects the accuracy of the pressure vs. impulse graph by only a small percentage.

	R (lb)	k (lb/in)	y_{el} (in)	PE_{component} (lb-in)	PE_{system} (lb-in)	% Difference
Stage 1	386,429	1,399,609	0.276	53,346	62,291	-14.36%
Stage 2	478,333	674,291	0.412	112,278	95,336	+17.77%
Stage 3	653,095	279,922	1.037	465,468	376,134	+23.75%
Stage 4	653,095	0	1.34	663,538	575,620	+15.27%

Table 10: Resistance Parameters for Component Model

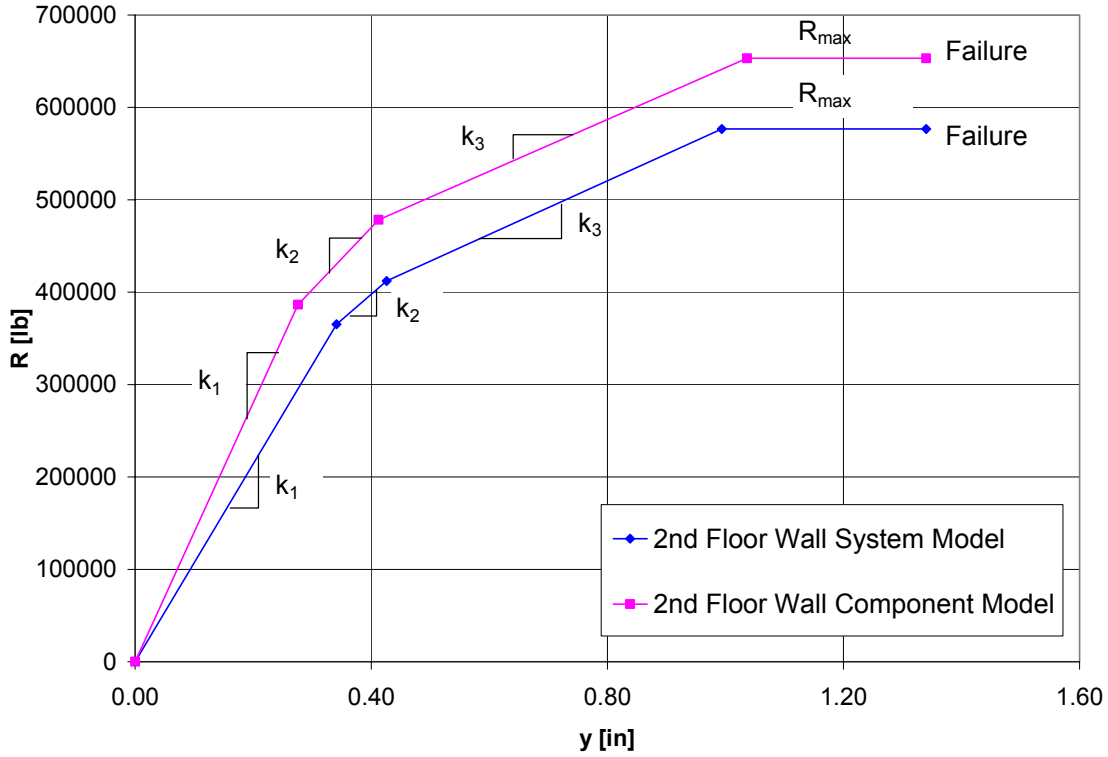


Figure 50: Static Resistance Curve (System vs. Component Model)

10.2. Equivalent SDOF Model

Now that the static resistance curve of the component model has been calculated, an equivalent SDOF model can be analyzed. Recall that development of the equivalent SDOF model requires that the actual mass, stiffness, and force (M, K, F) be converted to an equivalent mass, stiffness, and force (M_e, k_e, F_e). The assumption of a fixed-fixed wall now allows us to introduce the concept of *transformation factors*, K . These factors are used to convert the actual parameters of the wall directly into equivalent parameters without solving the integrals defined in Eqns. 1-3. The transformation factors are defined in Eqns. 11-13. The *mass factor*, K_M , is the ratio of the equivalent mass to the actual total mass of the structure. Similarly, the *load factor*, K_L , is defined as the ratio of the equivalent load to the actual total load. The *load-mass factor*, K_{LM} , is simply the mass factor divided by the load factor.

$$K_M = \frac{\int_0^L m(x)[\phi(x)]^2 dx}{M} = \frac{M_e}{M} \quad \text{Eqn. 11}$$

$$K_L = \frac{\int_0^L p(x)\phi(x) dx}{F} = \frac{F_e}{F} \quad \text{Eqn. 12}$$

$$K_{LM} = \frac{K_M}{K_L} \quad \text{Eqn. 13}$$

The resistance parameters of the actual wall can also be converted to equivalent values by use of a transformation

factor. The ratio of the equivalent resistance to the actual resistance is equal to the load factor, K_L . The ratio of the equivalent stiffness to the actual stiffness is also equal to the load factor (Biggs 1964), as shown in Eqn. 14. The EQM governing the equivalent SDOF system can now be represented in terms of the transformation factors defined in Eqn. 15. The transformation factors corresponding to the deformed shapes of Stages 1-4 wall have been previously derived and are presented in Table 11 (Biggs 1964). The values of R and k derived in Table 9 are re-tabulated below as well.

$$\frac{R_e}{R} = \frac{k_e}{k} = K_L \quad \text{Eqn. 14}$$

$$M_e y'' + k_e y = F_e(t) \Leftrightarrow K_M M y'' + K_L k y = K_L F(t) \quad \text{Eqn. 15}$$

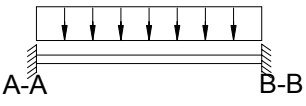
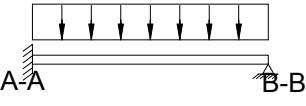
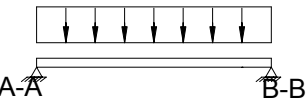
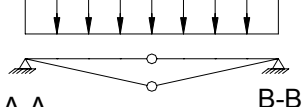
Loading Diagram	Stages	K_L	K_M	K_{LM}	R	k
	Stage 1 Elastic	0.53	0.41	0.77	$\frac{12 * M_{yB}}{L}$	$\frac{384 * EI}{L^3}$
	Stage 2 EI-PI I	0.58	0.45	0.78	$\frac{8 * M_{yA} + 4 * M_{yB}}{L}$	$\frac{185 * EI}{L^3}$
	Stage 3 EI-PI II	0.64	0.50	0.78	$\frac{12 * M_{yA} + 4 * M_{yB}}{L}$	$\frac{384 * EI}{5L^3}$
	Stage 4 Plastic	0.50	0.33	0.66	$\frac{12 * M_{yA} + 4 * M_{yB}}{L}$	0

Table 11: Component Model Parameters

The values of M_e , k_e , and R_e are tabulated in Table 12. The EQM describing the wall's dynamic behavior are shown in Eqns. 16-19. From these equations the pressure vs. impulse diagram can be calculated as before.

	M_e [lb-sec ² /in]	k_e [lb/in]	R_e [lb]	y_{el} [in]
Stage 1	15.61	741,792	204,807	0.276
Stage 2	17.14	391,088	277,433	0.412
Stage 3	19.04	179,150	417,981	1.037
Stage 4	12.57	0	417,981	1.34

Table 12: Equivalent Resistance Parameters of Component Model

Stage 1: $K_{M1} M y'' + K_{L1} k_1 y = K_{L1} F(t) \quad 0 < y < y_{el} \quad \text{Eqn. 16}$

Stage 2: $K_{M2}My''+K_{L2}[k_2(y-y_{el1})+R_1]=K_{L2}F(t)$ $y_{1el} < y < y_{2el}$ Eqn. 17

Stage 3: $K_{M3}My''+K_{L3}[k_3(y-y_{el2})+R_2]=K_{L3}F(t)$ $y_{2el} < y < y_{3el}$ Eqn. 18

Stage 4: $K_{M4}My''+K_{L4}R_{max}=K_{L4}F(t)$ $y_{3el} < y < y_m$ Eqn. 19

10.3. Pressure vs. Impulse Curve

The EQM of the component wall can be solved using the numerical analysis procedure previously discussed in Table 7 and presented in Appendix B. In order to quantify the structural strength of the component wall the pressure vs. impulse curves are graphed for all four damage states, as described in Section 9.3.2. Figure 51 shows the pressure vs. impulse curve of the component model compared to that of the system model. The results show that the simplifications made to represent the component model still produce a comparable solution. As mentioned previously the most common blast demands will load a structure impulsively. In the impulsive region for Stages 1-3 the strength of the component wall is calculated to be ~9% higher than the system model. In Stage 1 the component model underestimates the system response by ~7%. These values support the expected results corresponding to the allowable potential energy capacity for each stage, as described in Table 10.

The results of the component analysis yield a comparable solution to that of the system model. But it must be carefully noted that the simplifications of the component model assume the wall to be stiffer than it actually is, therefore the wall resistance will be over-estimated. The assumption of fixed-fixed ends should only be made on structures that exhibit a large stiffness. For the case of a flexible structure it may be prudent to derive a component model with pinned-pinned ends, in order to determine a lower-bound estimate of the response.

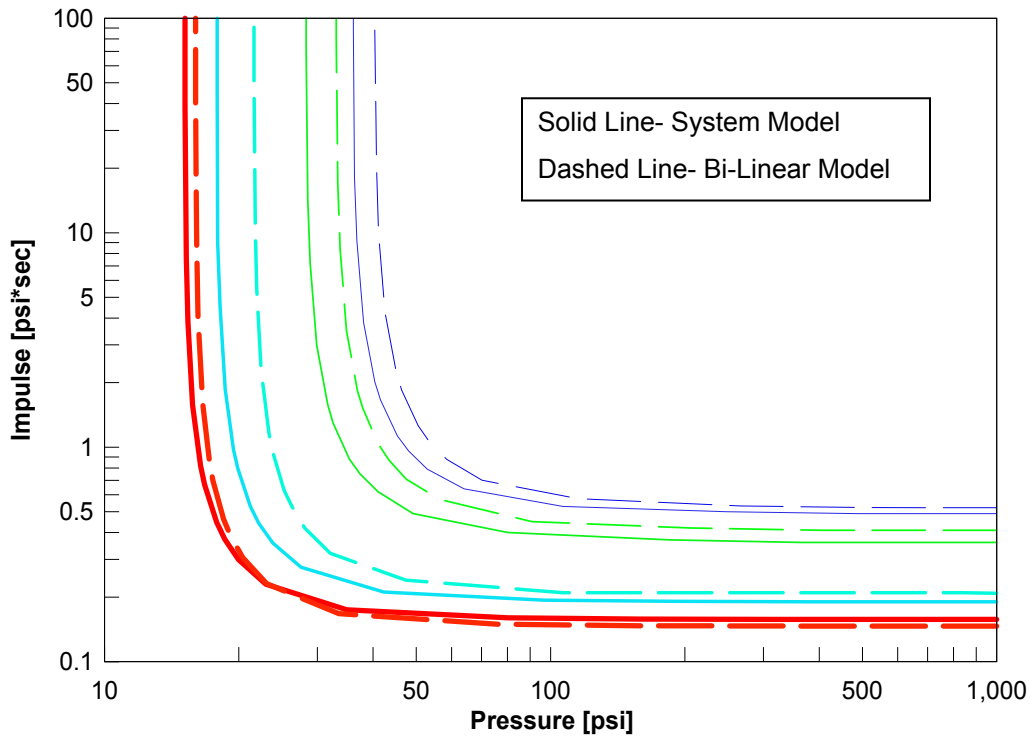


Figure 51: Pressure vs. Impulse Curve (Component & System Models)

10.4. Summary of Component Model Method

The complete procedure to calculate the dynamic response of the component model is summarized in the flow chart of Figure 52. The method to develop a pressure vs. impulse diagram is also summarized in Figure 53.

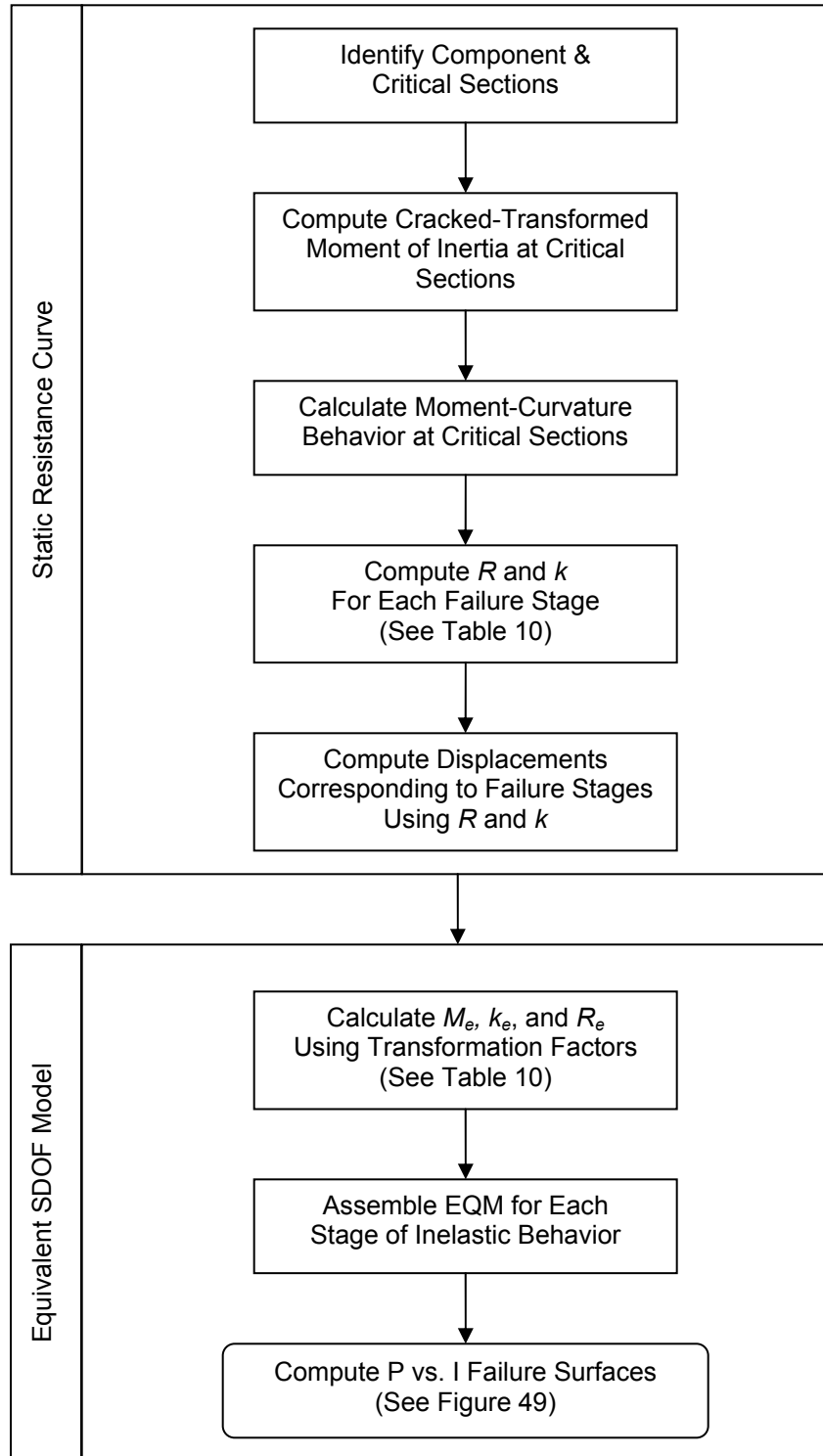


Figure 52: Flow Chart of Dynamic Response Methodology (Component Model)

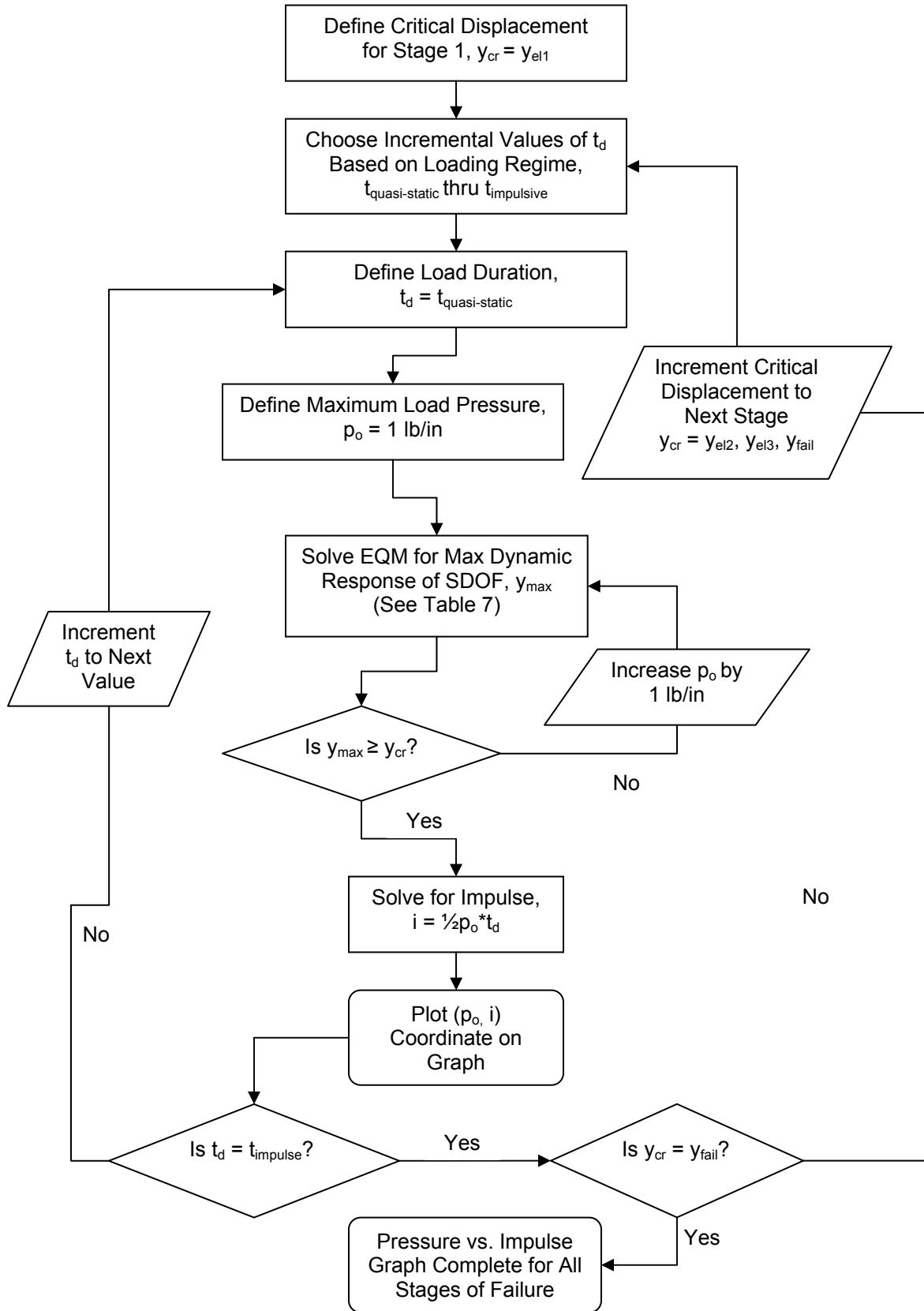


Figure 53: Flow Chart of Pressure vs. Impulse Curve Methodology

10.5. Component Analysis with Bi-linear Approximation

If it is not necessary to designate the intermediate stages of damage in a blast assessment, further simplifications can be incorporated. When only the yield and ultimate levels are needed it is advantageous to simplify the resistance curve as bi-linear or “elastic-plastic”. For the case of a bi-linear resistance curve graphs can be developed which correlate the natural period of a structure with its maximum midspan displacement under a certain blast demand. Figure 54 shows such a graph derived for a triangular load. Use of such tables allows a designer to quickly determine the blast resistance of a structure without ever having to solve the dynamic EQM problem. This is a much quicker way to gain information, but as the following results will show, the solution will differ somewhat from the previous estimate of response as a result of the simplification. This must be considered before a designer would choose to approximate a multi-linear resistance curve as bi-linear.

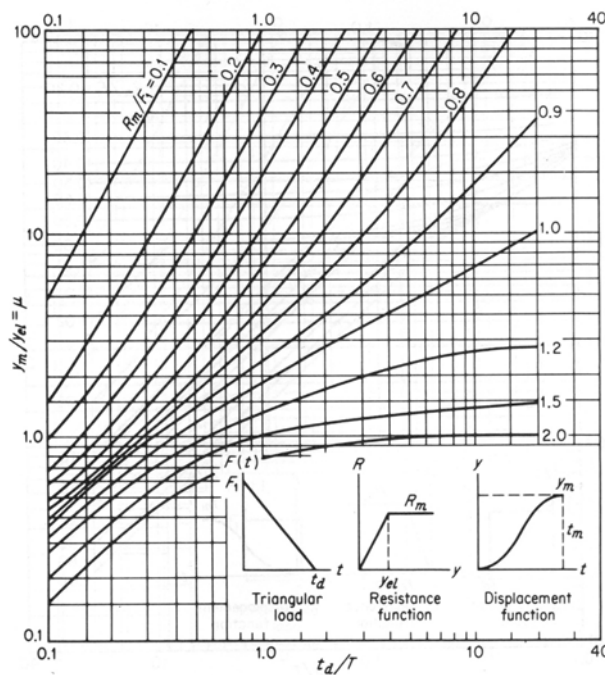


Figure 54: Maximum Response of Elastic-Plastic SDOF System Due to Triangular Load (Biggs 1964)

When converting the multi-linear resistance curve to bi-linear the stiffness values of Stage 1-3 will be replaced by an *effective spring constant*, k_e^E , as shown in Figure 55. The effective spring constant is chosen so that the areas under both curves are equal, which shifts the value of y_{el3} to y_{el}^E . This ensures that the energy absorbed by the two systems will be the same. The values of k_e^E and y_{el}^E are calculated to be 536,058 lb/in and 0.69” respectively. Using energy equivalence again, an effective displacement corresponding to failure stage 1 can also be calculated, y_{el1}^E . The point designating Stage 1 is found to be $(y_{el1}^E, R_{el}^E) = (0.325 \text{ in}, 174103 \text{ lb})$.

The parameters of the equivalent SDOF system (M_e , k_e , and F_e) must be estimated for the “elastic” stage, which now encompasses Stages 1-3 of the component model. It has been suggested that the parameters can be approximated by employing a weighted average of the transformation factors for each stage (Biggs 1964). Therefore, the transformation factors for each stage were weighted according to the area under the resistance curve for that stage, and the values were averaged to determine an *effective transformation factor*. Table 13 tabulates the effective load

and mass transformation factors, K_L^E and K_M^E respectively. The value of the effective equivalent mass, M_e^E , is calculated using the effective mass transformation factor, $M_e^E = M * K_M^E = 38.08 \text{ lb-sec}^2/\text{in} * 0.48 = 18.31 \text{ lb-sec}^2/\text{in}$. The effective equivalent load is found similarly, $F_e^E = F * K_L^E$. The value of F_e^E will be calculated for increasing values of p_o as illustrated in the numerical analysis program of Appendix B.

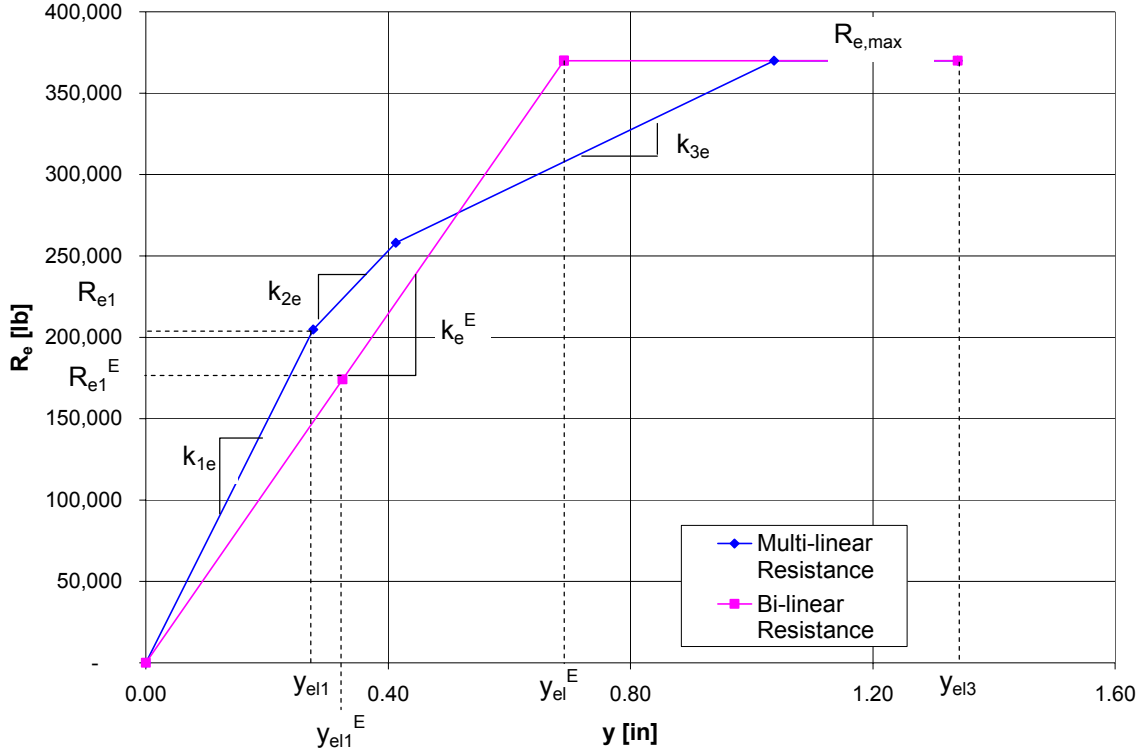


Figure 55: Effective Bi-linear Resistance Curve

	K_L	K_M
Stage 1	0.53	0.41
Stage 2	0.58	0.45
Stage 3	0.64	0.50
Effective Value	0.62	0.48

Table 13: Effective Parameters for Bi-Linear Resistance Curve

The EQM for the bi-linear model are represented in Eqn. 20-21. The transformation factors from Stage 4 in Table 11 apply to the plastic stage.

$$\text{Elastic: } K_M^E M y'' + k_e^E y = K_L^E F(t) \quad 0 < y < y_{el}^E \quad \text{Eqn. 20}$$

$$\text{Plastic: } K_{4M} M y'' + K_{4L} R_{\max} = K_{4L} F(t) \quad y_{el}^E < y < y_m \quad \text{Eqn. 21}$$

Figure 56 compares the results of the system model with the results of the bi-linear model. The error as a result of using a bi-linear resistance curve is apparent. When compared to the expected results of the system model the bi-linear model overestimates the system strength at Stage 4 by 15% in the impulsive region. This approximation is

non-conservative. The result of Stage 1 underestimates the response by 13%. These errors are a result of using a weighted average of the transformation factors to represent the bi-linear curve. The biggest drawback to the bi-linear model is that the intermediate stages of failure are not clearly delineated on the resistance curve. Therefore the pressure vs. impulse curve for Stages 2 & 3 cannot be generated by the bi-linear model. This technique is useful to determine the approximate response of the first and last stages, but it should be kept in mind that an unconservative answer may result.

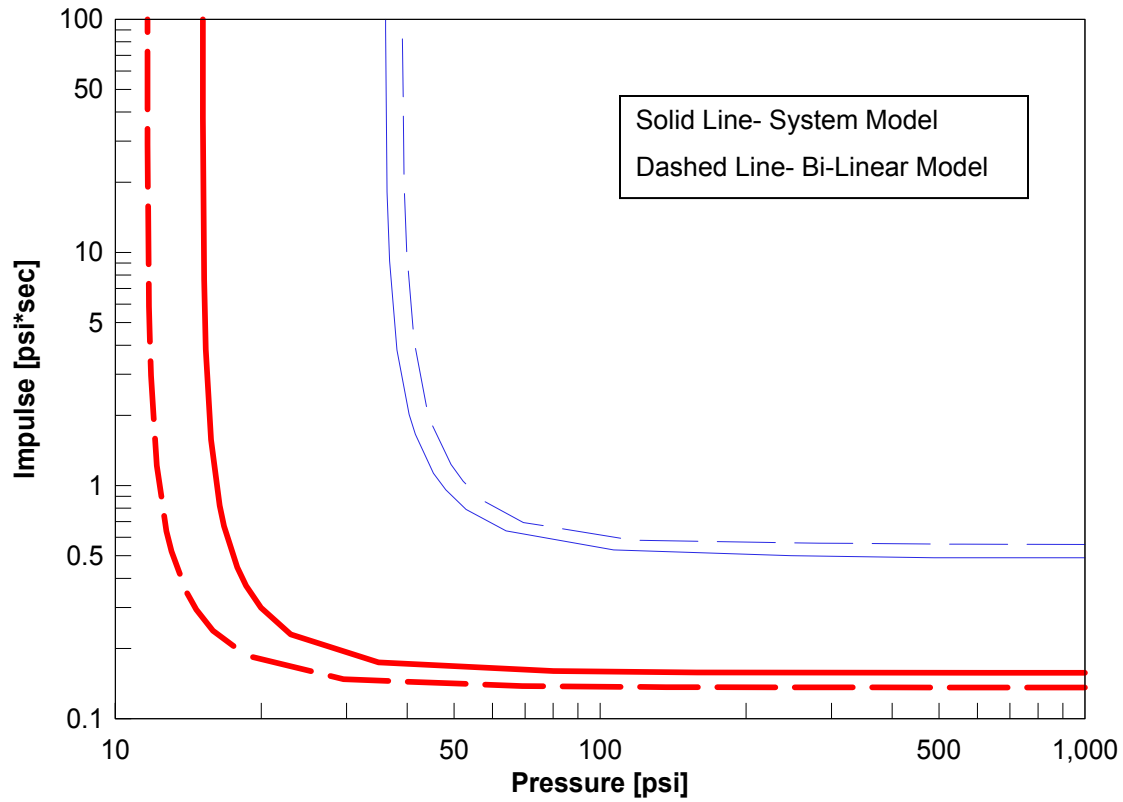


Figure 56: Pressure vs. Impulse Curve (Bi-Linear & System Models)

11. Conclusions and Recommendations

The purpose of this paper was to describe a procedure to determine the behavior of a reinforced concrete shear wall under a blast load. Consideration was made to develop an efficient calculation method that can be replicated in practice, while still yielding informative dynamic response information. A prototypical building was chosen which represents common office buildings constructed throughout the U.S. The building is three stories high with gravity bearing shear walls located at each corner. The shear walls have window openings at each floor and do not exhibit any special details or design for blast load. One of the corner shear walls was chosen for in-depth investigation. A combination of a static, FE analysis and a SDOF dynamic analysis was used to determine the response of the wall under a blast load.

The program BlastX was used to determine the blast demand of an explosion located 20 ft off the corner of the shear wall. As a preliminary study an FE model was constructed with static push-over loads to determine where failure likely occurs in the wall. It was determined that the 2nd floor, outer wall was the weak link in the total shear wall. This portion of the wall became the focus of further dynamic analysis. Two models were investigated. A system model was chosen that represented the actual end fixity of the 2nd floor, outer wall by including the stiffness contributions of its adjoining wall sections. Simplifying assumptions were then recommended to create a component model requiring less computational complexity. The component model assumed the ends of the 2nd floor, outer wall to be fixed-fixed.

First, the system model was analyzed to determine its dynamic response under a blast load. The static resistance curve of the wall was derived by calculating the stiffness of the wall pieces and their moment-curvature behavior. It was determined when and where plastic hinges form. An equivalent SDOF system was then developed to calculate the maximum dynamic response of the wall at four stages of failure. The final results were plotted as a pressure vs. impulse diagram which represented the level of damage the wall would sustain for varying sized blasts.

The dynamic analysis was replicated for the component model, requiring less rigorous calculation of the static resistance curve and equivalent SDOF parameters pertaining to the assumption of fixed ends. Comparison of the pressure vs. impulse curves for the system and component models showed that the component model is a close representation of the response predicted by the system model. For an impulsive blast demand, the component model overestimated the wall's resistance by 7%. While this is small percentage difference, it should be kept in mind that the component model results will always be non-conservative because it is assuming the wall is stiffer than actuality. For this reason the component model is recommended only for structures which exhibit a large amount of stiffness. For flexible structures, pinned-pinned end conditions could be used to represent the structure and would offer a lower bound estimate of the wall strength.

An additional simplification was studied in comparison to the system model results. In lieu of analyzing the dynamic problem using a multi-linear curve an equivalent elastic-plastic curve was derived. This model was used to estimate the blast resistance of the wall at first yield and failure. The intermediate stages of failure were not included because they are not delineated by a bi-linear model. The results yielded a pressure-impulse curve that was a 15% overestimate of the system model. For these reasons, a bi-linear approximation of the multi-linear resistance

curve would be recommended as a means to get an order of magnitude approximation of the response for elastic behavior or at failure.

It should be noted that this procedure considers the *flexural* resistance of the wall only. The consideration of a shear failure was not considered, but this is a very important failure mechanism which should be investigated in any blast design. Oftentimes, extra shear reinforcement will be necessary for a structure to reach its full flexural capacity. Two methods of shear failure should be considered, flexural shear and direct shear. A direct shear failure occurs when the load is applied at a high enough magnitude and rate that the wall does not have time to defect before it is sheared. This failure mechanism is a possibility under high impulse blast loads. Research into adequate detailing to resist flexural and direct shear failure would be highly informative to designers.

The methodology developed in this paper outlines an efficient procedure to determine the blast resistance of a wall under varying stages of inelastic behavior. The resulting pressure-impulse curves are a useful source of information to determine for a certain structure how much damage will result from a specific blast demand. This analysis is valuable for designers who are considering retrofit options to protect a structure against blast. Determining the blast resistance of existing structures is the first step towards determining what hardening options may be warranted.

12. References

- Applied Technology Council, and Building Seismic Safety Council. (1997). *NEHRP Commentary on the Guidelines for the Seismic Rehabilitation of Buildings (FEMA Publication 274)*, FEMA, Washington, D.C.
- Biggs, J. M. (1964). *Introduction to Structural Dynamics*, McGraw-Hill, New York.
- Britt, J. R., Ranta, D. E., and Joachim, C. E. (2001). "A Users Manual for the BlastX Code, Version 4.2." *ERDC/GSL TR-01-2*, US Army Corps of Engineers, Engineering Research and Development Center, Geotechnical and Structures Laboratory, Vicksburg, MD.
- Chopra, A. K. (1995). *Dynamics of Structures : Theory and Applications to Earthquake Engineering*, Prentice Hall, Englewood Cliffs, N.J.
- Conrath, E. J. (1999). *Structural Design for Physical Security : State of Practice*, American Society of Civil Engineers, Reston, Va.
- Crepeau, J. (2001). "SHAMRC Second-Order Hydrodynamic Automatic Mesh Refinement Code, Vol. 2: User Manual." Applied Research Associates, Inc, Albuquerque, NM.
- DSWA, D. S. W. A. (1998). "Protective Structures Automated Design System (PSADS), Version 1." Defense Special Weapons Agency (DSWA), Alexandria, VA.
- General Services Administration. (2003). "GSA Progressive Collapse Analysis and Design Guidelines for New Federal Office Buildings and Major Modernization Projects." Prepared by Allied Research Associates for GSA, Washington, D.C.
- Gere, J. M., and Timoshenko, S. P. (1997). *Mechanics of Materials*, PWS Pub Co., Boston.
- Hyde, D. W. (2003). "ConWep Version 2.0.2.0." USAE Engineer Research & Development Center, CEERD-GS-S, Vicksburg, Mississippi.
- Institution of Civil Engineers. (1964). "Ultimate Load Design of Concrete." Institution of Civil Engineers, London.
- International Code Council. (2003). *International Building Code*, Thomson Delmar Learning, Clifton Park, NY.
- Mays, G., and Smith, P. D. (1995). *Blast Effects on Buildings : Design of Buildings to Optimize Resistance to Blast Loading*, T. Telford, London.
- McVay, M. K. (1988). "Spall Damage of Concrete Structures." *U.S. Army Engr. Waterway Experiment Station Technical Rep. SL-88-22*, U.S. Army Engineer Waterways Experiment Station, Vicksburg.
- Park, R., and Paulay, T. (1975). *Reinforced Concrete Structures*, Wiley, New York.
- Prakash, V., Powell, G. H., and Campbell, S. (1993). "DRAIN-2DX Base Program Description and User Guide Version 1.10." *UCB/SEMM-93/17*, Department of Civil Engineering, University of California, Berkeley.
- Precast/Prestressed Concrete Institute. (1999). *PCI Design Handbook : Precast and Prestressed Concrete*, Precast/Prestressed Concrete Institute, Chicago.
- Priestly, M. J. N., Seible, F., and Calvi, G. M. (1996). *Seismic Design and Retrofit of Bridges*, John Wiley & Sons, Inc., New York.
- Smith, P. D., and Hetherington, J. G. (1994). *Blast and Ballistic Loading of Structures*, Butterworth-Heinemann, Oxford ; Boston.
- U.S. Army Corp of Engineers. (1998). "Protective Structures Automated Design System (PSADS)." Omaha, NE.
- U.S. Army Corp of Engineers. (2005). "Unified Facilities Criteria (UFC) Design of Buildings to Resist Progressive Collapse." Omaha, NE.
- U.S. Department of the Army. (1990). "Design of Structures to Resist the Effects of Accidental Explosions." *Army TM5-1300*, Washington, D.C.
- U.S. Department of the Army. (1998). "Design and Analysis of Hardened Structures to Conventional Weapons Effects." *Army TM 5-855-1*, Washington, D.C.
- Ugural, A. C., and Fenster, S. K. (1995). *Advanced Strength and Applied Elasticity*, PTR Prentice Hall, Englewood Cliffs, N.J.
- Witte, F. C. (2002). "DIANA – Finite Element Analysis User’s Manual: Release 8.1." TNO Building Construction and Research, Delft, The Netherlands.
- Ziemian, R. D., and McGuire, W. (2000). "MASTAN v2.0." The MathWorks, Inc., Natick, MA.

Appendix A: Mathcad Program to Solve System Model Equivalent SDOF Model

Define Constants:

E = Modulus of Elasticity

I = Moment of Inertia

L = Length of Wall

m = distributed mass of wall

$\varphi_1(x)$ = Stage 1 shape function

$\varphi_2(x)$ = Stage 2 shape function

$\varphi_3(x)$ = Stage 3 shape function

$\varphi_4(x)$ = Stage 4 shape function

M_{1e} = Stage 1 equivalent mass

M_{2e} = Stage 2 equivalent mass

M_{3e} = Stage 3 equivalent mass

M_{4e} = Stage 4 equivalent mass

k_{1e} = Stage 1 equivalent stiffness

k_{2e} = Stage 2 equivalent stiffness

k_{3e} = Stage 3 equivalent stiffness

k_{4e} = Stage 4 equivalent stiffness

F_{1e}' = Stage 1 equivalent force normalized by max pressure = F_{1e}/p_o

F_{2e}' = Stage 2 equivalent force normalized by max pressure = F_{2e}/p_o

F_{3e}' = Stage 3 equivalent force normalized by max pressure = F_{3e}/p_o

F_{4e}' = Stage 4 equivalent force normalized by max pressure = F_{4e}/p_o

y_{el1} = Stage 1 critical displacement

y_{el2} = Stage 2 critical displacement

y_{el3} = Stage 3 critical displacement

y_{el4} = Stage 4 critical displacement

R_{1e} = Stage 1 max equivalent resistance = $k_{1e} * y_{el1}$

R_{2e} = Stage 2 max equivalent resistance = $k_{2e}(y_{el2} - y_{el1}) + R_{1e}$

R_{3e} = Stage 3 max equivalent resistance = $k_{3e}(y_{el3} - y_{el2}) + R_{2e}$

R_{4e} = Stage 4 max equivalent resistance = R_{3e}

$y(\Delta t) :=$ for $p_0 \in 0, 1.. 500000$

* $p_0 = \text{lb/in}$

$t_d = \blacksquare$

* $F_{oe} = \text{lb}$

$t_{end} = \blacksquare$

$\Delta t = \blacksquare$

for $n \in 0.. \frac{t_{end}}{\Delta t} + 10$

$y_n \leftarrow 0$

$F1_{oe} \leftarrow p_0 \cdot F1'_e$

$F2_{oe} \leftarrow p_0 \cdot F2'_e$

$F3_{oe} \leftarrow p_0 \cdot F3'_e$

$F4_{oe} \leftarrow p_0 \cdot F4'_e$

$y_0 \leftarrow 0$

Initial calculation for $t = 0$

$f \leftarrow \frac{(F1_{oe})}{M1_e}$

$r \leftarrow \frac{y_0 \cdot k1_e}{M1_e}$

$y''\Delta t \leftarrow (f - r) \cdot \Delta t^2$

$y_1 \leftarrow \frac{1}{2} \cdot y''\Delta t$

$m \leftarrow 1$

for $i \in 1 \cdot \Delta t, 2 \cdot \Delta t.. t_{end}$

break if $y_m > y_{el1}$

$f \leftarrow \frac{\frac{-F1_{oe}}{t_d} \cdot i + F1_{oe}}{M1_e}$ if $f > 0$

$f \leftarrow 0$ otherwise

$r \leftarrow \frac{y_m \cdot k1_e}{M1_e}$

Elastic Stage until $y = y_{el1}$

$y''\Delta t \leftarrow (f - r) \cdot \Delta t^2$

$m \leftarrow m + 1$

$y_m \leftarrow 2 \cdot y_{m-1} - y_{m-2} + y''\Delta t$

for $j \in i, i + \Delta t \dots t_{end}$

break if $y_m > y_{el2}$

break if $y_m < y_{m-1}$

$y_{max} \leftarrow y_m$

$f \leftarrow \frac{\frac{-F_{2oe}}{t_d} \cdot j + F_{2oe}}{M_{2e}}$ if $f > 0$

$f \leftarrow 0$ otherwise

$r \leftarrow \frac{k_{2e} \cdot (y_m - y_{el1}) + R_{1e}}{M_{2e}}$

$r_{max} \leftarrow r \cdot M_{2e}$

$y''\Delta t \leftarrow (f - r) \cdot \Delta t^2$

$m \leftarrow m + 1$

$y_m \leftarrow 2 \cdot y_{m-1} - y_{m-2} + y''\Delta t$

Stage 2 until $y = y_{el2}$
or rebound begins ($y = y_{max}$)

for $k \in j, j + \Delta t \dots t_{end}$

break if $y_m > y_{el2}$

$f \leftarrow \frac{\frac{-F_{1oe}}{t_d} \cdot k + F_{1oe}}{M_{1e}}$ if $f > 0$

$f \leftarrow 0$ otherwise

$r \leftarrow \frac{r_{max} - k_{1e} \cdot (y_{max} - y_m)}{M_{1e}}$

$y''\Delta t \leftarrow (f - r) \cdot \Delta t^2$

$m \leftarrow m + 1$

$y_m \leftarrow 2 \cdot y_{m-1} - y_{m-2} + y''\Delta t$

Stage 2 rebound until $y = y_{el2}$

for $l \in k, k + \Delta t .. t_{end}$

break if $y_m > y_{el3}$

break if $y_m < y_{m-1}$

$y_{max} \leftarrow y_m$

$f \leftarrow \frac{\frac{-F3_{oe}}{t_d} \cdot l + F3_{oe}}{M3_e}$ if $f > 0$

$f \leftarrow 0$ otherwise

$r \leftarrow \frac{k3_e \cdot (y_m - y_{el2}) + R2_e}{M3_e}$

$r_{max} \leftarrow r \cdot M3_e$

$y''\Delta t \leftarrow (f - r) \cdot \Delta t^2$

$m \leftarrow m + 1$

$y_m \leftarrow 2 \cdot y_{m-1} - y_{m-2} + y''\Delta t$

Stage 3 until $y = y_{el3}$
or rebound begins ($y = y_{max}$)

for $n \in l, l + \Delta t .. t_{end}$

break if $y_m > y_{el3}$

$f \leftarrow \frac{\frac{-F1_{oe}}{t_d} \cdot n + F1_{oe}}{M1_e}$ if $f > 0$

$f \leftarrow 0$ otherwise

$r \leftarrow \frac{r_{max} - k1_e \cdot (y_{max} - y_m)}{M1_e}$

$y''\Delta t \leftarrow (f - r) \cdot \Delta t^2$

$m \leftarrow m + 1$

$y_m \leftarrow 2 \cdot y_{m-1} - y_{m-2} + y''\Delta t$

Stage 3 rebound until $y = y_{el3}$

```

for o ∈ n, n + Δt.. tend
    break if ym > yfail
    break if ym < ym-1
    ymax ← ym
    
$$f \leftarrow \frac{-F4_{oe}}{t_d} \cdot o + F4_{oe}$$

    if f > 0
        f ←  $\frac{-F4_{oe}}{M4_e}$ 
    else
        f ← 0
    
$$r \leftarrow \frac{R3_e}{M4_e}$$

    rmax ← r · M4e
    y''Δt ← (f - r) · Δt2
    m ← m + 1
    ym ← 2 · ym-1 - ym-2 + y''Δt

```

Stage 4 until y = y_{fail}
or rebound begins (y = y_{max})

```

for l ∈ k, k + Δt.. tend
    break if ym > yfail
    
$$f \leftarrow \frac{-F1_{oe}}{t_d} \cdot n + F1_{oe}$$

    if f > 0
        f ←  $\frac{-F1_{oe}}{M1_e}$ 
    else
        f ← 0
    
$$r \leftarrow \frac{r_{max} - k1_e \cdot (y_{max} - y_m)}{M1_e}$$

    y''Δt ← (f - r) · Δt2
    m ← m + 1
    ym ← 2 · ym-1 - ym-2 + y''Δt

```

Stage 4 rebound until y = y_{fail}

Po

```

break if ym > yfail

```

y(Δt) = ■

Appendix B: Mathcad Program to Solve Component Model Equivalent SDOF Model

Define Constants:

E = Modulus of Elasticity
 I = Moment of Inertia
 L = Length of Wall
 m = distributed mass of wall

Calculate per Table 10:

R_1 = Stage 1 max resistance
 R_2 = Stage 2 max resistance
 R_3 = Stage 3 max resistance
 R_4 = Stage 4 max resistance

k_1 = Stage 1 stiffness
 k_2 = Stage 2 stiffness
 k_3 = Stage 3 stiffness
 k_4 = Stage 4 stiffness

K_{1M} = Stage 1 mass transformation factor
 K_{2M} = Stage 2 mass transformation factor
 K_{3M} = Stage 3 mass transformation factor
 K_{4M} = Stage 4 mass transformation factor

K_{1L} = Stage 1 load transformation factor
 K_{2L} = Stage 2 load transformation factor
 K_{3L} = Stage 3 load transformation factor
 K_{4L} = Stage 4 load transformation factor

M_{1e} = Stage 1 equivalent mass = $K_{1M} * m$
 M_{2e} = Stage 2 equivalent mass = $K_{2M} * m$
 M_{3e} = Stage 3 equivalent mass = $K_{3M} * m$
 M_{4e} = Stage 4 equivalent mass = $K_{4M} * m$

k_{1e} = Stage 1 equivalent stiffness = $K_{1L} * k_1$
 k_{2e} = Stage 2 equivalent stiffness = $K_{2L} * k_2$
 k_{3e} = Stage 3 equivalent stiffness = $K_{3L} * k_3$
 k_{4e} = Stage 4 equivalent stiffness = $K_{4L} * k_4$

y_{el1} = Stage 1 critical displacement = R_1/k_1
 y_{el2} = Stage 2 critical displacement = R_2/k_2
 y_{el3} = Stage 3 critical displacement = R_3/k_3
 y_{el4} = Stage 4 critical displacement = R_4/k_4

R_{1e} = Stage 1 max equivalent resistance = $k_{1e} * y_{el1}$
 R_{2e} = Stage 2 max equivalent resistance = $k_{2e}(y_{el2} - y_{el1}) + R_{1e}$
 R_{3e} = Stage 3 max equivalent resistance = $k_{3e}(y_{el3} - y_{el2}) + R_{2e}$
 R_{4e} = Stage 4 max equivalent resistance = R_{3e}

$y(\Delta t) :=$ for $p_0 \in 0, 1.. 500000$

*** $p_0 = lb/in$**

$t_d = \blacksquare$

```

for n ∈ 0..  $\frac{t_{end}}{\Delta t} + 10$ 
   $y_n \leftarrow 0$ 
   $F1_{0e} \leftarrow p_0 \cdot L_2 \cdot K1_L$ 
   $F2_{0e} \leftarrow p_0 \cdot L_2 \cdot K2_L$ 
   $F3_{0e} \leftarrow p_0 \cdot L_2 \cdot K3_L$ 
   $F4_{0e} \leftarrow p_0 \cdot L_2 \cdot K4_L$ 
   $y_0 \leftarrow 0$ 
   $f \leftarrow \frac{(F1_{0e})}{M1_e}$ 
   $r \leftarrow \frac{y_0 \cdot k1_e}{M1_e}$ 
   $y''\Delta t \leftarrow (f - r) \cdot \Delta t^2$ 
   $y_1 \leftarrow \frac{1}{2} \cdot y''\Delta t$ 
   $m \leftarrow 1$ 

```

$t_{end} = \blacksquare$

$\Delta t = \blacksquare$

Initial calculations when $t = 0$

- Continue numerical analysis as for the system model in Appendix A.